Government of **Western Australia**
Department of **Water**

Projected impacts of climate change on the Serpentine catchment

Downscaling from multiple General Circulation Models

Water Resource Technical Series

Report No. WRT 36
February 2009

Projected impacts of climate change on the Serpentine catchment

Downscaling from multiple General Circulation Models

by

A Kitsios[1], MA Bari[2], SP Charles[3]

(1) Department of Water
(2) Bureau of Meteorology
(3) CSIRO Land and Water

Department of Water

Water Resource Technical Series

Report no. WRT 36

February 2009

Department of Water
168 St Georges Terrace
Perth Western Australia 6000
Telephone +61 8 6364 7600
Facsimile +61 8 6364 7601
http://www.water.wa.gov.au

February 2009

ISSN 1327-8436 (print) and 1449-8901 (online)
ISBN 978-1-921508-37-0 (print) and 978-1-921508-38-7 (online)

Recommended reference

Kitsios, A, Bari, MA & Charles, SP 2009, *Projected impacts of climate change on the Serpentine catchment, Western Australia: Downscaling from multiple General Circulation Models*, Department of Water, Water Resource Technical Series, WRT 36.

For more information contact Mark Pearcey.

Acknowledgements

The authors thank the following for their help and contributions: The Australian Greenhouse Office for funding for the project, Mary-Ann Coppolina, Mark Pearcey, Ed Hauck and John Ruprecht from the Department of Water, Naomi Kerp and Amanda Reed from Alcoa, and Charles Jeevaraj and Colin Terry (formerly) from the Water Corporation of Western Australia.

Cover photograph: A tributary of the Serpentine River — Jayrup catchment
Photographer: Artemis Kitsios

Contents

Appendices

Figures

Tables

Summary

Climate change has serious implications for the management of water resources. The hydrologic cycle has been altered by the climatic change that has occurred as a result of both increased greenhouse gases and natural climate variability. Changes in rainfall and streamflow patterns in the south-west of Western Australia have had the effect of reducing the available water resources. As the population increases, so will demand for water supplies, and evaluating the effects of climate change is therefore important for the future management of water resources.

This study is an extension of the *Climate change, catchment runoff and risks to water supply in the south-west of Western Australia* — or Stage 1 study — undertaken for the Australian Greenhouse Office (Berti et al. 2004). The Stage 1 study evaluated the effects of climate change on the Stirling Dam catchment in the south-west of Western Australia. Stage 1, which used a General Circulation Model (CSIRO Mk3 GCM) under the A2 (high emissions scenario), found that by mid-century there would be an 11% reduction in rainfall, resulting in a 31% reduction in annual catchment yield into Stirling Dam. This study assesses impacts of climate change on the Serpentine Dam catchment using four global climate models and compares their results. Two of the models were developed at CSIRO Australia (CCAM and Mk3), one at the Hadley Centre in the UK (HadAM3P) and one at the Max Planck Institute in Germany (ECHAM4). All used the A2 emission scenario, which corresponds to a 1.7 times increase in CO_2 emissions by 2090. This is also the emission scenario used in Stage 1 of the study. Downscaled rainfall datasets from these GCMs were used as inputs into a catchment model, LUCICAT, in order to evaluate streamflow under the future climate.

The results of this study (Stage 2) are based on averages from forty current and forty projected downscaled rainfall datasets for each of the GCMs. The CCAM and Mk3 results show 12–14% reductions in annual rainfall by mid-century. This corresponds to a 30–44% decline in streamflow. The HadAM3P, which modelled the 2070–99 period, shows a 24% decline of rainfall, corresponding to 69% streamflow reduction. The ECHAM4 shows a 24% decline of rainfall for the same period, but, due to inconsistencies, has not been used for streamflow analysis.

Although this study has modelled only one of the IPCC emission scenarios, a range of other scenarios could be modelled. These results represent fairly extreme possible outcomes, as the A2 scenario corresponds to a constantly increasing emission rate. The majority of other scenarios tend to peak in mid-century, then stabilise by 2100.

This study assumes no change to current land use, temperature and vegetation response to changes in CO_2 concentrations.

1 Introduction

Human-induced climate change is predicted to seriously affect many aspects of the environment, including water resources, with major implications for agriculture, industry and urban water supply. The population in Western Australia is expected to increase to over 3 million by 2051 (ABS 2002), putting further pressure on water resources.

Climatic variables exert a large influence on a catchment's water balance, affecting rainfall, evaporation, streamflow and soil moisture as well as recharge to groundwater. The effects of climate change on streamflow will be seen at time scales that range from storm events to multi-decadal. It is important to document the seasonal variations of these changes as they may have more impact on catchment yield than the predicted annual changes (Stonefelt et al. 2000).

The south-west of Western Australia has experienced declining rainfall since the late 1970s. Reduction in catchment rainfall often results in an amplified reduction in streamflow (Chiew & McMahon 2002). Reduced streamflows have been observed in the Perth water-supply catchments since the 1970s (Bari & Ruprecht 2003). The inflow into reservoirs supplying the Integrated Water Supply System (IWSS) decreased from an annual average inflow of 338 GL for the 1911–74 period to 177 GL for the 1976–96 period and then to 115 GL in the 1997–2004 period (Water Corporation 2005b). For streams in high-rainfall areas, the flow duration at various flow rates has decreased (Rodgers & Ruprecht 1999).

Many studies have increased our understanding of the potential impacts of climate change on surface water resources. Most have been completed globally; few have focused on Australia and fewer still on Western Australia. The studies usually employ General Circulation Models (GCMs), sometimes called Global Climate Models, to simulate atmospheric pressure, velocity, temperature and moisture through time to project possible climatic changes in future years.

There has been modelling of climate-change scenarios using GCMs in numerous regions of the world (Arora & Boer 2001; Voss et al. 2002). The effects of climate change on extreme events have been studied in Northern Germany (Bronstert et al. 2002) and in New York City (Blake et al. 2000). Mean changes to rainfall and runoff have been studied in the United States (Wolock & McCabe 1999; Hay et al. 2000). Within Australia, there have been several studies modelling the effects of climate change on hydrology. Specific rivers studied have included the Macquarie River (Hassal & Associates 1998) and the Border River catchment (Ritchie et al. 2004). Other studies have compared the effects in different regions of Australia (Nathan et al. 1988; Chiew et al. 1995; Schnur & Lettenmaier 1998; Chiew & McMahon 2002). In the south-west of Western Australia there have been a various climate-change studies (Viney & Sivapalan 1996; Rodgers & Ruprecht 1999; Evans & Schreider 2002; IOCI 2002). Stage 1 of this study (Berti et al. 2004) focused on the Stirling catchment.

Different GCMs often produce quite different outcomes despite modelling the same emission scenario. The accuracy of GCMs is highest at the global scale; however, they have also

been applied on regional scales, as the resolution of such models is of the order of 200 km (Hassall & Associates 1998; CIESIN 1995). When applied on a local scale, the GCM projections become more uncertain, as the resolution is too coarse to include local-scale features such as topography (Hassall & Associates 1998) and rainfall from convective systems.

As decision making usually takes place at the regional or local scale, these GCM projections may lead to levels of uncertainty. A variety of methods can increase the spatial resolution of GCM projections and enable their application at smaller scales. These include increasing the resolution of the components of the GCM (IPCC 2001) as well as coupling the GCM with a regional climate model (RCM). RCMs have larger computational requirements.
They run on finer spatial and temporal scales and enable the study of regional changes in climate (Suchita 2004). Another, used in Stages 1 and 2 of this study, is stochastic downscaling, which uses statistical methods to relate GCM characteristics to the local scale. The downscaled rainfall is used as input to hydrologic models to simulate the effects of a changing climate on river flow and subsequent storage yields. Stochastic downscaling was chosen in preference to using RCM precipitation directly as (1) it simulates individual gauge-scale precipitation (2) it allows generation of multiple realisations (conditional on GCM atmospheric output) and (3) previous studies have found that RCMs do not reproduce measured precipitation statistics as well as stochastic downscaling (Wilby et al. 2000; Hay & Clarke 2003; Wood et al. 2004).

Stage 1 analysed streamflow outputs generated from one GCM, the CSIRO Mk3, and reported the percentage change in catchment yield projected for the future scenario. In Stage 2, downscaled rainfall series from four GCMs have been used as data inputs to simulate the streamflows within the Serpentine Dam catchment, one of the main water-supply catchments for the Perth Metropolitan Area. The purpose of this report is to compare results from the four GCMs and determine a range of projected outcomes rather than to calculate a single value for catchment yield reduction.

2 Catchment description

2.1 Location

The Serpentine catchment is approximately 55 km south-east of Perth, and includes the towns of Serpentine, Jarrahdale, Mundijong and Byford. The town of Serpentine was developed in the early 1890s as a result of the declaration of the Serpentine Agricultural Area. Jarrahdale was also developed at this time, being officially gazetted as a town site in 1913.

2.2 Land use

This study focuses on the Serpentine Dam catchment (Fig. 2.1). The main land use is jarrah forest forming an upperstorey vegetation cover. Smaller trees and shrubs produce a significant understorey throughout the catchment. The catchment is largely forested, with only small parts cleared. Dieback is present within the catchment. The Jack Rocks subcatchment was mined for bauxite in the 1990s while parts of the Cameron West and Cameron Central subcatchments were logged in 1995/96 (Water and Rivers Commission 1999). There has been selective logging within the Jayrup subcatchment (Water and Rivers Commission 1999). Alcoa currently has mine operations in the Jayrup subcatchment. The company has a mining tenement for all of the Serpentine Dam catchment, while others, including Hedges Gold, Moutier and Trovex, have mining tenements south of the catchment. South of Serpentine Dam, the subcatchments are mainly mined for bauxite.

Fires influence land use within the catchment. Prescribed burning has a role in reducing the incidence of wildfires, regenerating native forests and conserving biodiversity. Hot wildfires convert much more surface vegetation and leaf litter to nutrient-rich ash and expose the soil surface to rainfall, which can increase the risk of soil erosion (NSW EPA 2003). Soils can become water repellent, which increases runoff and therefore nutrient and sediment transport into receiving waters (NSW EPA 2003). Chemicals mobilised from the fire can also enter streams (Martin 2001). The Department of Environment and Conservation has proposed that parts of the Serpentine Dam catchment will be subjected to prescribed burning over the 2006–09 period (CALM 2005).

2.3 Elevations

Topographic elevations vary from a maximum of 530 m AHD at the southern edge of the River Road subcatchment to a minimum of 250 m AHD at the dam outlet. Within the major subcatchments elevations vary widely; in particular, the eastern part of Big Brook and Jack Rocks at subcatchments 42 and 47 and subcatchments within River Road (Fig. A.2).

2.4 Climate

The climate of the Serpentine catchment area is classified as temperate (Bureau of Meteorology 2005), with hot dry summers and cool wet winters. Rainfall is heavier in the western part of the catchment, as shown by the spatial distribution of mean annual rainfall (Fig. A.3) and mean monthly rainfall at subcatchments 1, 28 and 86 (Fig. A.4). Average annual rainfall varies from 680 mm in the east to 1150 mm in the west of the catchment.

2.5 Serpentine Reservoir

The Serpentine Reservoir was created when the Serpentine Dam was constructed in 1961. It has a catchment area of 664 km^2 and a storage capacity of 138 million m^3. The Serpentine Scheme began with the need for additional water-supply sources for industrial and urban use. It is one of many south-west WA reservoirs that provide water to the Integrated Water Supply System (IWSS). The water stored in the reservoir is released under controlled conditions and discharged into the lower Serpentine River and then into the Serpentine Pipehead Reservoir. Here, the water is piped under gravity through two 55-km pipelines to supply water to the Perth Metropolitan Area as part of the Integrated Water Supply System (IWSS) (Water Corporation 2005a).

2.6 Rivers and gauging stations

Three main streams enter the Serpentine Reservoir (Fig. 2.3). The Serpentine River is the main river, originating in the east of the catchment and then flowing north-west towards the reservoir. Big Brook is the main southern tributary, flowing from the south along the western edge towards the reservoir. The third significant stream enters from the north-east, originating from the Jack Rocks subcatchment. Two other minor streams also enter the reservoir.

All tributaries flowing into the reservoir have water with salinity <150 mg/L TDS. The more distant streams are also fresh, including those of the Jayrup and Cameron Central subcatchments. This is typical of a forested catchment within the high-rainfall zone where the high rainfall develops a permanent flow of groundwater that allows most of the salt in the rainfall to discharge from the catchment without accumulating (Mayer et al. 2005). In the drier eastern areas salt may accumulate in the soil but is rarely mobilised into the streams unless the forest is permanently cleared.

Evidence suggests that the changing climate has affected streamflow into Serpentine Reservoir. The average annual (modelled) inflow to the reservoir over the 1912–94 period was 66 GL; when averaged over 1975–94, the figure falls to 41 GL (Bari & Ruprecht 2003). The salinity of the reservoir is approximately 195 mg/L TDS (Figure 2.2).

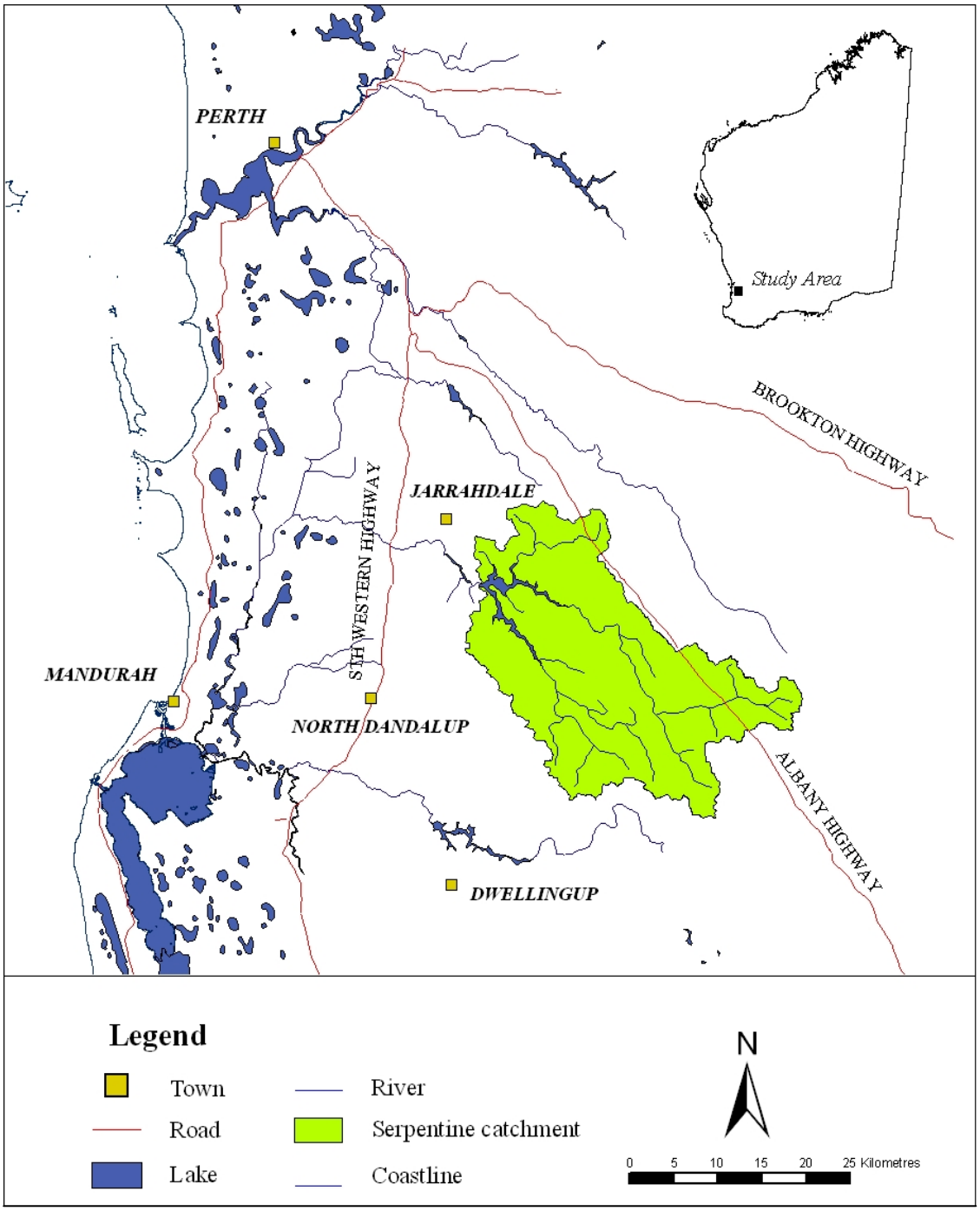

Figure 2.1 Location of the Serpentine Reservoir catchment

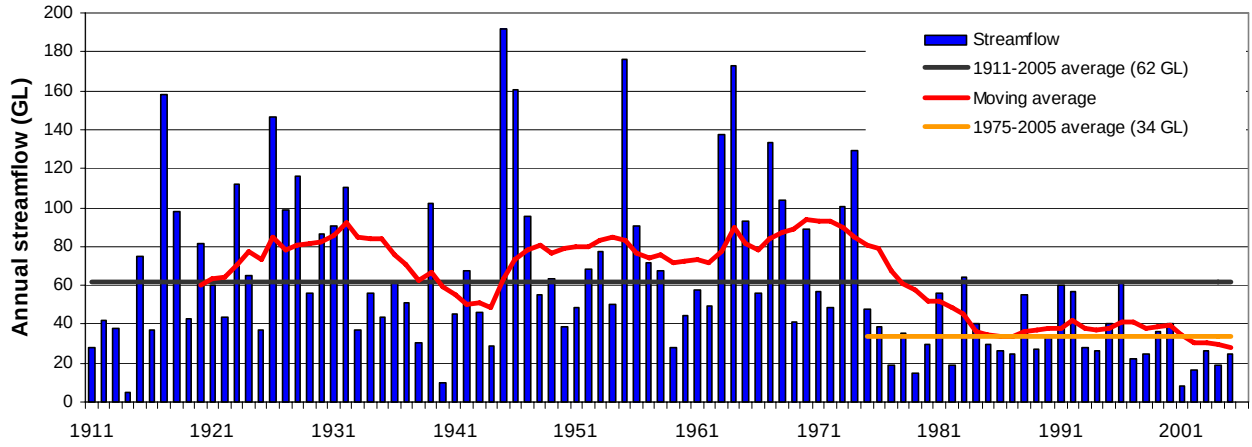

Figure 2.2 Modelled and observed flows to the Serpentine Reservoir

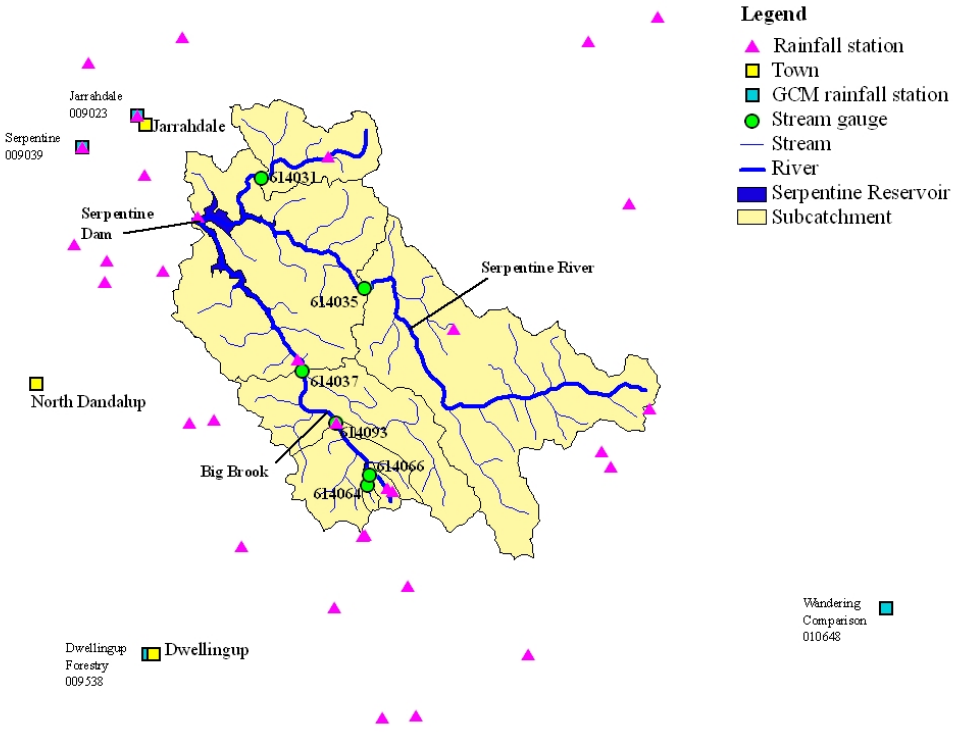

Figure 2.3 Stream gauges and rainfall stations throughout the Serpentine catchment

River Road (614035) is the only gauging station situated on the Serpentine River. It lies within the study area, approximately halfway between the dam and the origin of the river (Fig. 2.3). Site data indicates that the river flows for approximately six months of the year. The Jack Rocks gauging station (614031) is situated approximately 5 km from where the Jack Rocks tributary meets the Serpentine River. In the 1980s and early 1990s this stream flowed on average for eleven months of the year, but by the middle to late 1990s it flowed

only about nine months of the year. The gauging station at Big Brook (614037) is the most downstream gauge along this tributary, 15 km from the dam. Here, the river flows for approximately six months of the year. At the Jayrup gauging station (614093), about 6 km upstream of Big Brook, water flows for approximately five months of the year. The Cameron Central gauging station (614066) is further upstream, where there is flow for about four months of the year. The Cameron West gauging station (614064) is situated along a minor stream that meets the main tributary at Cameron Central, where flow is recorded for approximately four months of the year.

2.7 Runoff characteristics

The mean runoff throughout the catchment varies spatially between 1% and 10%. It is similar at the River Road and Big Brook stations, at just over 3%, while at the Jack Rocks station the runoff rate equates to approximately 10% (Table 2.1). Rainfall and runoff relating to the reservoir are representative of the entire catchment. Further information regarding observed and modelled runoff characteristics can be read in Section 4.3.1.

Table 2.1 Average annual rainfall, streamflow and runoff rate at the reservoir and all gauging stations for corresponding period of record

Station No.	Name	Recorded data	Catchment area ($km^{2)}$	Rainfall (mm)	Runoff (mm)	Streamflow (GL)	Runoff rate (%)
614031	Jack Rocks	1981–1998	55	1024	100	5.6	9.8
614035	River Road	1982–1998	243	806	28	6.8	3.5
614037	Big Brook	1983–2004	149	937	31	4.6	3.3
614093	Jayrup	1995–2003	46	911	17	0.8	1.8
614066	Cameron Central	1992–2003	5	875	7.5	0.04	0.86
614064	Cameron West	1991–2003	2	982	5.3	0.01	0.54
	Serpentine Dam	1975–2003	664	921	57	38	6.2

3 Climate scenarios

General Circulation Models (GCMs) are sophisticated computer programs that simulate the physical processes of the atmosphere and oceans. They solve the equations of conservation of mass, momentum and energy for many points on a three-dimensional grid covering the globe. Climate-change projections are obtained from GCM simulations that use projected future concentrations of greenhouse-gases and aerosols. 'Emissions scenarios' set the rate of change of the greenhouse gas and aerosol concentrations used in these simulations. These emission scenarios have been determined by the Intergovernmental Panel on Climate Change (IPCC) as representative of possible future paths of world population, economic growth, technological development and energy use (Bureau of Meteorology 2003). The distinction between 'projections' and 'predictions' is important. As there is no way to determine future emissions with any degree of certainty, it is impossible to 'predict' future climate.

Six scenario groups emerged from the Third Assessment Report of the IPCC, with different levels of emphasis on economic, regional, environmental and global issues (Fig. 3.1). These are the A1 (A1FI, A1T, A1B), A2, B1 and B2 scenario 'families'.

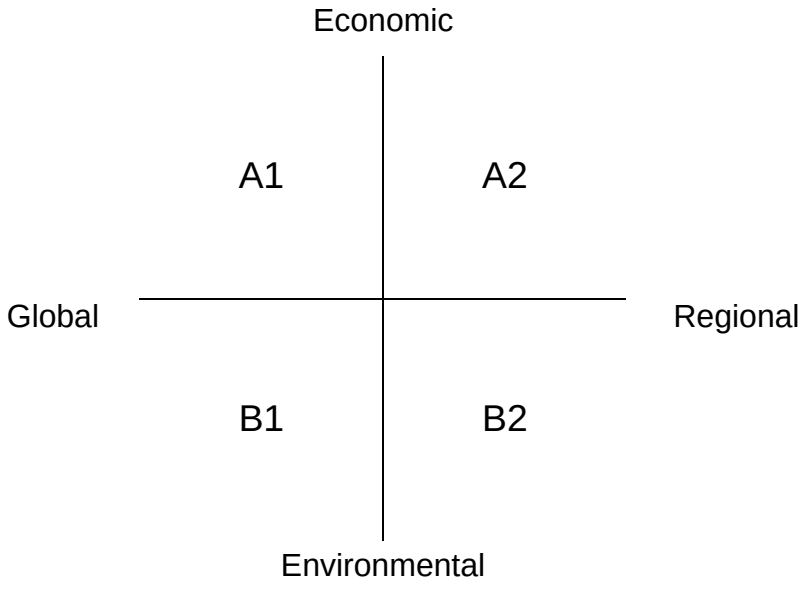

Figure 3.1 Emission scenario families

The A1 scenario family describes a world with rapid economic growth, new technologies and increased cultural and social interactions. The global population is set to peak at 8.7 billion by 2050 and to decline to 7 billion by 2100. This family splits into three groups distinguished by the direction of future energy sources: A1FI is fossil-fuel intensive, A1T uses non-fossil energy sources and A1B uses a balance (IPCC 2000).

The A2 scenario is at the higher end of emissions scenarios, with continued high rates of greenhouse-gas emissions reaching 1320 parts per million by volume (ppmv) by 2100 (CCCMA 2004). It is characterised by a regionally-oriented, self-reliant, heterogeneous world with continuously increasing populations (15 billion by 2100) and a focus on regional economic development rather than technological change and global environmental concerns.

The B1 scenario family describes a world with an emphasis on global sustainability, with a move towards an information-focused economy and resource-efficient technologies. The global population peaks in mid-century and then declines (IPCC 2000).

The B2 scenario family has an emphasis on local sustainability, and a local and regional focus on environmental protection and social equity. Economic development is considered intermediate, technological change is diverse and global population increases continuously to 10.4 billion. The CO_2 concentration for the B2 scenario by 2100 is 915 ppmv (CCCMA 2004).

This study uses climate-change projections obtained from four climate models and the A2 IPCC emissions scenario. Three fully coupled GCMs were the Hadley Centre HadAM3P (UK), the Max Planck Institute ECHAM4 (Germany) and the CSIRO Mk3 (Australia). The fourth was the Conformal Cubic Atmospheric Model (CCAM, CSIRO [Australia]) which is a stretched-grid atmospheric GCM linked to the Mk3 through far-field forcing. CCAM gives the ability to assess gains achieved by dynamical downscaling prior to statistical downscaling. Table 3.1 presents the resolutions of the GCMs.

Table 3.1 Resolution of GCMs

Organisation	Time period		GCM name	Resolution
Hadley Centre	1960–1989	2070–2099	HadAM3P AGCM	1.875° long x 1.25° lat with 19 vertical levels
			HadCM3 OGCM	1.25° x 1.25° with 20 vertical levels
Max Planck Institute	1975–2004	2035–2064	ECHAM4 AGCM	3.75° x 3.75° with 19 vertical levels
			HOPE-G OGCM	2.80° x 2.80° with 20 vertical levels
CSIRO	1975–2004	2035–2064	Mk3 AGCM	1.875° x 1.875° with 18 vertical levels
			Mk3 OGCM	1.875° lon x 0.93° lat with 31 vertical levels
CSIRO	1975–2004	2035–2064	CCAM	60 km over Australasia with 18 vertical levels

From each GCM A2 transient run, a ‘current’ and a ‘future’ period time slice is extracted. As in the initial study (Berti et al. 2004), the current period used for the Mk3, CCAM and ECHAM4 models is 1975–2004. The HadAM3P output is for the 1960–89 period, as daily output for the 1975–2004 period was not available. The future projections for the Mk3, CCAM and ECHAM4 models are for the 2035–64 period, while the HadAM3P uses 2070–99. The IPCC A2 scenario projects an approximate 1.7-fold increase in CO_2 (equivalent) by 2050, which is the midpoint of the 2035–64 time slice and a 2.4-fold increase by the end of the 21st century.

3.1 CSIRO Mk3 GCM

The CSIRO Mk3 couples an atmospheric GCM (atmospheric, land and sea-ice components) to an ocean GCM derived from the GFDL Modular Ocean Model. The Mk3 allows for the interactions of different components, taking into account the different time scales of each. Major improvements over previous model generations (e.g. the Mk2) include better physical parameterisations, thus removing the need for flux adjustments, and inclusion of a prognostic cloud scheme, allowing the model to generate physically-based cloud properties (Gordon et al. 2002).

The Mk3 atmospheric GCM (AGCM) has been developed specifically to use horizontal spectral resolution T63 (1.875^0 EW x 1.875^0 NS) with 18 vertical levels. The number of grid boxes in the horizontal for the Mk3 AGCM (nominally T63) is thus 18 432. This is a substantial increase on the number of horizontal grid boxes (3584) as used in the Mk2 model. The dynamic framework of the atmospheric model is based upon the spectral method (Bourke 1974), with the equations cast in the flux form that conserves predicted variables (Gordon 1981). An important model development concerns the treatment of atmospheric moisture within the Mk3 model. The earlier method entailed having the atmospheric water vapour carried as a grid field with only the advection of the vapour being computed by the spectral method. This has been replaced by a semi-Lagrangian transport method (Gordon et al. 2002).

The oceanic component of the CSIRO Mk 3 model is based on the code of the GFDL Modular Ocean Model (MOM), version 2.2 (Pacanowski 1996). It supersedes the oceanic code in the CSIRO Mk 2 model, which was based on the earlier GFDL Bryan-Cox code (Cox 1984). The MOM 2.2 has several major improvements in model physics and numerics compared to the earlier version. The oceanic component has horizontal resolution matching that of the atmospheric model's (T63) in the east-west direction, and twice that in the north-south direction. Thus the grid spacing is 1.875^0 longitude by 0.93^0 latitude (approximately: latitude is on a Gaussian grid). The ocean grid boxes have the same horizontal layout, but with two ocean model grid boxes per AGCM grid box meridionally. There are 31 levels in the vertical, with the spacing of the levels gradually increasing with depth, from 10 m at the surface to 400 m in the deep ocean.

3.2 CSIRO CCAM

This study also examines outputs from the CSIRO Conformal-Cubic Atmospheric Model (CCAM) which is run at high spatial resolution over Australia with far-field forcing from the Mk3 GCM A2 run. CCAM is a two-time-level, semi-Lagrangian, semi-implicit, finite-difference primitive equations model, formulated on the quasi-uniform conformal-cubic grid. It includes a variable-resolution capability for modelling the atmosphere at fine resolution over selected regions and is run at a horizontal resolution of 60 km over the Australasian region (McGregor 2005).

Using a fine resolution climate model is termed ‘dynamical downscaling’. Studies assessing the suitability of dynamically downscaled output for use in hydrologic modelling have often concluded that statistical downscaling is necessary to produce rainfall time series that reliably reproduce the observed rainfall properties (Wilby et al. 2000; Wood et al. 2004).

3.3 Hadley Centre HadAM3P GCM

HadAM3P is an atmospheric general circulation model, developed primarily to assess European climate change. It focuses on surface air temperature, precipitation and snow mass, and has a higher resolution than the previous HadAM3. Output is in the form of high-resolution global time-slice experiments for both a control (1960–89) and a future scenario (2070–99) (Rowell 2005).

3.4 Max Planck Institute ECHAM4

The ECHAM4 is the atmospheric component of the atmospheric/ocean-coupled model, ECHO-G. The ECHO-G was driven by historical climate data and focused on reconstructing observed Northern Hemisphere temperatures. Von Storch et al. (2004) emphasise that the most important aspect of the model is that it simulates a constant and reasonable climate and that the applied forcing is within reasonable values. The ocean component of the ECHO-G is referred to as the HOPE-G.

4 Methodology

The objective of this study was to assess possible future changes in catchment yield to the Serpentine Dam catchment resulting from projected future climate changes from four climate models. Firstly, the LUCICAT model was used to represent the current rainfall – runoff processes occurring within the catchment. This was achieved by calibrating LUCICAT against observed datasets. Current and future rainfall datasets were then produced by statistically downscaling the atmospheric predictors extracted from the four GCMs. These statistically downscaled rainfall simulations were then used to run the LUCICAT model in order to simulate the runoff response that would occur within the Serpentine catchment. Following from this, the change in catchment yield of the catchment was estimated. A conceptual figure of this methodology relating to the current-climate analysis is presented below (Fig. 4.1). The future climate analysis is similar, with the exception that modelled GCM streamflow for future conditions is compared with the modelled GCM streamflow from the current climate.

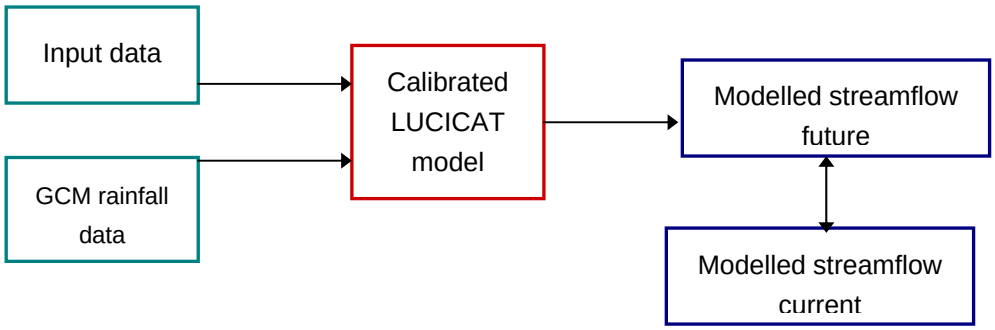

Figure 4.1 Conceptual figure of methodology

4.1 Downscaled rainfall

Downscaled rainfall data was produced for a selected network of 31 meteorological stations across south-west Western Australia (Berti et al. 2004). Station selection reflected data availability and coverage of important surface-water catchments, groundwater recharge areas and relevance to agricultural production.

A statistical downscaling process was applied to each GCM in order to generate precipitation time series. The non-homogeneous hidden Markov model (NHMM) of Hughes et al. (1999) was used to downscale atmospheric predictors to multi-site daily precipitation occurrence; then conditional multiple linear regression was used to simulate multi-site daily precipitation amounts (Charles et al. 1999). The NHMM predicts multi-site patterns of daily precipitation occurrence as a finite number of ‘hidden’ (i.e. unobserved) weather states. The temporal evolution of these daily states is modelled as a first-order Markov process with state-to-state

transition probabilities conditioned on a small number of synoptic-scale atmospheric predictors such as sea-level pressure.

By determining distinct multi-site daily precipitation occurrence patterns, rather than atmospheric circulation patterns, the NHMM captures much of the spatial and temporal variability of daily multi-site precipitation occurrence records. For each weather state of a selected NHMM, precipitation amounts at each site are modelled by regressions of transformed amounts on precipitation occurrence at key neighbouring sites. This approach captures both the first- and second-order moments (i.e. mean and variability) of the daily precipitation data (Charles et al. 1999).

The model for generation of multi-site daily temperatures (maximum and minimum) is fitted subsequent to the NHMM selection, with parameters conditional on the weather states. It uses a weather-generator approach (Wilks & Wilby 1999), with multi-site daily residuals of temperature simulated as a multivariate normal process, maintaining inter-site cross-correlations and at-site lag-1 auto-correlations.

The NHMM was fitted to observed data for 1978 to 2002 as described in Berti et al. (2004). The atmospheric predictors used in fitting are 'centred', i.e. their means are subtracted (Hughes et al. 1999). Similarly, the atmospheric predictors extracted from the climate models have their current period means subtracted from both the current and future periods. This is a form of bias correction, allowing direct comparison between the climate model current period and the observed data of the fitting period (Timbal & McAvaney 2001). In the case of HadAM3P, centring the 1960–89 predictors also produces predictor series with zero means. Thus the downscaled rainfall from the HadAM3P current period can be compared directly to the downscaled rainfall series from the other GCMs for the current period.

4.2 Application of the LUCICAT model

The LUCICAT model was used as a tool to estimate the effects of different climate projections on the catchment yield of Serpentine Reservoir (Bari & Smetten 2004; Beverly et al. 2005; Bari & Smettem 2006a & b; Charles et al. 2007) In order to do this, the model was prepared and calibrated first as described in Appendix A. The model was then used to simulate streamflows using rainfall data representing various climate projections, and the results were compared to a simulation using rainfall for the period 1964–2004. Further information regarding the input files can be read in Appendix A, Application of LUCICAT model to the Serpentine Reservoir catchment (Fig. 4.1).

4.3 LUCICAT calibration

The subcatchments modelled ranged in area from 1.91 km^2 to 16.42 km^2. The model was calibrated manually over the period 1981–2004, as data from gauging stations were recorded only during this period. The base parameter set was taken from the LUCICAT modelling of the Helena catchment. In the final calibration parameter set, two of the parameters varied across the catchment: the infiltration threshold, which varied from 0.0001 in the high-rainfall

area near Jack Rocks to 0.0079 and 0.0091 in the smaller experimental catchments of Cameron Central and Cameron West respectively. Topsoil thickness varied from 1.9 m in the east part of the catchment to 2.9 m at the dam outlet. The topsoil thickness at the Cameron West and Central subcatchments increased to 3.8 m and 3.5 m respectively. Other parameters are shown in Table A.1.

Groundwater level

Simulated groundwater levels in all subcatchments peak between 1968 and 1975 and then, in most, steadily decrease. Groundwater reaches the surface only in some subcatchments. In subcatchments 48 and 49 groundwater reaches the surface in 1974 and remains near the surface for the rest of the simulated period. The groundwater in subcatchments 81, 83 and 85 also discharges to the surface and into streams for long periods of time. This is a realistic result, as the mean annual rainfall in these subcatchments is higher than 1000 mm.

Annual runoff

There was a good correlation between the observed and modelled annual hydrographs at all gauging stations. As shown in Figure 4.2, the annual runoffs at (a) Jayrup and (b) River Road are predicted well, in the range of 0–60 mm/year and 5–80 mm/year respectively. Less accurate are runoffs for the smaller subcatchments (c) Cameron West and (not shown) Cameron Central. The calibration plots of the remaining gauging stations, as well as an in-depth analysis of annual streamflow trends for all gauging stations, are described in Appendix A.

The LUCICAT model simulated the high-flow years (1991 and 1996) well, and was more successful in larger catchments. The 1996 modelled annual flows at the Big Brook and River Road gauging stations were within 3% and 4% respectively of observed flows. The 1991 modelled flows at Big Brook, Jack Rocks and River Road were within 6%, 4% and –6% respectively of observed flows. The annual modelled flows of the smaller catchments, Cameron West and Cameron Central, followed the trend of the observed data.

The year 1997 was a low-flow year. The 1997 modelled runoff at River Road is 4 mm higher than the observed flow, with a high 48% difference. Similarly, the modelled value for Big Brook is 6 mm, or 63% higher than the observed value.

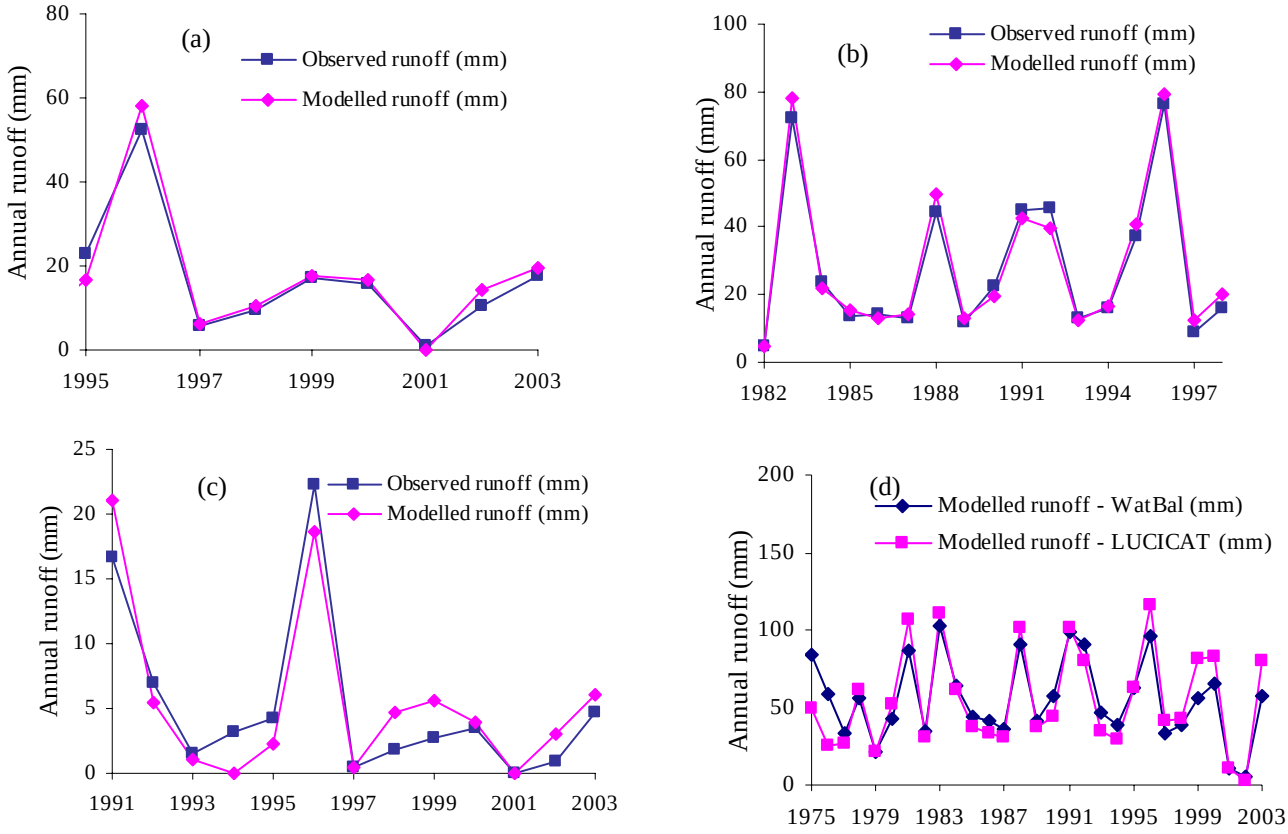

Figure 4.2 Observed and modelled annual runoff at (a) Jayrup, (b) River Road, (c) Cameron West, (d) Serpentine Dam

The accuracy of the dam-outlet calibration is difficult to determine, as the 'observed' data for this site are calculated using a water-balance approach, which takes into account the release of water from the dam. The LUCICAT simulations are similar to the water-balance calculations, supporting the accuracy of the LUCICAT results.

As discussed for the examples above, LUCICAT models runoff well at all magnitudes. The magnitude of annual runoff at gauging stations varies, with Jack Rocks recording the highest and Cameron West and Central the lowest. Despite the differences in magnitude, the accuracy of each calibration is good, ranging over 2–7%, with the model results on average 5% greater than the observed records (Table A.3). The percentage changes correspond to the average annual runoff for the period of record of the individual sites. The accuracy of the LUCICAT predictions is best displayed in Figure A.8, where the relationships between the observed and modelled annual runoffs are shown. Jayrup and River Road gauging stations have R^2 values of 0.97 and 0.98 respectively. The correlations between observed and

modelled flow at the Cameron West and Cameron Central gauging stations are lower, at 0.88 and 0.84 respectively.

An overview of the relationship between observed and modelled flow can be seen in Figure 4.3 which plots mean annual observed runoff against mean annual modelled runoff for all gauging stations. As can be seen, LUCICAT is able to simulate the observed runoff at all magnitudes, and the bias in the trendline indicates that the modelled values are higher than the observed at the high magnitudes. This is also supported by the statistics in Table 4.1, with the 90th percentiles and means generally slightly higher than the observed datasets.

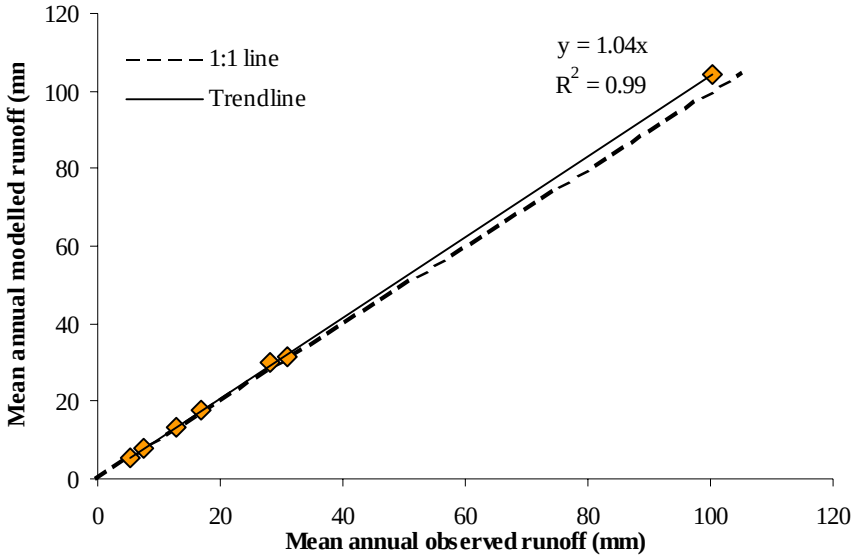

Figure 4.3 Scatter graph of mean annual observed and modelled runoff for all gauging stations

Table 4.1 Observed and modelled annual runoff statistics (mm)

Gauging station	Data period	10th percentile		Median		Mean		90th percentile		CV	
		Obs.	Mod.	Obs.	Mod.	Obs.	Mod.	Obs.	Mod.	Obs.	Mod.
Big Brook	1983–2004	10.0	13.8	23.5	24.8	30.8	31.5	63.2	67.1	0.7	0.7
Jayrup	1995–2003	4.8	4.9	15.5	16.8	16.9	17.8	28.6	27.4	0.9	0.9
River Road	1982–1998	10.6	12.6	15.9	19.5	28.0	29.0	56.0	60.9	0.8	0.8
Jack Rocks	1981–1998	55.5	55.5	85.3	86.8	100.3	104.5	162.1	176.2	0.4	0.5
Cameron Central	1992–2003	1.9	1.6	5.6	6.4	7.5	8.0	12.3	8.7	0.9	1.2
Cameron West	1991–2003	0.5	0.1	3.2	4.0	5.3	5.6	14.8	16.2	1.3	1.2
Dam inflow (WBAL)	1975–2003	30.5	24.8	55.5	44.1	55.0	54.9	92.1	102.2	0.5	0.6

Monthly runoff

Streamflow was also calibrated at the monthly scale, with good results. The Jack Rocks hydrograph is shown in Figure 4.4. LUCICAT tended to model higher than observed values for high-flow events (greater than 40 mm/month) and was very accurate with the intermediate flows (15–40 mm/month). Accuracy was lower in the smaller subcatchments, particularly the Cameron Central gauging station. At smaller scales, small modelling differences (1 mm) can lead to large percentage differences. This is also reflected in the correlation coefficients. The R^2 correlation between the observed and modelled monthly flows at River Road and Jack Rocks were 0.97 and 0.96 respectively. The correlation was also high at Big Brook (0.95) and Jayrup (0.94). The correlation was not as high at the Cameron sites, with coefficients of determination 0.80 and 0.85 at Cameron Central and West respectively. Further information regarding statistics and trends of monthly streamflow calibration can be found in Appendix A.

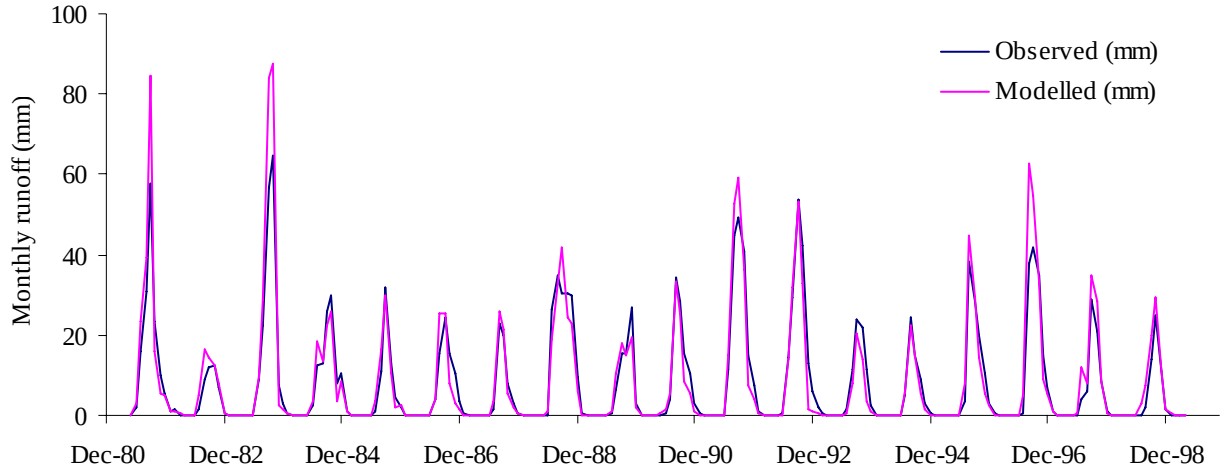

Figure 4.4 Observed and modelled monthly runoffs at Jack Rocks gauging station

The modelled inflow into the dam was not calibrated against an observed dataset, but compared with output from a water-balance model (WatBal). Figure 4.5 illustrates that, during peak runoff events, LUCICAT simulates higher flows than the water-balance data. For the low runoff events, the LUCICAT flows are below those of the water-balance dataset.

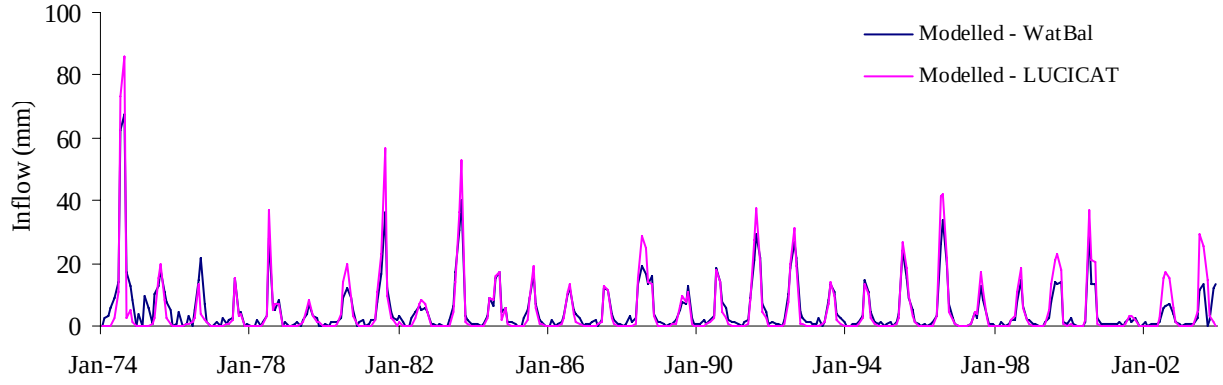

Figure 4.5 Monthly LUCICAT and water-balance-modelled dam inflow

Daily streamflow

At all gauging stations, the general pattern of the hydrographs was simulated well by LUCICAT. The daily hydrographs at the Jack Rocks, Cameron Central, Big Brook and River Road gauging stations are displayed in Figure 4.6, with the remaining daily hydrographs and analyses in Figure A.10. In some hydrographs LUCICAT models higher flows than observed

and earlier ‘cease-to-flow’. The gauging stations at the smaller subcatchments, Cameron West and Cameron Central, recorded lower streamflows. For these gauging stations, LUCICAT tended to predict higher runoff than observed.

The modelled and observed daily hydrographs of the Jack Rocks gauging station correspond well. Daily runoff is high at this site, recording a maximum of 7.4 mm in 1987 (Fig. 4.6a). For all years, LUCICAT correctly models the duration of flow, picking up all runoff events. There is a tendency for LUCICAT to model higher than observed values during high runoff events, such as those in 1981 and 1996. For example, in 1981 LUCICAT models 9.4 mm of runoff for a 4.9 mm event. There is also a tendency for the baseflow component of the hydrograph to be greater than observed in the early part of the year and less than observed in the latter part.

The Cameron West and Central subcatchments, being first order, experience very low flows and have small mean annual runoff rates of 0.54% and 0.85% respectively. Due to the small scale of streamflow, small variations from observed data (<1 mm) appear to have a high magnitude of error. The Cameron Central calibration is quite well matched. The duration and magnitude of runoff in 1997 and 2000 is predicted very well. There are some years (1992, 1993, 1995) when the modelled flow begins later than observed. In other years (1994, 1999) the first runoff event is missed, and as a result records of modelled runoff begin later than observed (Fig. 4.6b). At this site, LUCICAT models runoff better in the over-0.4 mm range.

The modelled and observed daily flows correspond well at both the Big Brook and River Road gauging stations (Figs. 4.6c & d) and comparisons between modelled and observed data at these gauging stations are similar. At both sites, LUCICAT models the duration of flow well, and also tends to model higher than observed runoff during peak events. During the dry conditions of 2001, modelled runoff is higher than observed at the Big Brook gauging station but is correctly modelled in the dry conditions in 1987. The modelled data at both sites can at times show drier conditions towards the end of the hydrograph. At Big Brook this is particularly the case for 1990, 1992 and 1993, while at River Road, this occurs in 1986 and 1992.

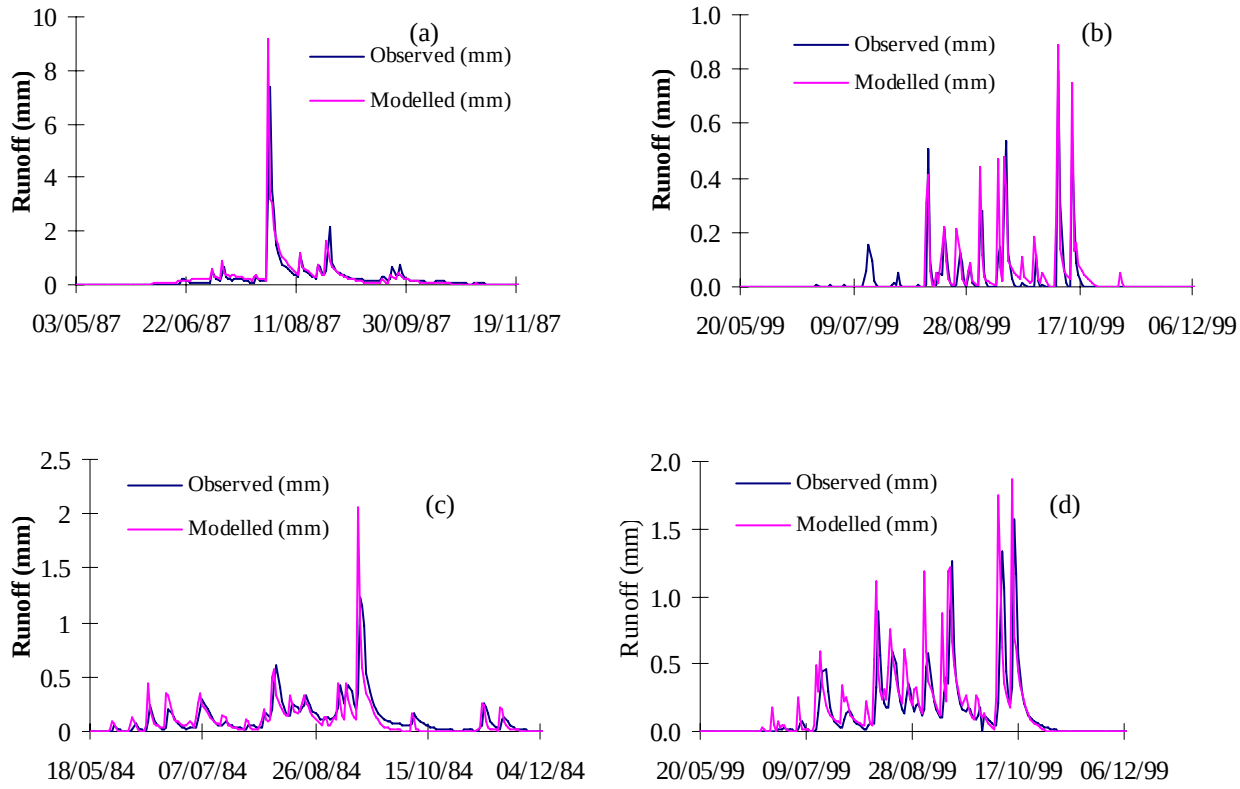

Figure 4.6 Observed and modelled daily streamflow at (a) Jack Rocks, (b) Cameron Central, (c) Big Brook and (d) River Road

Flow duration

Flow duration curves have been produced for all the gauging stations, with those for Jack Rocks and Cameron West shown in Figure 4.7. The plots show a good match for the median to high flows and a deviation from the observed flow in the low-flow periods. Further plots and description of flow duration for other gauging stations can be seen in Figure A.11.

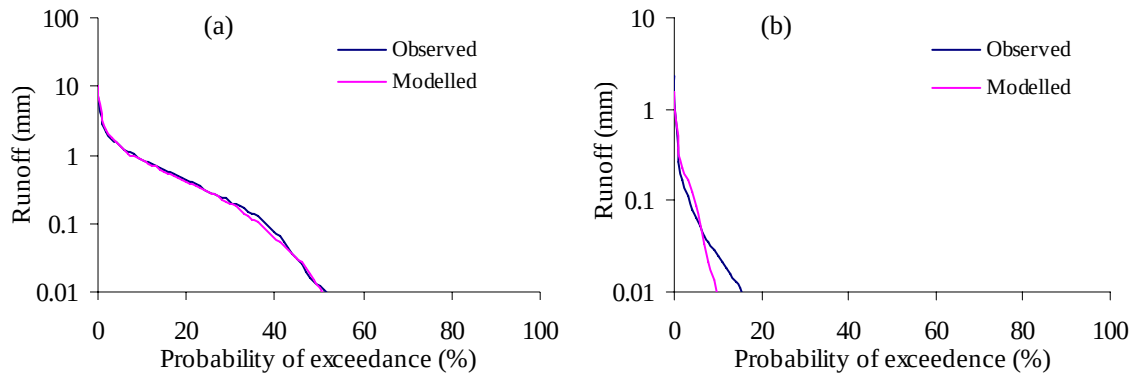

Figure 4.7 Flow duration curves for (a) Jack Rocks and (b) Cameron West

Reservoir inflow

The monthly inflow into the Serpentine Dam was calculated using two different methods. LUCICAT was used to compute the monthly inflow into the reservoir. The other method was using a reverse water-balance calculation, which takes into account rainfall, pan evaporation, storage-level change, reservoir releases and scour. A comparison of the cumulative monthly inflows, illustrated in Figure 4.8, shows that generally the two curves fit well, with mean annual values for the LUCICAT and water-balance data during the 1975–2003 period at 54.9 and 55.0 mm respectively. Due to different methods of calculation, at times the LUCICAT values and water-balance-calculated data differ.

The runoff statistics show some variations between the two datasets (Table 4.1). The 90th percentile is higher for LUCICAT (102 mm) than for water balance (92 mm), indicating that in high-flow events LUCICAT may predict higher than observed flow. A higher LUCICAT maximum value of 116 mm opposed to 103 mm also supports this. The 10th percentile is higher for the water-balance data (31 mm) than for LUCICAT (25 mm). This indicates that during low-flow events LUCICAT may have a tendency to predict a lower runoff than estimated by the water balance method. LUCICAT models a smaller minimum inflow (3 mm) than water balance (5 mm), also supporting this idea. These two characteristics were also noted in the monthly inflows (Fig. 4.5).

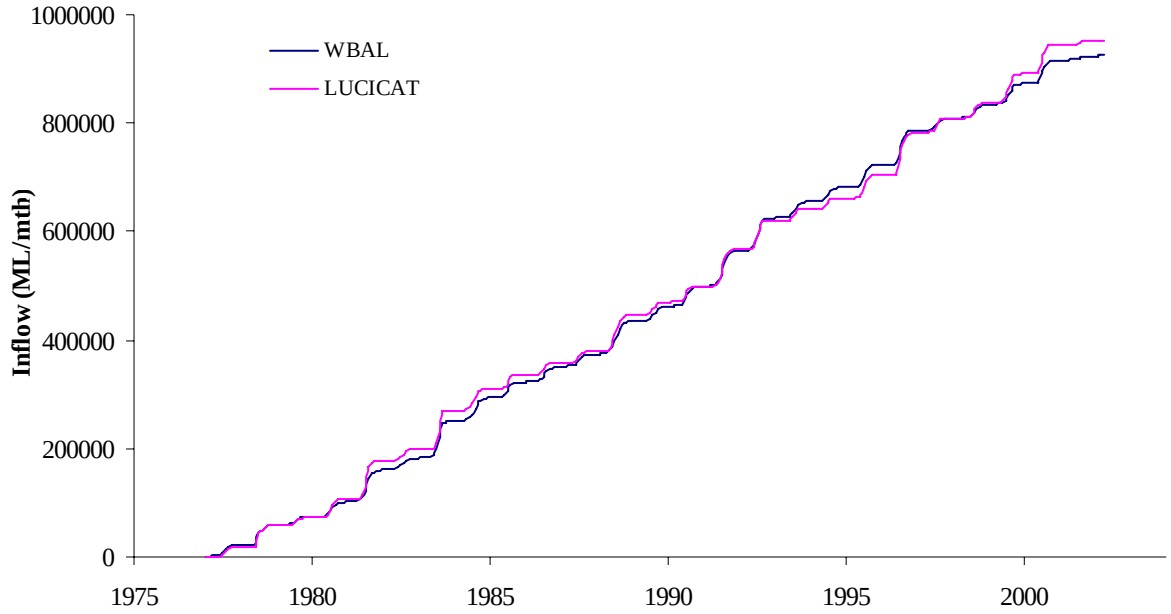

Figure 4.8 Cumulative LUCICAT and water-balance monthly dam inflows

Table 4.2 Runoff statistics of the LUCICAT and water-balance datasets

Runoff statistic	LUCICAT (1975–2003) (mm)	Water balance (1975–2003) (mm)
Mean	54.9	55.0
Median	44.1	55.5
10th Percentile	24.8	30.5
90th Percentile	102.2	92.1
Coefficient of variation	0.6	0.5
Standard deviation	31.5	26.2

Catchment water balance

A catchment water-balance assessment was undertaken for the Serpentine Dam catchment (Table 4.3). The water balance shows the partitioning of the model inputs and outputs in terms of rainfall, flow components, transpiration and evaporation from soil. Annual data were averaged over the time period 1975–2003. Interflow comprises the majority of the

streamflow, at 76%, with baseflow contributing least (3%). Average annual transpiration is quite high, at 721 mm. During the simulation period, there was a storage change of 2 mm.

Table 4.3 Water-balance components based on modelling results

Water balance component	Division	Average (1975–2003) (mm)
Rainfall	Total	921
Soil evaporation		17
Transpiration		721
Interception		121
Streamflow*	Total	61.0
	Surface runoff	*13.4*
	Interflow	*48.2*
	Baseflow	*2.0*
Storage change		–2

*Total streamflow is less than the sum of the individual streamflow components due to transmission and evaporation losses.

4.3.1 Runoff characteristics

Modelled mean annual runoff followed a similar spatial distribution to mean annual rainfall, increasing from upstream to downstream (Fig. 4.9). A summary of the runoff at the gauging stations is shown in Table 2.1. The two areas of the catchment with the lowest runoff (less than 20 mm/year) are the upstream section of the River Road catchment (subcatchments 1–15) and the upper section of the Jayrup catchment (subcatchments 58–65). This may be due to any combination of the low rainfall in these areas, the small catchment areas (2–10 km^2), soil properties (infiltration capacity, porosity and hydraulic conductivity) and evaporation rates.

Generally, the eastern side of the catchment has lower runoff than the western side. However, runoff in subcatchments 14, 18 and 19 slightly higher than at nearby subcatchments can be attributed to the convergence of streams and tributaries. Another area (subcatchments 23, 24, 25) also has higher runoff than nearby subcatchments. This area, on the edge of the catchment, has an area of high elevation. The higher runoff can therefore be attributed to steep gradients. Such subcatchments characteristically have high runoff, as flows from different points in the catchment reach the outlet at the same time. Runoff increases towards the reservoir. The Jack Rocks catchment has high runoff rates (in the range of 100–130 mm/year) which can be attributed to high rainfall in this area as well as large areas of impervious ground (the Department of Water's internal database classifies soils in the north-eastern corner of the subcatchment as 'steep granitic ranges and hills with bare rock'). The runoff at the dam is highest, at approximately 210 mm/year.

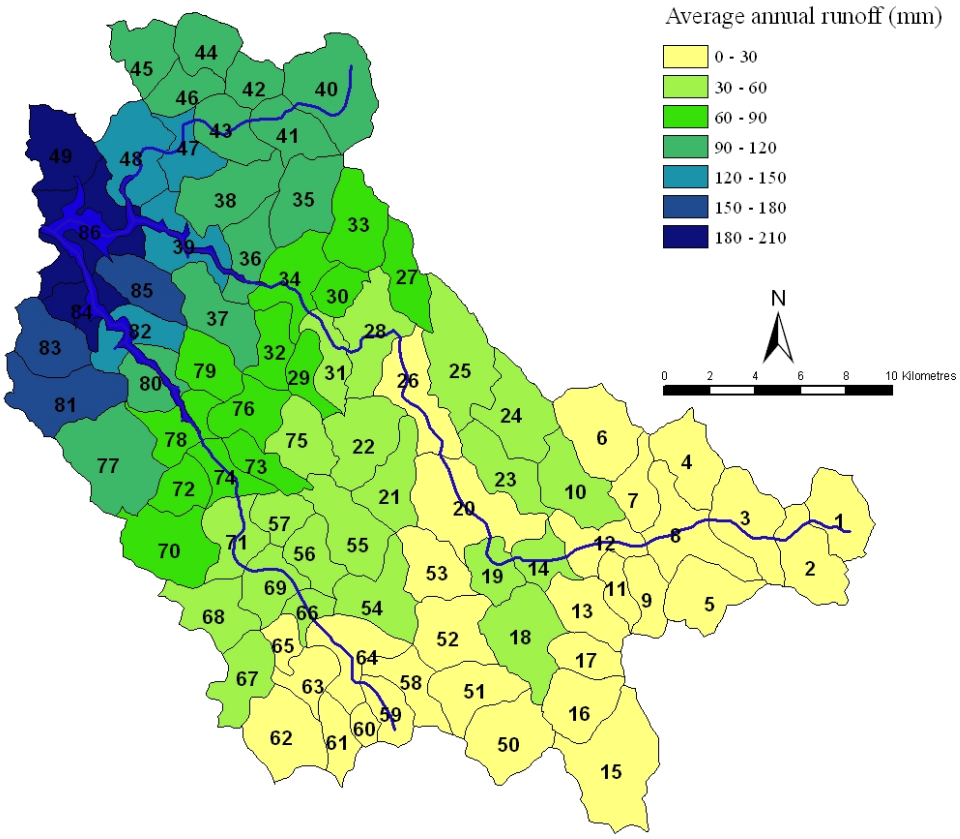

Figure 4.9 Modelled mean annual runoff 1975–2003

5 Results of GCM downscaling

5.1 Rainfall

When running LUCICAT using the downscaled rainfall, only four stations of the 31 downscaled rainfall sites across the south-west of Western Australia were close enough to the Serpentine Dam catchment to be used for calculating the spatial distribution of daily rainfall: Serpentine (009039), Jarrahdale (009023), Wandering (010648) and Dwellingup Forestry (009538) (Fig. 2.3). None of the stations is within the catchment.

Using the CCAM data from only these four sites, a spatial distribution of rainfall was calculated using the Dean and Snyder method (1977). The distribution was derived from data observed at 31 rainfall stations (Fig. A.3). As a result, the distribution calculated using the CCAM data for the current climate did not reflect that created using observed data. Due to this, further analysis was done to form a relationship between each subcatchment and each of the four rainfall stations. This relationship was then used to create the spatial distribution of rainfall for all GCM downscaled rainfall datasets. More information regarding this methodology can be found in Appendix B.

There are 100 simulations of 30 years of downscaled rainfall data corresponding to each GCM for both a current and a future scenario. Forty simulations were used in this study for data analysis. The statistical significance of this sample size is discussed in Appendix C. The following analysis focuses on the catchment aggregate rainfall evaluated at subcatchment 86, which represents the whole Serpentine Dam catchment. Each of the downscaled rainfall datasets for the current climate was compared with its observed current-climate dataset (1975–2004) as well as its corresponding future scenario. Monthly rainfall plots and cumulative monthly rainfall plots were developed for the observed data as well as the current and future downscaled rainfall datasets.

Observed monthly rainfall refers to the monthly rainfall data computed using LUCICAT, averaged over the 1975–2004 period. For example, observed January rainfall is the mean rainfall for all Januaries over that 30-year period. Monthly means of rainfall were also developed for each GCM for both the current climate and the future climate. Firstly, mean monthly rainfall for the 30-year period was calculated for each simulation. This produced 40 datasets of monthly rainfall. An average of these 40 datasets was then taken in order to illustrate the range of the simulations. The ‘annual rainfall’ is the sum of these monthly rainfalls.

5.1.1 Cumulative rainfall — current

When analysing climate data, a large time period is required in order to take into account the natural climate variability. As a result, the following analysis has focused on the cumulative rainfall at the end of the 30-year simulation period. The downscaled rainfall from all GCMs for

the current climate was compared to the observed data for 1975–2004 (Fig. 5.1), with the last 7 years of simulations shown enlarged. Generally, simulations for the first 10 years of the downscaled rainfall deviate most from the observed data, with the latter 20 years corresponding well. A plot of the percentage differences between the observed data and each of the current-climate datasets at the end of the 30-year period is shown in Figure 5.2. The figure also shows the percentage differences between the current climate and the corresponding future climate. The error bars show the range of percentage differences from the 40 simulations. The downscaled mean of those three and observed rainfall are shown in Table 5.1.

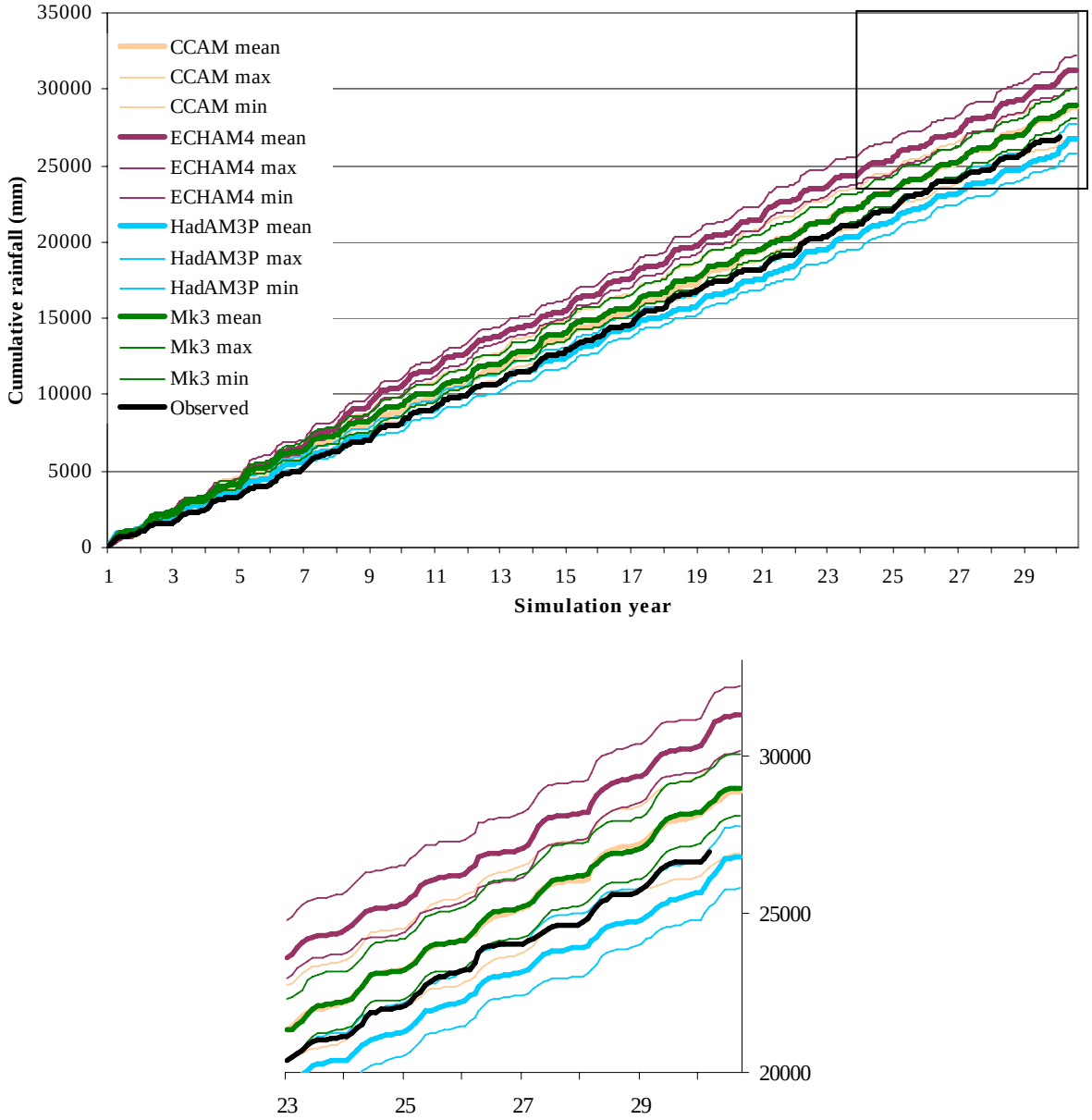

Figure 5.1 Cumulative rainfall — current period

ECHAM4

The ECHAM4 downscaled rainfall shows the greatest deviation from the observed data. At the end of the 30-year period, the average of the ECHAM4 cumulative rainfall is 14% higher than the observed. This is mainly due to high rainfall during the first 10 years, with the trend in the following 20 years being similar to the observed data. This is reflected in the fact that, from 1985 to 2003, the mean annual ECHAM4 rainfall is 984 mm, compared to the observed 928 mm, which corresponds to a 6% difference. Due to the difference in the two datasets, downscaled rainfall from this GCM was not used to generate streamflow in LUCICAT. For more information see Section 6.1.1.

CSIRO Mk3

The maximum, mean and minimum of the Mk3 simulations are plotted in Figure 5.1. At the end of the 30-year simulation period, the mean of the Mk3 simulations is 6% higher than the observed. The minimum of the simulations is similar in magnitude to the observed data. As the case of the ECHAM4 data, the first 10 years of the Mk3 data deviate most from the observed dataset, while in the following 20 years the datasets are similar, with the average of the Mk3 rainfall only 2.5% higher than the observed data.

CCAM

The CCAM rainfall trend corresponds well with the observed data trend. At the end of the 30-year period, the mean of the CCAM plot is 5% higher than the observed data. The plot of the observed data sits above the CCAM minimum plot and below the CCAM mean plot, indicating that the observed data lie within the lower range of the CCAM simulations (Fig. 5.1).

HadAM3P

The HadAM3P simulations show a drier trend than the observed current climate. At the end of the 30-year period, the final average value of all simulations was approximately 3% lower than that of the observed data. The observed data are within the upper range of the HadAM3P simulations (Fig. 5.1).

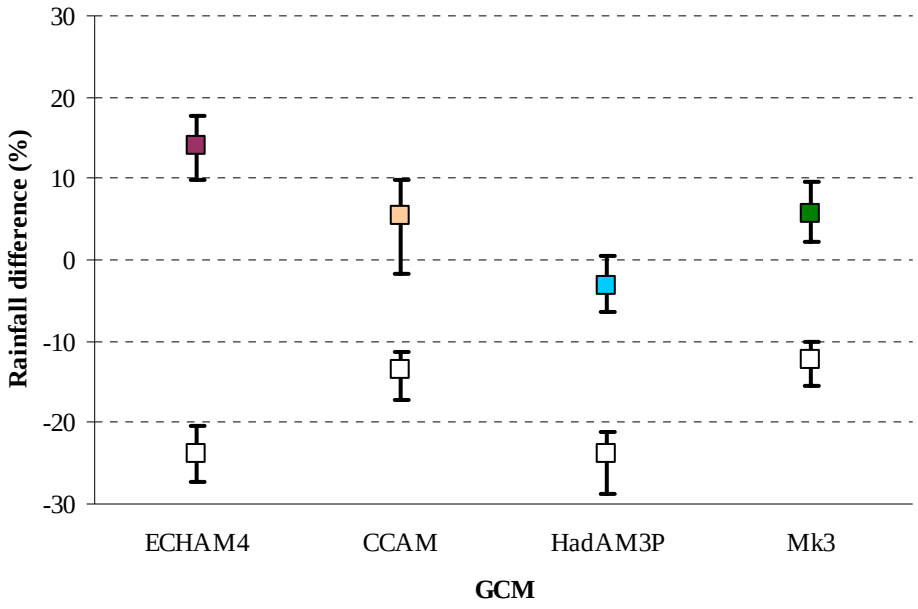

Figure 5.2 Differences between (1) the observed and the current downscaled rainfall from GCMs (coloured) and (2) current and future downscaled simulations (30-year simulation period)

5.1.2 Cumulative rainfall – future

The future climate scenarios were not all projected for the same time period (Table 3.1). The Mk3, CCAM and ECHAM4 rainfall data were projected for the period 2035–64, with HadAM3P for 2070–99. The projections developed from the Mk3 and the CCAM runs were very similar, with the ECHAM4 projection lower. Figure 5.3 shows cumulative plots of the mean, minimum and maximum of the simulations for the Mk3, CCAM and ECHAM4 models.

The similarity between the Mk3 and the CCAM results is expected, as the CCAM is conditioned on the Mk3 far-field forcing. At the end of the 30-year future period, the mean cumulative rainfall for the Mk3 and CCAM was 25 400 mm and 24 900 mm respectively. This equates to a 0.4% difference. Both models have a similar range of simulations. In both cases the maximum is approximately 3% higher than the corresponding average, while the minima are 7% (CCAM) and 3% (Mk3) lower. The ECHAM4 result is lower in magnitude than the other two datasets. The mean rainfall plot at the end of the 30-year period is 4% lower than the CCAM mean.

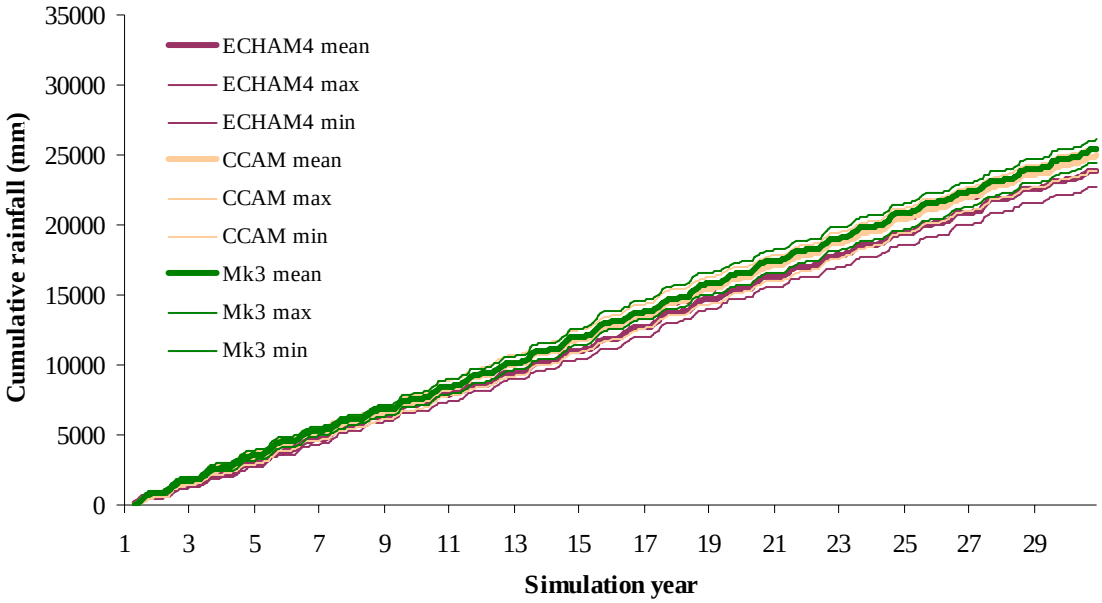

Figure 5.3 Cumulative rainfall — future climate, Mk3, CCAM and ECHAM4 (2035–64)

The cumulative rainfall total derived by the HadAM3P model (Fig. 5.4) in the later climate (2070–99) was lower than that predicted by the other GCMs for the 2035–64 period. This is an expected result, as the CO_2 signature for this simulation period is higher, and would have implications in terms of rainfall and temperature changes. The mean of the 40 HadAM3P simulations was 18% lower than the CCAM mean. The range of the simulations is similar to that of the other GCM results.

In all cases, the future climates had smaller cumulative rainfall totals than their corresponding current scenarios. The ECHAM4 dataset had the greatest difference, with a 24% reduction in rainfall. The CCAM and Mk3 results were similarly reduced: 14% and 12% respectively. A visual inspection of these differences can be seen in Figure 5.2 (white boxes), which show the 40 simulation average at the end of the 30-year period as well as the range of averages for each GCM.

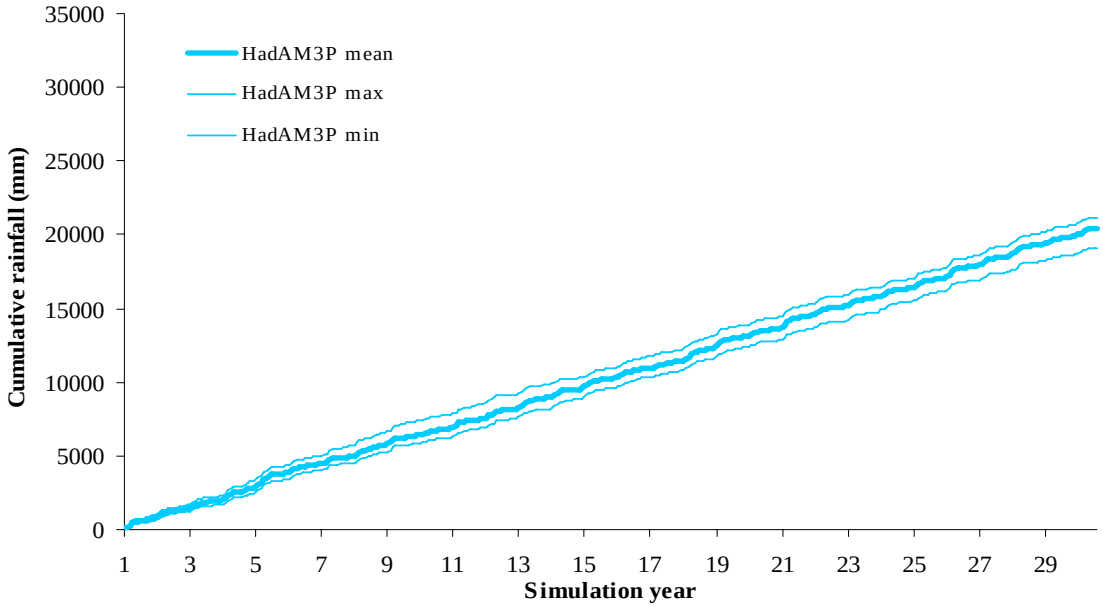

Figure 5.4 Cumulative rainfall — future climate, HadAM3P simulations (2070–99)

5.1.3 Annual and monthly rainfall

Monthly rainfall was calculated for the current and future scenarios from downscaled data from each of the four GCMs (Figs 5.5, 5.6, 5.7 & 5.8). A description of the seasonal patterns for each dataset is given below. An analysis of monthly differences is given in Appendix B (Table B.1 & Fig. B.5). The annual rainfall differences for the current climate are summarised in Table 5.1. The current and future scenario results are compared, with the Mk3, CCAM and ECHAM4 future downscaled rainfall datasets corresponding to the years 2035–64 and the HadAM3P dataset corresponding to 2070–99 (Table 5.2).

Mk3

The mean annual downscaled rainfall for the current period was 5.1% higher than the observed data. There is a shift in the timing of the peak rainfall from June–July (observed) to July–August (Mk3) (Fig. 5.5). Due to the shift, rainfall totals are 25% less than observed for the April–June period and 29% higher than observed for the July–October period. This seasonal shift is due to temporal biases in the Mk3 mean sea level pressure (MSLP)-derived atmospheric predictors (Fig. 5.9a). The future dataset follows the same seasonal pattern as the current dataset, with peak rainfall in July–August. The mean annual rainfall decreases by 12% (Table 5.2), with the majority of the reduction occurring from May to August. Rainfall in the future scenario during the drier months is also reduced, apart from February, when there is a slight increase. Due to the seasonal bias of this GCM, during the latter half of the year (August–October) future rainfall is higher than the observed rainfall.

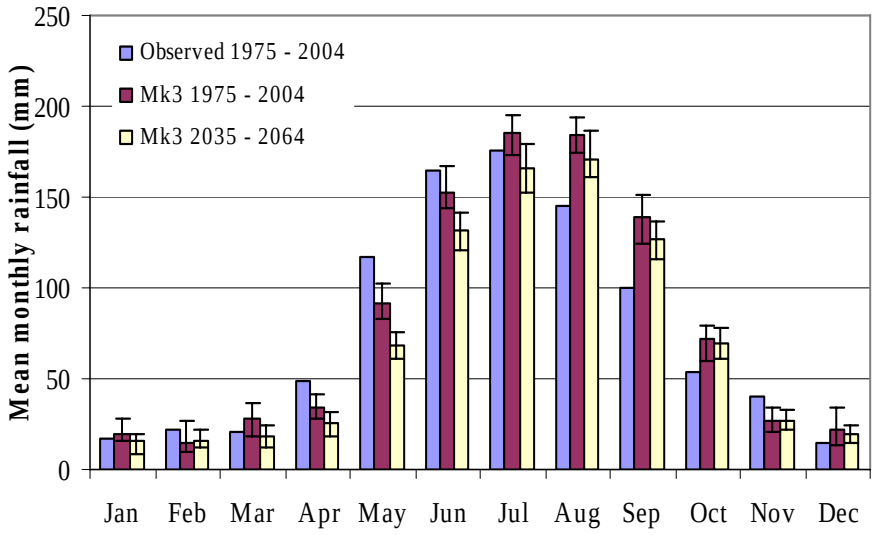

Figure 5.5 Mk3 mean monthly rainfall

Table 5.1 Difference between observed and current-simulated rainfall

	Annual average (mm)	Difference compared to observed (%)
Observed (1975–2004)	921	
Mk3 (1975–2004)	969	5
CCAM (1975–2004)	966	5
ECHAM4 (1975–2004)	1047	14
HadAM3P (1960–1989)	897	–2.4

Table 5.2 Percentage change in rainfall from current to future scenarios

	Mean annual rainfall (mm)	Difference compared to current (%)
2035–2064 projection		
ECHAM4	799	–23.8
CCAM	835	–13.6
Mk3	854	–11.9
2070–2099 projection		
HadAM3P	685	–23.6

CCAM

The mean annual downscaled rainfall for the current climate is 1.5% higher than the observed data. The mean monthly rainfall matches observed data fairly well, although there is a slight bias (Figure 5.6). The bias is similar in its timing to that of the Mk3, although the difference is smaller. Thus, it appears that the CCAM corrects for some of the temporal bias seen in Mk3 MSLP. Mean annual rainfall for the future scenario is 14% less than for the current scenario, the majority of this reduction occurring from May to June. As with the Mk3, due to the seasonal bias some months in the future scenario (September and October) have higher rainfall than observed rainfall. During some summer months, the average rainfall in the future scenario is higher than in either the current or observed scenario for the month.

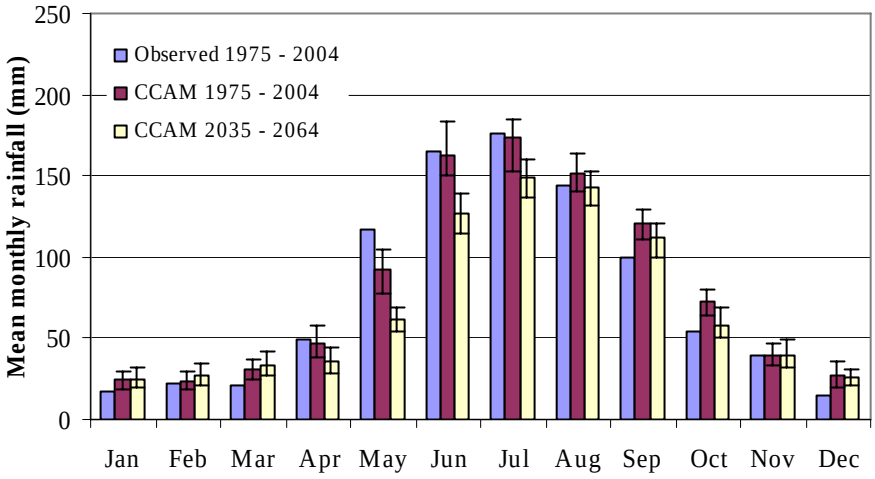

Figure 5.6 CCAM mean monthly rainfall

ECHAM4

The ECHAM4 mean annual downscaled rainfall is 10% higher than the mean annual observed rainfall. Simulated rainfall during the high rainfall months of June–August is 37% higher than the observed data. LUCICAT-simulated rainfall for the remaining months is within 14% of the observed data. The seasonality of the downscaled rainfall data is similar to that of the observed. Similarly to the Mk3, the inability of the ECHAM4 model to reproduce the observed MSLP seasonal cycle over the region (Fig. 5.9c) contributes to the periods of high rainfall. Mean annual rainfall modelled for the future scenario is 24% less than for the current climate. Mean monthly rainfall for the future scenario is less than that for the current scenario for all months, with the largest reductions in the May–August period.

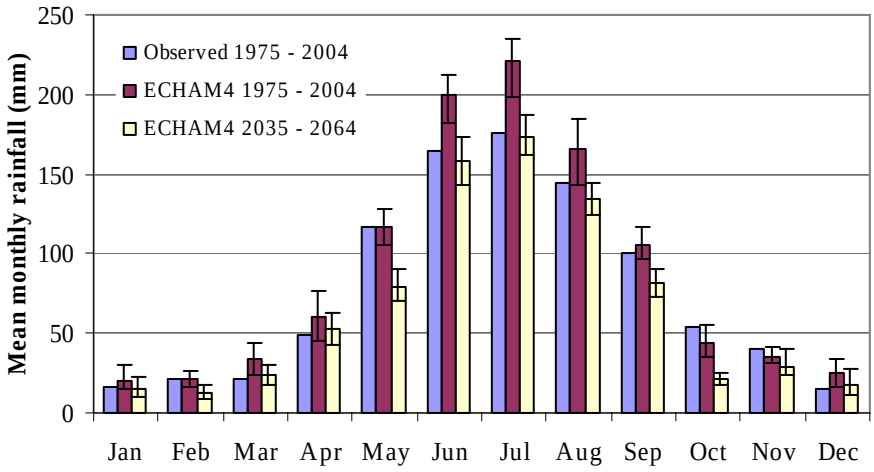

Figure 5.7 ECHAM4 mean monthly rainfall

HadAM3P

The mean annual rainfall downscaled from the HadAM3P model was 6% lower than the observed rainfall. The timing of peak rainfall shifts from mid June (observed) to early July (HadAM3P). Simulated rainfalls for April to June are on average 53% lower than the observed. Again, this seasonal bias can be partly explained by the errors associated with the GCM reproduction of the seasonal cycle of atmospheric predictors (Fig. 5.9). The mean annual rainfall for the future scenario is 24% less than for the current climate. The majority of this reduction occurs during the May–September period. In some of the drier months, rainfall in the future scenario is reduced (February, April and October) and in others increased (January, March, November and December).

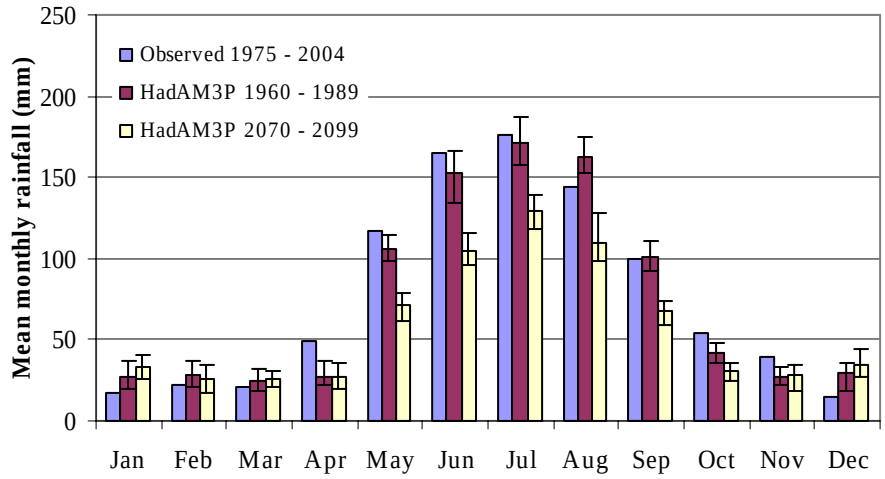

Figure 5.8 HadAM3P mean monthly rainfall

The seasonal bias seen in the downscaled rainfall data (Figs 5.5–5.8) can be partly explained by biases in the seasonality of the atmospheric predictors as reproduced by the GCMs. As the largest rainfall mismatch occurs during the winter months, the biases in one of the winter atmospheric predictors — mean sea level pressure (MSLP) — have been plotted for each GCM (Fig. 5.9). The bias is the difference between the GCM and observed anomaly. A positive bias should correspond to a lower value of downscaled rainfall and a negative bias to a higher value of downscaled rainfall data. Thus, MSLP biases can explain some, but not all, of the biases evident in the downscaled rainfall datasets.

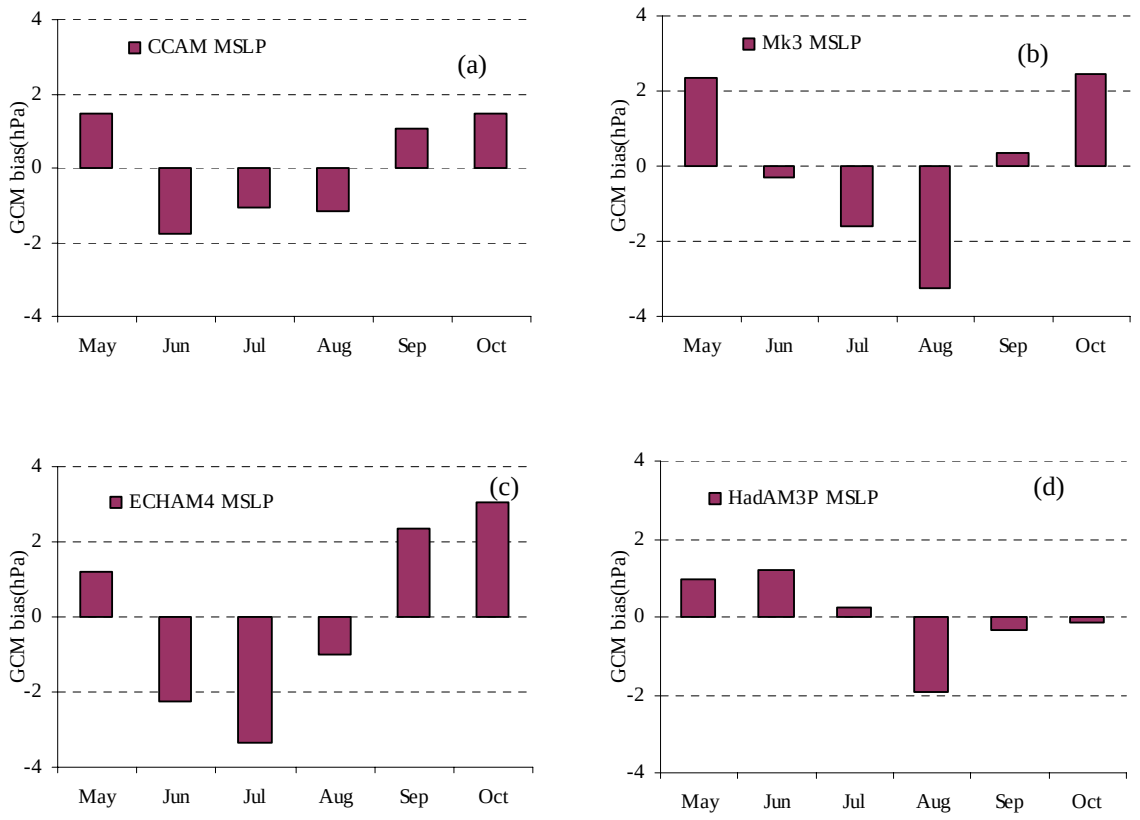

Figure 5.9 Anomalies of winter MSLP for (a) Mk3 (b) CCAM (c) ECHAM4 and (d) HadAM3P

The CCAM, Mk3 and ECHAM4 MSLP biases all have similar trends (positive bias in May, September and October; negative bias in June, July and August). For the Mk3, the positive bias in MSLP during May explains the lower downscaled rainfall and the negative biases in July and August explain the higher downscaled rainfalls for those months (Fig. 5.9a). For the CCAM, May MSLP has a positive bias, which corresponds with lower than observed downscaled rainfall, and the negative bias in August explains its higher simulated rainfall (Fig. 5.9b). Downscaled rainfalls for September and October are higher than observed, yet the MSLP biases for these months are positive.

The MSLP bias for the ECHAM4 corresponds to the correct rainfall patterns (higher or lower than the observed data) for all months apart from September. For example, the negative MSLP biases in June and July explain the higher downscaled rainfalls for these months (Fig. 5.9c). The HadAM3P is similar in that the MSLP bias explains the rainfall discrepancies for all months apart from October. The MSLP biases for this GCM are different from the other GCMs in that the biases are smaller and do not follow the same seasonal pattern (Fig. 5.9d).

The biases seen in downscaled rainfalls that do not appear related to MSLP biases may be due to other atmospheric predictors used in the models, such as the North–South MSLP gradient or the Dew Point Temperature Depression at 850 hPa, or to biases in another component of the modelling framework.

5.2 Streamflow

Ten years of observed rainfall data were used before the 30-year period as a 'warm-up run' in order to stabilise the LUCICAT model. Due to the high rainfall simulated by the ECHAM4 model, it was decided that this dataset would not be used. Forty simulations of 30 years of downscaled rainfall data for the CCAM, Mk3 and HadAM3P GCMs were used as input to model streamflow in LUCICAT. While running the model, no parameters were altered from when the model was run using observed data. The modelled streamflow at Serpentine Reservoir produced by using downscaled rainfall data was compared with two streamflow datasets — that evaluated by LUCICAT using observed records of rainfall (LUCICAT) and the water balance data (WBAL). Each current-scenario simulated dataset was also compared with its corresponding future-scenario dataset.

5.2.1 Cumulative streamflow — current

The range of streamflow projections encompasses both the LUCICAT and the water-balance (WBAL) datasets. The HadAM3P projected the lowest volumes of streamflow, and the Mk3 the highest. At the end of the 30-year period, the average of the Mk3 streamflow simulations overestimates the LUCICAT data by 29% (Fig. 5.10). The average of the CCAM streamflows also overestimates LUCICAT but only by 14%. The average of the HadAM3P streamflows underestimates LUCICAT by 10%.

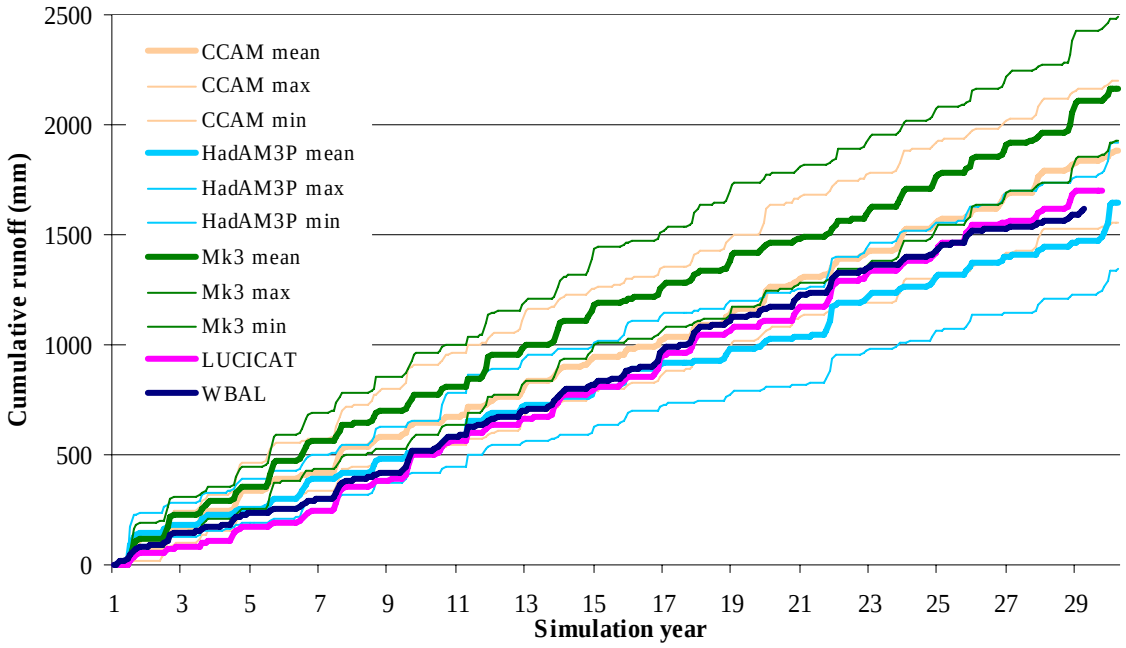

Figure 5.10 Cumulative runoff at Serpentine Dam — current climate

5.2.2 Cumulative streamflow — future

Cumulative runoff plots were also constructed for the Mk3, CCAM and HadAM3P future scenarios. The Mk3 and CCAM simulations both modelled the 2035–64 period (Fig. 5.11) and have similar results during the first 18 years. The upper range of the CCAM simulations corresponds well with the mean of the Mk3 simulations, and the minimum plot of the Mk3 corresponds well with the mean plot of the CCAM curve (Fig. 5.11). After that, the Mk3 simulations deviate further from those of CCAM. At the end of the 30-year period, the average of the Mk3 projection (1377 mm) is 25% higher than for CCAM (1039 mm). The HadAM3P simulations, modelled for a later time period (2070–99), record the smallest runoff accumulation (Fig. 5.12). At the end of 30 years, the average of cumulative runoffs is calculated to be 478 mm, which equates to being 54% lower than the CCAM end result and 65% less than the Mk3 end result. Compared to the current-scenario simulations, the HadAM3P future scenario accumulates 71% less runoff.

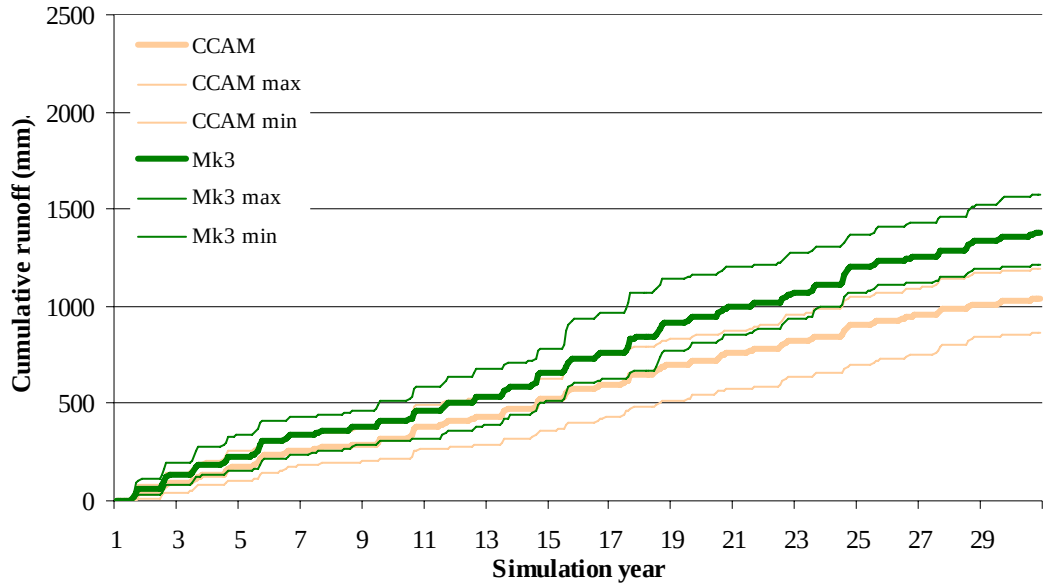

Figure 5.11 Cumulative runoff — future climate, CCAM and Mk3 simulations

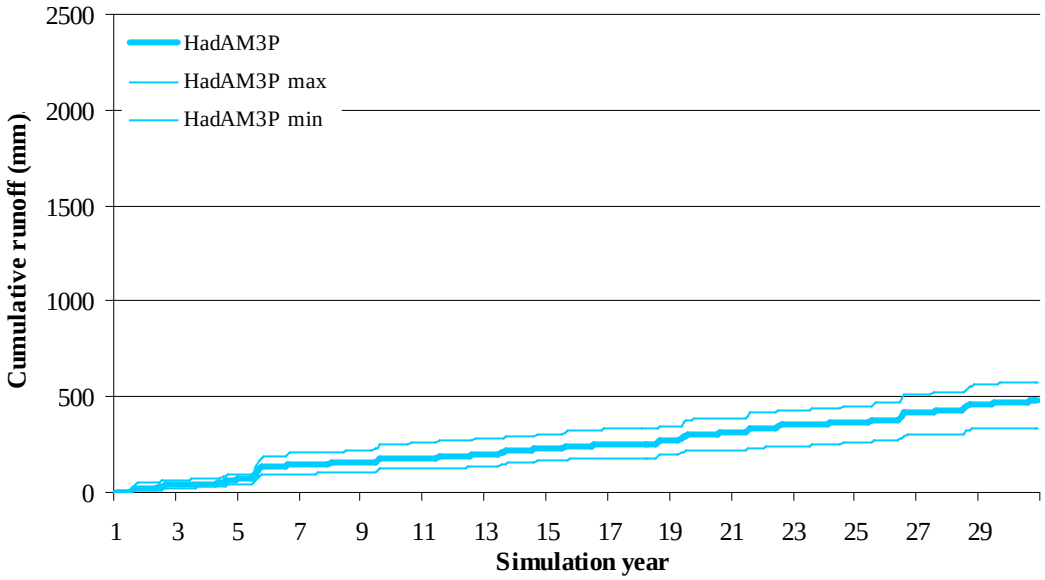

Figure 5.12 Cumulative runoff — future climate, HadAM3P simulation

5.2.3 Monthly streamflow

Mean monthly streamflows were evaluated for the current and future scenarios corresponding to the Mk3, CCAM and HadAM3P GCMs. Each current-scenario dataset was compared with the LUCICAT simulation of observed records, and each future scenario dataset was compared with its corresponding current scenario. The summary of annual differences is given in Table 5.3 with statistics relating to the monthly runoff in Appendix D. The Mk3 and CCAM results for the current-climate scenario are both higher than the observed records, while the HadAM3P figures are lower.

The CCAM simulations for the current scenario are close to the observed data, with an annual average overestimation of 14% (Fig. 5.13). Outputs for June and July are lower than the observed; though, the observed values for both months are within the range of data for the current scenario. Figures for August to December are higher than the observed data. The mean monthly runoffs for the future scenario are lower than for the current scenario in all months apart from March, where they are the same. On an annual scale, runoff reduces by 44%. The current and future scenario data have similar seasonal biases so, in some months (October and December) the mean runoff for the future scenario is greater than for the observed data.

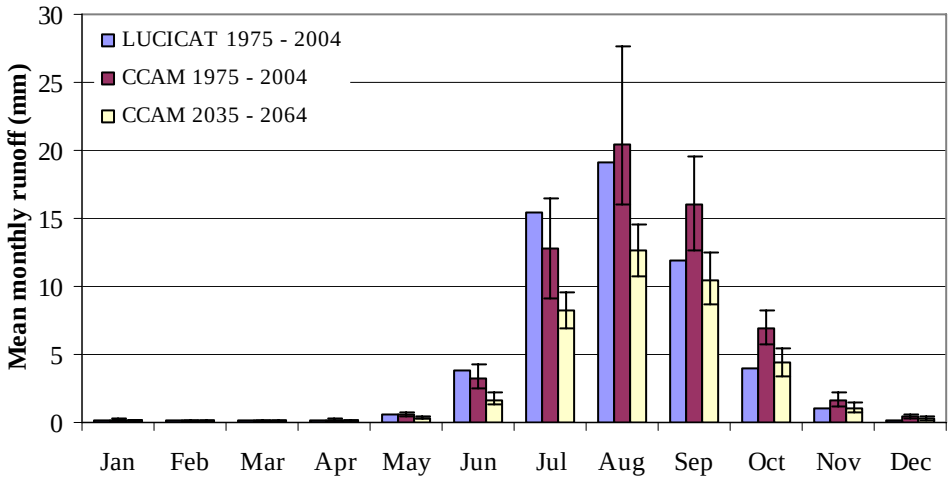

Figure 5.13 CCAM mean monthly runoff

On an annual scale, the Mk3 current-scenario simulations are 29% higher than the observed data — largely due to mean monthly runoffs for August and September being 7.4 mm and 9.3 mm higher than the observed data (Fig. 5.14). The estimations for the other wet months are better: within 3 mm. The dry months (November–May) are simulated well: within 1 mm. The seasonal bias in the Mk3 data when comparing the current-scenario to the observed dataset is greater than in CCAM and results in larger discrepancies in monthly runoff. The mean monthly runoffs of the future scenario are lower than for the current scenario in all months apart from February where they are the same.

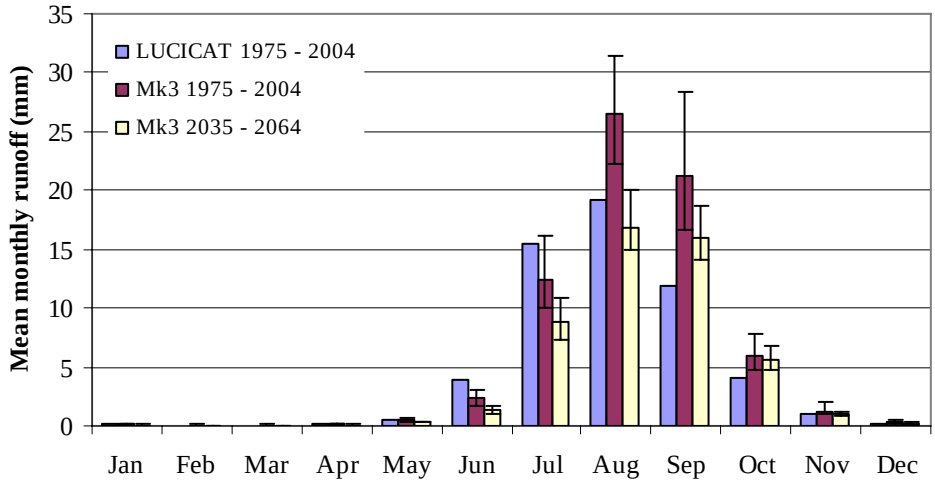

Figure 5.14 Mk3 mean monthly runoff

The Mk3 mean annual runoff in the future scenario is 29% less than in the current. As with the CCAM data, the current and future scenario data share similar seasonal biases and, as a result, in some months (September, October and December) the mean runoffs for the future scenario are greater than for the observed data.

Unlike CCAM and Mk3, HadAM3P streamflows are less than LUCICAT flows. On an annual scale, they are 10% lower, mainly due to low streamflows during July (Fig. 5.15). The error bars indicate, however, that the LUCICAT data are within the range of the simulated July streamflows. Future mean monthly runoffs are lower than current scenario runoffs in all months except January, where future runoff is higher. At the annual scale, the future scenario produced 69% less runoff than the current scenario. This is a larger reduction than for the other two GCMs but expected as the projection period is later: 2070–99. Runoffs decrease most in July, August and September: by 8, 14 and 7 mm respectively. The largest percentage reductions occur in May, June and October (73, 82 and 72% respectively).

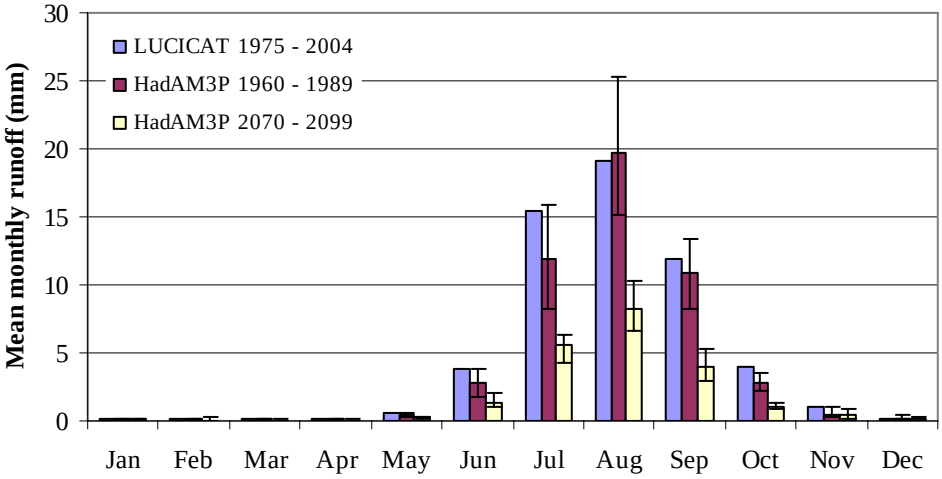

Figure 5.15 HadAM3P mean monthly runoff

Table 5.3 Percentage changes in annual streamflow, observed to current climate and current to future climate

Current climate	Average (mm/yr)	Average (GL/yr)	Difference compared to observed (%)
Observed (LUCICAT 1975-2004)	54.9	36.4	
CCAM (1975–2004)	62.5	41.5	13.8
HadAM3P (1960–1989)	49.6	32.9	–9.6
Mk3 (1975–2004)	70.9	47.1	29.1
Future climate	**Average (mm/yr)**	**Average (GL/yr)**	**Difference compared to current (%)**
CCAM (2035–2064)	35.2	23.4	–43.7
HadAM3P (2070–2099)	15.5	10.3	–68.7
Mk3 (2035–2064)	50.4	33.5	–29

5.3 Water-balance components

Water-balance components were calculated for the current and future scenarios of the CCAM, Mk3 and HadAM3P simulations for a 30-year period and compared with observed data from the LUCICAT model (Table 5.4; Figs 5.16 & 5.17) For all GCM runs, interflow is

the most significant flow component, while baseflow contributes the least to the total streamflow. Interflow changes most between the present to the future scenarios, decreasing by 43%, 37% and 72% for the CCAM, Mk3 and HadAM3P simulations respectively. In the Stage 1 study, for the Stirling Dam catchment, during future scenario, baseflow (19% of total streamflow), changed most. In this Stage 2 study, the baseflow component is only 2% (see Table 5.4) of total flow, so a reduction in a future climate is not as noticeable.

Table 5.4 Annual mean water-balance components for observed data, current and future CCAM, Mk3 and HadAM3P scenarios

Water balance component	Observed (1975–2004) (mm)	Current climate CCAM (mm)	Future climate CCAM (mm)
Rainfall – total	921	964	864
Interception	121	127	118
Soil evaporation	17	18	16
Transpiration	721	751	704
Streamflow — total*	61.0	62.4	35.8
— *Surface runoff*	*13.4*	*13.9*	*8.9*
— *Interflow*	*48.2*	*49.3*	*28.2*
— *Baseflow*	*2.0*	*2.3*	*1.3*
Storage change	–2	2	–13

Water balance component	Current climate Mk3 (mm)	Future climate Mk3 (mm)	Current climate HadAM3P (mm)	Future climate HadAM3P (mm)
Rainfall — total	965	854	896	682
Interception	131	119	125	105
Soil evaporation	18	16	16	13
Transpiration	734	688	701	593
Streamflow — total*	74.5	47.5	56.9	16.5
— *Surface runoff*	*15.4*	*10.7*	*11.8*	*4.8*
— *Interflow*	*59.8*	*37.7*	*46.1*	*12.9*
— *Baseflow*	*2.3*	*1.6*	*1.7*	*0.6*
Storage change	5	–19	–6	–47

*Total streamflow is less than the sum of the individual streamflow components due to transmission and evaporation losses.

For the future climate scenarios, all streamflow components reduce. (Fig. 5.17). As shown in Figure 5.16a, there was significant variation between simulations for the current-climate

interflow components. The interflow components averaged over the 30-year period were 33 GL. This variation was not as prominent in the simulations for the future scenario.

With the Mk3 simulations, the percentage reductions were less than those of the CCAM (Fig. 5.16b). Baseflow and surface runoff components were both lower by 30%. The flow components from the HadAM3P simulations are the lowest mainly due to lower rainfalls in the future climate during 2070-99 (Fig. 5.16c).

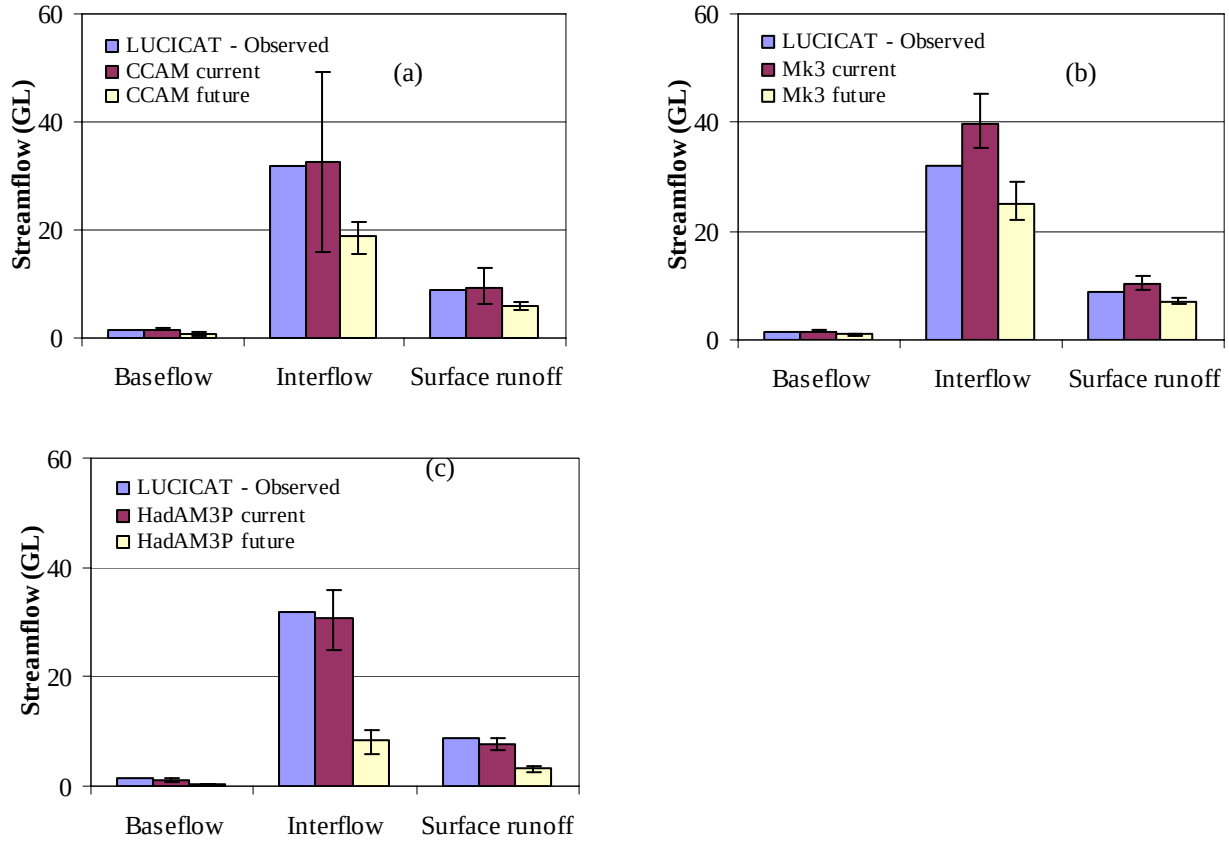

Figure 5.16 LUCICAT streamflow components at Serpentine Dam: observed, current and future simulations for (a) CCAM, (b) Mk3 and (c) HadAM3P

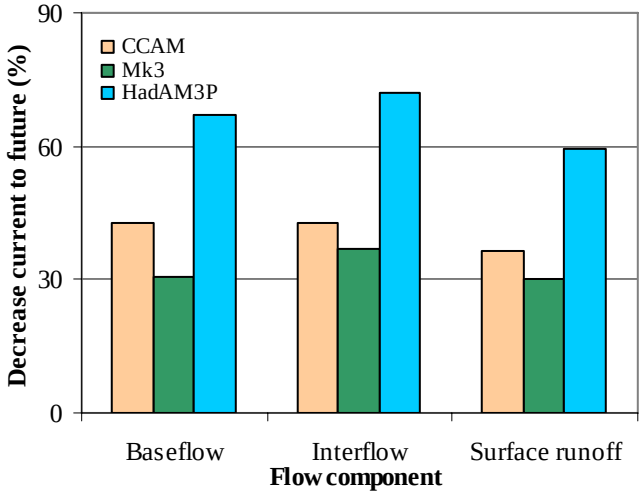

Figure 5.17 Percentage decreases in flow components for the CCAM, Mk3 and HadAM3P LUCICAT models

6 Discussion

This study is not aimed at calculating the exact future declines in rainfall, streamflow or catchment yield into the Serpentine Dam catchment, but in estimating the extent of the likely declines. As climate modelling is a relatively new science, uncertainty exists in its application, and only projections — not predictions — can be given. Climate models will only ever provide projections, as the actual trajectory of greenhouse-gas emissions scenarios will remain uncertain regardless of improvements in climate models.

6.1 GCM results relating to the Serpentine Dam catchment

Not all downscaled rainfall datasets were appropriate for use in this study. The current-scenario downscaled rainfall derived from the ECHAM4 GCM was significantly higher than the data generated by the three other models and the observed data, and was therefore not used in the streamflow analysis. The other downscaled rainfall datasets were deemed appropriate for use in modelling streamflow and catchment yield into the Serpentine Dam. Both current and future scenarios were modelled for each of the three GCMs. The HadAM3P data are closest to the observed data. Using CCAM increased the resolution of the Mk3 GCM and produced results that related more closely to the observed data than the Mk3. In all future scenarios streamflows, and consequently catchment yields, decline.

6.1.1 Rainfall — applicability of the ECHAM4 model

Mean monthly rainfall was calculated for each of the current-scenario downscaled rainfall datasets. The ECHAM4 rainfalls are significantly higher than those produced by the other models and the observed data. One possible reason for this is the larger grid spacing of the GCM causing a coarser reproduction of the atmospheric predictors. On analysing the downscaled rainfall, the increase was mainly due to a 10-year period of high rainfall. This indicates that the ECHAM4 model captures a higher variability of rainfall, and may be less applicable for this part of Western Australia. Its atmospheric data may still be valid, as the current climate does not relate to a specific time period. However, in this study, downscaled rainfall datasets from different GCMs were compared to a specific 30-year period of observed rainfall. Since the ECHAM4 data did not correspond as well as the other downscaled rainfall datasets, they were not included in the streamflow modelling.

6.1.2 Rainfall – CCAM improvement on the Mk3

There was a noticeable improvement in the current-climate dataset from the Mk3 run to the CCAM run. The CCAM data shows a weaker seasonal bias in the timing of the peak rainfall than the Mk3 run (Fig. 6.1). So, the mean monthly rainfalls are closer to the observed values. This improvement can be partly explained by the accuracy of the atmospheric predictors (Fig. 5.9). The GCMs aim to reproduce the monthly anomaly of the observed atmospheric predictors. Figure 5.9 shows the anomaly bias (GCM anomaly – observed anomaly) of all GCMs. A bias of zero indicates a very good match. The CCAM model has a narrower range of biases than the Mk3, which indicates that the model is more accurately reproducing the predictors. As the CCAM code is continually undergoing improvement and refinement, it is reasonable to expect future versions to perform even better. Although the seasonality of the monthly rainfall has changed, the mean annual rainfall for both datasets is very similar at 967 mm for CCAM and 969 mm for Mk3 (Table 5.1).

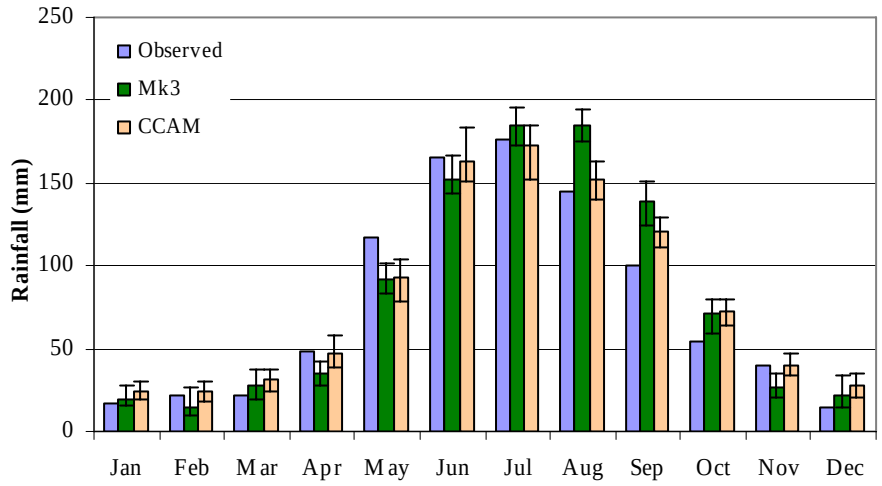

Figure 6.1 Mean monthly rainfall at Serpentine Dam: observed data, CCAM and Mk3 simulations

The two models computed similar annual rainfall averages for the 30-year period, but quite diverse streamflow values. A better match can be seen in the CCAM data when comparing the modelled streamflow for both datasets. This variation between the CCAM and Mk3 simulations can be attributed to the seasonal bias of the Mk3 rainfall data, which show higher rainfall from July to August (Fig. 6.2) This pattern was also observed in streamflow data. The Mk3 mean annual streamflow was 29% higher than the observed data, whereas the CCAM figure was only 14% higher (Fig. 6.2). This supports the idea that the seasonality of rainfall has a large influence on streamflow and catchment yield.

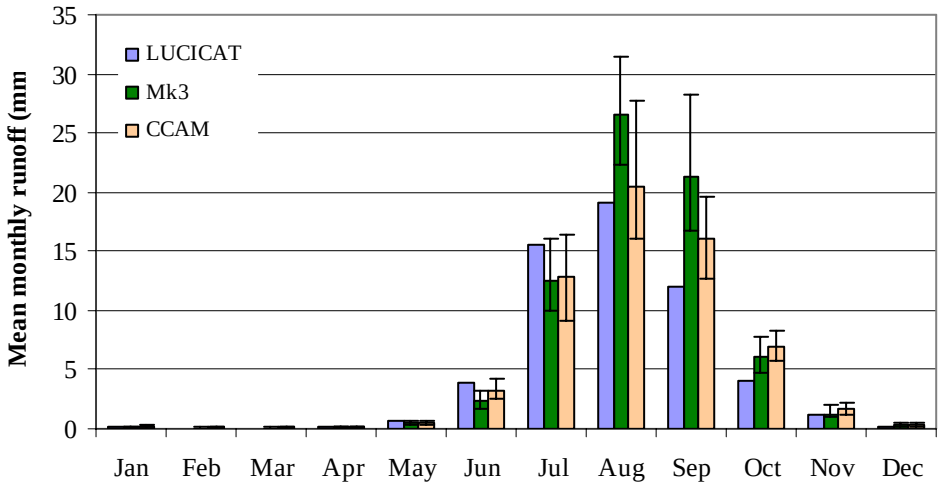

Figure 6.2 Mean monthly runoff at Serpentine Dam: observed data, CCAM and Mk3 simulations

6.1.3 Rainfall and streamflow reduction

The results from Stages 1 and 2 of this study indicate that the reduction in streamflow is approximately three times the reduction in rainfall for the A2 emissions scenario (Table 6.1).

This relationship is consistent with results of similar studies. Chiew and McMahon (2002) modelled rainfall and runoff for the present (1990) and future climates (2030) in catchments around Australia. For results with future rainfall and runoff declines, the runoff decline is 2.8 times rainfall decline. A similar study on the Salmon catchment in south-west Western Australia (Viney & Sivapalan 1996) found a 10% reduction in rainfall leads to approximately 30% decline in streamflow. Rainfall and runoff were modelled for six catchments around Australia for 2035 and 2085 using the CSIRO Mk2 GCM and the SIMHYD rainfall/runoff model (Harrold et al. 2005). Of the catchments with reductions in rainfall and streamflow, the average ratio of streamflow to rainfall reduction is 2.15.

Table 6.1 Rainfall and runoff decline for the future climate

Catchment	GCM & catchment model	Rainfall decline (%)	Runoff decline (%)	Ratio
Stirling	Mk3/LUCICAT	11	31	2.82
Serpentine	Mk3/LUCICAT	12	29	2.42
Serpentine	CCAM/LUCICAT	14	44	3.14
Serpentine	HadAM3P/LUCICAT	24	69	2.88
			Average	**2.80**

6.1.4 Modelled changes in climate patterns

All future scenarios project a decline in rainfall. Average annual rainfall for the 30-year period for the CCAM and Mk3 datasets declines by 14% and 12% respectively and by 24% for the ECHAM4 and HadAM3P datasets. The larger declines can be explained by the initially higher rainfall average for the ECHAM4 data (i.e. higher variability), and by a later modelling period for HadAM3P.

The currently high rainfall months (April–October) have lower rainfall in all future rainfall datasets. In the other, drier months some future datasets have a slight increase in rainfall (Table 6.2). In some cases, the timing of future peak flows also shifts: This is particularly so for the CCAM-generated data where peak rainfall shifts from June–July to July–August (Fig. 5.6). Peak rainfalls for the Mk3 and ECHAM4 also shift though not as markedly (Figs 5.5 & 5.7).

Table 6.2 Mean monthly downscaled and observed rainfall (mm)

	Jan	Feb	Mar	Apr	May	Jun	Jul	Aug	Sep	Oct	Nov	Dec
Observed	17	22	21	49	117	165	176	145	100	54	40	15
ECHAM4 current	20	21	34	60	117	199	221	166	105	44	35	25
ECHAM4 future	16	13	24	52	79	158	173	134	82	21	29	18
CCAM current	25	24	31	47	93	163	173	152	121	72	39	27
CCAM future	24	27	33	35	62	127	150	142	112	58	39	26
Mk3 current	19	15	28	34	92	153	185	185	138	71	26	22
Mk3 future	15	16	18	25	69	132	166	171	127	69	26	20
HadAM3P current	27	29	24	27	106	153	171	162	100	42	27	29
HadAM3P future	33	26	26	27	71	104	129	109	68	30	28	34

The seasonal shifts in rainfall are very influential in the modelled streamflow outputs. The mean annual streamflows into the Serpentine Dam in the current-scenario are 47.1 GL (Mk3) and 41.5 GL (CCAM). The streamflows are fairly similar, unlike the very different streamflows in the future-scenario. The Mk3 mean annual streamflow into the reservoir drops 29% to 33.5 GL while CCAM streamflow drops 44% to 23.4 GL (Table 5.3). This is a large difference in streamflow reduction, considering that the annual downscaled rainfall decreases are similar, at 12% and 14% for the Mk3 and CCAM respectively. The large difference in future streamflow decline can be attributed to the differences in seasonality of the future-climate rainfall.

Flow frequency

The flow duration of the CCAM current and future scenarios were compared in a flow duration curve developed using the median simulation from the current climate (simulation 31) and that from the future climate (simulation 30) (Fig. 6.3).

The future simulation indicates that runoffs at all magnitudes will decrease, with the greatest effects being seen at high-flow periods. For months with high runoff (10–100 mm/month) the CCAM current data revealed a probability of exceedence between 0 and 20%. For the same probability, the CCAM future data showed a decrease in monthly runoff (6 mm of the current 17 mm at 10% probability of exceedence), indicating a decrease in the frequency of high flows — with adverse effects on catchment yield. This finding is supported by the modelling results, which revealed a 44% reduction in mean annual catchment yield.

The reduction at low runoff periods is also significant in terms of catchment water processes (0.2 mm out of the current 0.4 mm at 60% probability of exceedence), putting further stress on the environment.

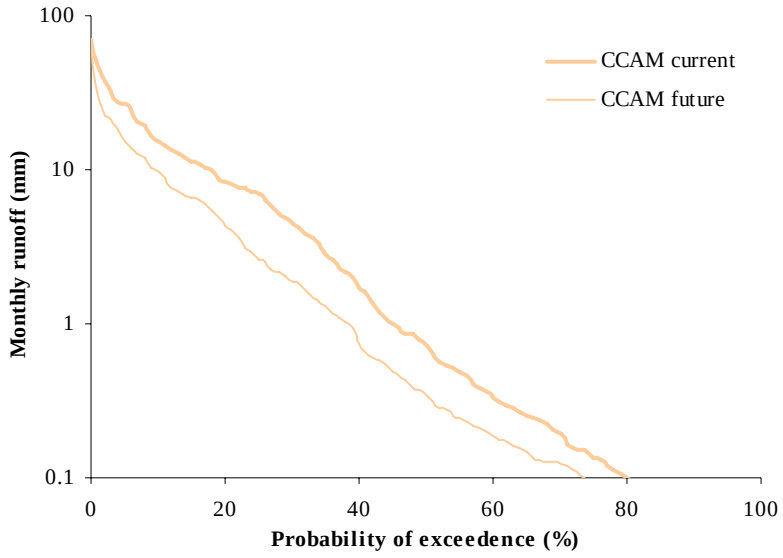

Figure 6.3 Flow duration curves

6.2 Modelling uncertainty

A level of uncertainty is inherent in climate modelling. Different GCMs modelling the same scenario often produce different outcomes; as in this study, where four climate models driven by the A2 emission scenario and downscaled for the Serpentine Dam catchment, produced different rainfall results. The variation in results can be attributed to the mechanics of the climate models, including the use of climate predictors. Wilby (2005) notes that different

climate models produced widely differing projections at the regional scale when used to drive a statistical downscaling model for estimating daily flows of the River Thames in the UK. Uncertainty also exists in deciding which climate scenario is to be modelled. Future greenhouse-gas emissions are only projections of possible situations, and different outcomes will result from using different projections. Uncertainty also exists in hydrological modelling. Historical data are essential in such studies, yet complete records are not always available. Other data used in hydrologic modelling also have associated uncertainties, particularly evapotranspiration and its role in water-balance models associated with a warmer climate.

6.2.1 Hydrologic modelling

In this study, uncertainty exists in each model step. The model's structure is an approximate representation of the real hydrologic processes, and many parameters used by the model have been derived from data with various degrees of uncertainty. An example is the computation of the spatial distribution of rainfall in the Serpentine Dam catchment from records of rainfall stations across the catchment. The stations are unevenly distributed, so certain areas are unequally represented. In addition, there are data gaps in the 30 years at the rainfall stations. If records from a low-rainfall station stop, the distribution of rainfall from this time can become biased. In addition, topography influences local-scale rainfall and, with large elevation variations within the catchment, the rainfall stations would not capture all local-scale variations.

Modelled data are calibrated against observed data — in this case, streamflow at various gauging stations throughout the Serpentine catchment. Parameters are altered so that the modelled data correspond as well as possible with the observed data. A common problem in hydrologic modelling is that of equifinality. This occurs when several parameter sets are considered 'equivalent' (Hreiche et al. 2002). For example, overestimating one parameter and underestimating another can give the appearance of an accurate result (Frederick & Major 1997). This type of uncertainty has been reported as being of a magnitude similar to that of the emission scenario choice up to about 2030 (Wilby 2005).

6.2.2 Projections

The extent of greenhouse-gas emissions to be experienced in the future will always be uncertain. A method of characterising this uncertainty is to use a number of different emission scenarios to project a range of possible outcomes. This study has used the A2 scenario, which is at the high end of the projections. As only one emission scenario has been studied, the results represent only one possible outcome. Projected changes in regional circulation and hence rainfall using this scenario may be larger than changes from scenarios with less greenhouse forcing. For example, the projected carbon dioxide emission for the B2 scenario is 915 ppmv by 2100, whereas on the A2 scenario it is 44% higher, at 1320 ppmv. Thus the results of this study could be viewed as being at the high end of runoff response to climate change.

6.2.3 Atmospheric predictors

There is a recurring, pervasive problem of climate models incorrectly modelling the annual cycle of key predictors. This caused the resultant mismatch between the seasonality of the observed data used to fit LUCICAT and that generated by downscaling GCMs. This seriously limits confidence in projected catchment yield response. The results presented here suggest that model resolution is a factor related to the ability of a climate model to reproduce the annual cycle of atmospheric predictors required for statistical downscaling. Notably, the ECHAM model, with the coarsest grid resolution, produced the poorest reproduction of the annual cycle of key predictors, and HadAM3P, with finer spatial resolution, better reproduced the annual cycle (Fig. 5.9). CCAM improved on the Mk3 reproduction of the annual cycle, showing the benefit of dynamic downscaling as a precursor to statistical downscaling.

6.2.4 Evapotranspiration

Pan evaporation is a measure of potential evapotranspiration, or atmospheric demand (Land and Water Australia 2004). It is a topical subject, with opinions differing in the direction of historical pan-evaporation trends (increasing or decreasing) and the reasons for this trend.

There is some indication that greenhouse-induced climate change will lead to increased evaporative demand and actual evaporation. Higher concentrations of carbon dioxide in the atmosphere may lead to changes in forest density and structure, and may result in greater evapotranspiration. Against this is the lack of evidence of long-term, large-scale increases in pan evaporation. This may be due to the dependence of pan evaporation on other climatic variables including solar radiation, wind speed and vapour-pressure deficit, none of which have changed in a way to promote an increase in pan evaporation (Gifford et al. 2005). Strengthening this argument is evidence that, from the 1960s to the 1990s globally, there has been a decreasing trend in pan evaporation. One potential reason for this is a reduction in solar radiation reaching the Earth's surface, due to global dimming, that occurred during the same time period in the Northern Hemisphere (Gifford et al. 2005).

The annual pan evaporation rate has decreased 2.8 mm/yr for the last 30 years. Likewise, annual lake evaporation has decreased by 2.9 mm/yr (Gifford et al. 2005; Roderick & Farquhar 2004). The effects of lower pan and lake evaporation rates on actual evapotranspiration depend upon how 'wet' or 'dry' a particular area is. In a 'wet' area (annual rainfall greater than pan evaporation), reduced pan evaporation may mean reduced actual evaporation and so increased streamflow. Observations from the Northern Hemisphere (Russia and other parts of Europe) support this hypothesis. In a 'dry' area (like south-west Western Australia), if annual rainfall does not change, reduced pan evaporation may lead to increased plant growth due to a reduction in moisture deficit. The effects of reduced pan evaporation and reduced annual rainfall on soil moisture deficit, plant growth and streamflow are still unclear.

There are numerous areas of uncertainty in using pan evaporation for climate modelling. Firstly, there is a significant difference between actual and potential evapotranspiration. During drought conditions, the atmospheric demand is high, causing a high potential evapotranspiration but, from a lack of soil moisture, a low actual evapotranspiration (Land and Water Australia 2004). Long-term records are also difficult to obtain. Standard measuring devices were only installed in the 1960s, so analysing trends using data recorded before this time can bias the results. Urbanisation also has a role in affecting pan evaporation, influencing wind speeds through obstructions.

Pan evaporation has been calculated from first principles in a recent CCAM simulation downscaling NCEP reanalysis from 1951–2000. In these 60 km simulations, at every grid point a pan water temperature is updated each time step, based on the latent and sensible heat fluxes from the pan water surface, and also including sensible heat fluxes from the bottom and sides of the pan. In this simulation, the modelled pan evaporation trends from 1975–2000 were found to be generally consistent with the observed trends over most of Australia (J McGregor, pers. comm. 2007).

6.2.5 Other factors

Other atmospheric factors are not always incorporated into climate modelling. These include the incorporation of ocean evaporation and its response to climate change. Cloud cover is another factor with uncertain influences on climate change, as many GCMs are not able to properly model the physics of clouds (Franks 2002). As a result, the effects of cloud cover on radiation and the influence of greenhouse gases on cloud formation and cloud properties are uncertain (Gifford et al. 2005).

7 Conclusion

The current-climate downscaled rainfall datasets from the four GCMs were compared with observed rainfall. Mean annual rainfalls from three GCMs (HadAM3P, CCAM and Mk3) were within ±5% of the observed mean annual rainfall (1975–2003) of 921 mm, while those from ECHAM4 rainfall was higher. As a result, only rainfall data from the first three GCMs were used in the streamflow analysis. The Mk3 and the CCAM current-climate downscaled rainfalls have seasonal biases at the monthly scale. The CCAM bias is not as strong as the Mk3, yet still models lower rainfall in the early months and higher rainfall later in the year.

All GCMs model a future climate with a reduction in rainfall from 12% to 24%. The projected declines are12% and 14% by mid-century for the two Australian climate models (CCAM and Mk3). The projected 24% decline by mid-century for ECHAM4, approximately twice the reduction of CCAM and Mk3, can be attributed to the initially higher current-climate rainfall. The HadAM3P also projects a 24% reduction, explained by referring to a later climate (2070–99). For all models, the majority of the decline occurs during the wet months and the drier months remain fairly constant.

Downscaled GCM rainfall was used as data input into the LUCICAT model. Before doing so, the model was calibrated for the Serpentine Dam catchment using measured rainfall, streamflow and catchment characteristics data. The LUCICAT model was calibrated on the annual, monthly and daily time scales and mirrors the historical streamflow trends very well. Flow magnitudes are also predicted well, with generally better results in the larger gauged areas. Daily calibrations are at times higher than the observed data and also give some earlier cease-to-flow results. Calibration reveals that mean annual flow (1975–2003) into the Serpentine Dam is 36.5 GL.

The correlation between the observed and the current-climate catchment yields is optimal with the CCAM simulations, the CCAM annual flow of 41.5 GL corresponding to a 14% overestimation. The seasonal bias of the Mk3 rainfall has a large impact on the annual flow result. Annual rainfall for the Mk3 and the CCAM simulations varies by 2%; however, the seasonality of the rainfall carries through into the streamflow results. As a result, the Mk3 simulations overestimate calibrated annual streamflow by 29%. The HadAM3P simulations show streamflow 10% lower than the calibrated mean annual flow. Streamflow components are best modelled by the CCAM simulations, which also have the largest simulation range.

In the future climate, mean annual streamflow is projected to decrease more than rainfall — this is typical of the relationship between rainfall and streamflow. By mid-century (2035–64), the annual average streamflows projected by the Australian models (Mk3 and CCAM) would decrease to 33.5 GL and 23.4 GL or by 29% and 44% respectively. By late century (2070–99), the HadAM3P simulations produced a 69% reduction in annual flow to 10.3 GL.

This study has focused on the mean annual variations in rainfall and streamflow over a 30-year period. Reporting at this time scale can mask the within-year variations. When analysing the downscaled rainfall datasets, accurate simulations at the annual scale masked, for some

models, the seasonal biases that influence both monthly and annual variations of modelled streamflow.

With the completion of this study it has become apparent that not all GCMs are suitable for use in the south-west of Western Australia. It is clear that there are many sources of uncertainty involved with climate/hydrology modelling, which can be undefinable, ambiguous or unavoidable. The A2 emission scenario used assumes constant high-emission rates, so results are taking into account a possible 'worst-case' scenario. If future emission rates are lower than envisaged in the A2 scenario, climate patterns could be different, with possibly less reduction in rainfall and streamflow.

The study assumed no catchment land-use changes in the next 100 years (though changes due to prescribed burning, mining and land development are possibilities) and kept pan evaporation and plant transpiration efficiency unchanged in the future climate.

Additional studies can be carried out to reduce the uncertainties. Similar climate change/hydrology studies that use more than one emission scenario will provide a broader range of results to analyse and take into account the range of possible future climates given the current state of knowledge. Further studies should also consider combining available catchment yield results with investigations into water demand. Further research is currently under way in relation to the direction of pan evaporation. Once relationships are established between evaporation and other climatic variables, uncertainty in the parameterisation of hydrologic/climate models will be reduced. Performing similar studies in different areas of Western Australia will allow additional comparisons and further refinement of sources of error.

The use of four climate models generated a broad spectrum of results. Each model re-created the current-climate rainfall to varying levels of success, while the GCM with the coarsest spatial resolution (ECHAM4) deviated the most from the observed dataset. The use of a Regional Catchment Model produced more accurate results, as shown in comparing the CCAM results with those of the Mk3.

The results are projections of possible scenarios, which will change depending on the emission scenario and future land use as well as the response of rainfall and actual evaporation to future climate conditions.

8 References

Arora, VK & Boer, GJ 2001, 'The effects of simulated climate change on the hydrology of major river basins', *Journal of Geophysical Research*, vol.106(D4), pp. 3335–3348, available at <http://www.cccma.bc.ec.gc.ca/papers/varora/impact_report_for_wgne.pdf>, accessed 5/1/06.

Bari MA, 2005, 'A distributed conceptual model for stream salinity generation processes: A systematic data-based approach', Doctor of Philosophy thesis, The University of Western Australia, 267p.

Bari, MA & Smettem, KRJ 2004, Modelling monthly runoff generation processes following land use changes: groundwater-surface runoff interactions, *Hydrology and Earth Systems Science,* vol. 8(5), pp. 903–922.

Bari, MA & Smettem, KRJ 2006a, 'A conceptual model for daily water balance following partial clearing from forest to pasture', *Hydrology and Earth Systems Science*, vol. 10, pp. 321–337.

Bari, MA & Smettem, KRJ 2006b, 'A daily salt balance model for stream salinity generation processes following clearing from forest to pasture', *Hydrology and Earth Systems Science* vol. 10, pp. 519–534.

Bari, MA, Berti, MA, Charles, S, Hauck, E & Pearcey, M 2005, *Modelling of streamflow reduction due to climate change in Western Australia – A case study*. MODSIM 2005, Melbourne, December 2005, Australia.

Bari, MA, Charles, SP, Kitsios, A, Coppolina, M, Boniecka, L, & Crossley, K 2007, 'Predicting streamflow reduction due to climate change in the southwest of Western Australia — A review', in: *Greenhouse 2007, Latest Science and Technology*, October 2007, Sydney, Australia.

Bari, MA & Ruprecht, JK 2003, *Water yield response to land use change in south-west Western Australia*, Department of Environment, Western Australia, Salinity and Land Use Impacts Series, Report No. SLUI 31.

Berti, ML, Bari, MA, Charles, SP & Hauck, EJ 2004, *Climate change, catchment runoff and risks to water supply in the south-west of Western Australia*, Department of Environment, Western Australia.

Beverly, C, Bari, MA, Christy, B, Hocking, M & Smettem, KRJ 2005, 'Predicted salinity impacts from land use change: comparison of rapid assessment approaches and a detailed modelling framework', *Australian Journal of Experimental Agriculture*, vol. 45, p. 117.

Blake, R, Khanbilvardi, R & Rosenzweig, C 2000, 'Climate change impacts on New York City's water supply system', *Journal of the American Water Resources Association, vol.* 36, no. 2, pp. 279–292.

Bourke, W 1974, 'A multi-level spectral model. I. Formulation and hemispheric integrations', *Monthly Weather Review,* vol. 102, pp. 687–701.

Bronstert, A, Niehoff, D & Burger, G 2002, 'Effects of climate and land-use change on storm runoff generation: present knowledge and modelling capabilities', *Hydrological Processes,* vol. 16, pp. 509–529. Available at <http://www3.interscience.wiley.com/cgi-bin/fulltext/89015871/PDFSTART>, accessed 5/1/06.

Bureau of Meteorology 2003, *The greenhouse effect and climate change,* Commonwealth Bureau of Meteorology, Melbourne, p. 74.

Bureau of Meteorology 2005, Australian climate zones — all climate classes (based on the Koppen classification, Commonwealth Bureau of Meteorology, Melbourne.

CALM 2005, '*6 season indicative burn program, spring 2005 – autumn 2008, Swan Region'* [map], *Indicative prescribed burning plan, south-west Western Australia, autumn 2006*, Naturebase, Department of Conservation and Land Management, Western Australia, <http://www.naturebase.net/projects/indicative_prescribed_burning_plan_2008-08.html>, accessed 15/11/05.

CCCma 2004, *CGCM runs forcing: Equivalent CO_2 concentrations used in CCCma coupled global climate model simulations,* Canadian Centre for Climate Modelling and Analysis, <http://www.cccma.bc.ec.gc.ca/data/cgcm/cgcm_forcing.shtml>, accessed 15/11/05.

Charles, SP, Bari, MA, Kitsios, A & Bates, BC 2007, 'GCM downscaling for precipitation and runoff projection in the Serpentine catchment, Western Australia', International Journal of Climatololgy, vol. 27, pp. 1673–90.

Charles, SP, Bates, BC & Hughes, JP 1999, 'A spatio-temporal model for downscaling precipitation occurrence and amounts', *Journal of Geophysical Research*, vol. 104, pp. 31657–31669.

Chiew, FHS & McMahon, TA 2002, 'Modelling the impacts of climate change on Australian streamflow', *Hydrological Processes,* vol.16, pp. 1235–1245.

Chiew, FHS, Whetton, PH, McMahon, TA & Pittock, AB 1995, 'Simulation of the impacts of climate change on runoff and soil moisture in Australian catchments', *Journal of Hydrology,* vol. 167, pp. 121–147.

Consortium for International Earth Science Information Network (CIESIN) 1995, *Thematic guide to integrated assessment modeling of climate change,* University Center, Michigan, <http://sedac.ciesin.org/mva/iamcc.tg/TGHP.html>, accessed 7/10/05.

Cox, MD 1984, *A primitive equation, three-dimensional model of the ocean,* Technical Report No. 1, Ocean Group, Geophysical Fluid Dynamics Laboratory, Princeton University, Princeton, NJ.

Dean, JD & Snyder, WM 1977, 'Temporally and areally distributed rainfall', *Journal of Irrigation and Drainage Engineering,* vol. 123, IR2, pp. 221–229.

Dixon, NRM & Bari, MA 2008, 'Modelling of stream salinity management options for the Warren River', in: *Hydrology and Water Resources Symposium*, The Institution of Engineers, Adelaide, Australia, 2008.

Evans, J & Schreider, S 2002, 'Hydrological impacts of climate change on inflows to Perth, Australia', *Climatic Change,* vol. 55**,** pp. 361–393.

Franks, SW 2002, 'Assessing hydrological change: deterministic general circulation models or spurious solar correlation?', *Hydrological Processes,* vol*.* 16**,** pp. 559–564.

Frederick, KD & Major, DC 1997, 'Climate change and water resources', *Climatic Change,* vol. 37, no. 1, pp. 7–23.

Gifford, RM, Farquhar, GD, Roderick, ML & Nicholls, N 2005, 'Workshop summary on pan evaporation: an example of the detection and attribution of climate change variables', *Proceedings of a workshop held at the Shine Dome, Australian Academy of Science,* ed. R.M. Gifford, pp. 4–19.

Gordon, HB, 1981, 'A flux formulation of the spectral atmospheric equations suitable for use in long-term climate modeling', *Monthly Weather Review,* vol. 109, pp. 56–64.

Gordon, HB, Rotstayn, LD, McGregor, JL, Dix, MR, Kowalczyk, EA, O'Farrell, SP, Waterman, LJ, Hirst, AC, Wilson, SG, Collier, MA, Watterson, IG & Elliott, TI 2002, *The CSIRO Mk3 Climate System Mode,* Technical Paper No. 60, CSIRO Atmospheric Research, Melbourne.

Harrold, TL, Chiew, FHS & Siriwardena, L 2005, 'A method for estimating climate change impacts on mean and extreme rainfall and runoff', in A Zerger, & RM Argent, (eds) *MODSIM 2005 International Congress on Modelling and Simulation*, Modelling and Simulation Society of Australia and New Zealand, pp. 497–504, available at <http://mssanz.org.au/modsim05/papers/harrold.pdf>, accessed 27/3/2005.

Hassall & Associates, NSW Department of Land and Water Conservation, NSW National Parks and Wildlife Service and CSIRO Atmospheric Research 1998, *Climate change scenarios and managing the scarce water resources of the Macquarie River. Final report,* Environment Australia, Canberra.

Hay, LE & Clarke, MP 2003, 'Use of statistically and dynamically downscaled atmospheric model output for hydrologic simulations in three mountainous basins in the eastern United States', *Journal of Hydrology,* vol. 282, no. 1, pp. 56–75.

Hay, LE, Wilby, RL & Leavesley, GH 2000, 'A comparison of delta change and downscaled GCM scenarios for three mountainous basins in the United States', *Journal of the American Water Resources Association,* vol. 36, no. 2, pp. 387–397.

Hreiche, A, Mezher, D, Bocquillon, C, Dezetter, A, Servat, E & Najem, W 2002, 'Parallel processing for a better understanding of equifinality in hydrologic models', in AE Rizzoli, & AJ Jakeman, (eds), *Integrated assessment and decision support,* Proceedings of the First Biennial Meeting of the International Environmental Modelling and Software Society, vol. 1, pp. 410–415, available at <http://www.iemss.org/iemss2002/proceedings/pdf/volume%20uno/194_hreiche.pdf>, accessed 14/3/2006.

Hughes, JP, Guttorp, P & Charles, SP 1999, 'A non-homogeneous hidden Markov model for precipitation occurrence', *Applied Statistics,* vol. 48, pp. 15–30.

IOCI 2002, *Climate variability and change in south west Western Australia,* Indian Ocean Climate Initiative Panel, Western Australia.

IPCC 2000, *Emissions scenarios. Summary for policymakers,* Intergovernmental Panel on Climate Change, <http://www.grida.no/climate/ipcc/spmpdf/sres-e.pdf>, accessed 10/1/06.

IPCC 2001, *Climate change 2001: the scientific basis,* Intergovernmental Panel on Climate Change, <http://www.grida.no/climate/ipcc_tar/wg1/378.htm>, accessed 10/6/05.

Johnson, RA & Bhattacharyya, GK 1996, *Statistics: principles and method*s, 3rd edn., John Wiley & Sons Canada, Toronto.

Land and Water Australia 2004, 'Pan evaporation defying the trends: new research', *CLIMAG,* vol. 8, no. 1, p. 4.

Luke, GJ, Burke, KL & O'Brien, TM 1988, *Evaporation data for Western Australia,* Technical Report No. 65, Division of Resource Management, Department of Agriculture, Western Australia.

Martin, DA 2001, *'A comprehensive approach to post-fire water quality monitoring and decision-making'* US Geological Survey, available at http://firescience.cr.usgs.gov/html/martin_abs.html, accessed 15-11-05.

Mauger, GW 1996, *Modelling dryland salinity with the M.A.G.I.C. system,* Water and Rivers Commission, Western Australia, Water Resources Technical Series, Report No. WRT 7.

Mayer, XM, Ruprecht, JK & Bari, MA 2005, *Stream salinity status and trends in south-west Western Australia,* Department of Environment, Western Australia, Salinity and Land Use Impacts Series, Report No. SLUI 38.

McGregor, JL 2005, *C-CAM geometric aspects and dynamical formulation,* Technical Paper 70, CSIRO Atmospheric Research, Melbourne.

Nathan, RJ, McMahon, TA & Finlayson, BL 1988, 'The impact of the greenhouse effect on catchment hydrology and storage yield relationships in both winter and summer rainfall zones', in Pearman, GI (ed.), *Greenhouse: planning for climate change,* E.J. Brill, New York, pp. 273–295.

NSW EPA 2003, *State of environment report*, chapter 6, Department of Environment and Conservation, New South Wales, <http://www.epa.nsw.gov.au/soe/soe2003/chapter6/chp_6.5.htm>, accessed 15/11/05.

Pacanowski, RC (ed.) 1996, *MOM 2 Version 2: Documentation, User's Guide and Reference Manual,* GFDL Ocean Technical Report 3.2, Geophysical Fluid Dynamics Laboratory/NOAA, Princeton, NJ.

Ritchie, JW, Zammit, C & Beal, D 2004, 'Can seasonal climate forecasting assist in catchment water management decision-making? A case study of the Border Rivers catchment in Australia', *Agriculture, Ecosystems and Environment*, vol. 104, pp. 553–565.

Roderick, ML & Farquhar, GD 2004, Changes in Australian pan evaporation from 1970 to 2002', *International Journal of Climatology*, vol. 24, pp. 1077–1090.

Rodgers, SJ & Ruprecht, JK 1999 (unpublished), 'The effect of climate variability on streamflow in the south-west of Western Australia', Surface Water Hydrology Report Series, Report No. SWH 25, Water and Rivers Commission, Western Australia.

Rowell, DP 2005, *A scenario of European climate change for the late 21st century: seasonal means and interannual variability,* Hadley Centre for Climate Prediction and Research, Exeter, UK.

Schnur, R & Lettenmaier, DP 1998, 'A case study of statistical downscaling in Australia using weather classification by recursive partitioning', *Journal of Hydrology,* vol. 212–213, pp. 362–379.

Smith, RA, Bari, MA, Dixon, NRM & Rowlands, D 2007, Helena River: Salinity Situation Statement, Department of Water, Division of Water Resources Management, Water Resources Technical Series WRT 34, 177p.

Stonefelt, MD, Fontaine, TA & Hotchkiss, RH 2000, 'Impacts of climate change on water yield in the Upper Wind River Basin', *Journal of the American Water Resources Association,* vol. 36, no. 2, pp. 321–336.

Suchita, P 2004 'Application of stochastic downscaling techniques to global climate model data for regional climate prediction', Thesis for the Degree of Master of Science in Civil Engineering, Department of Civil & Environmental Engineering, Louisiana State University, available at <http://etd.lsu.edu/docs/available/etd-08192004-224424/unrestricted/Chapters.pdf>, accessed 20/6/05.

Timbal, B & McAvaney, BJ 2001, 'An analogue-based method to downscale surface air temperature: application for Australia', *Climate Dynamics,* vol. 17, pp. 947–963.

Viney, NR & Sivapalan, M 1996, 'The hydrological response of catchments to simulated changes in climate', *Ecological Modelling,* vol. 86, pp. 189–193.

Von Storch, H, Zorita, E, Jones, M, Dimitriev, Y, Gonzalez-Rouco, F & Tett, SB 2004, 'Reconstructing past climate from noisy data', *Science,* vol. 306, pp. 679–682.

Voss, R, May, W & Roeckner, E 2002, 'Enhanced resolution modelling study on anthropogenic climate change: changes in extremes of the hydrological cycle', *International Journal of Climatology,* vol. 22, pp. 755–777, available at <http://www3.interscience.wiley.com/cgi-bin/fulltext/94517540/PDFSTART>, accessed 4/1/06.

Water and Rivers Commission 1999, *Review of the experimental catchments in the Joint Immediate Rainfall Zone Research Programme,* Water and Rivers Commission, Western Australia, Water Resource Technical Series, No. WRT 13.

Water Corporation 2005a, 'Our water sources … Serpentine Dam', Water Corporation, Western Australia, http://www.watercorporation.com.au/D/dams_serpentine.cfm, accessed 23/5/05.

Water Corporation 2005b, 'Our water sources … Yearly streamflow for major surface water sources', Water Corporation, Western Australia, http://www.watercorporation.com.au/D/dams_streamflow.cfm, accessed 13/3/06.

Wilby, RL 2005, 'Uncertainty in water resource model parameters used for climate change impact assessment', *Hydrological Processes,* vol. 19, pp. 3201–3219.

Wilby, RL, Hay, LE, Gutowski Jr, WJ, Arritt, RW, Takle, ES, Pan, Z, Leavesley, GH & Clark, MP 2000, 'Hydrological responses to dynamically and statistically downscaled climate model output', *Geophysical Research Letters,* vol. 27, no. 8, pp. 1199–1201.

Wilks, DS & Wilby, RL 1999, 'The weather generation game: a review of stochastic weather models', *Progress in Physical Geography,* vol. 23, no. 3, pp. 329–357.

Wolock, DM & McCabe, GJ 1999, 'Estimates of runoff using water balance and atmospheric general circulation models', *Journal of the American Water Resources Association,* vol. 35, no. 6, pp. 1341–1350.

Wood, AW, Leung, LR, Sridhar, V & Lettenmaier, DP 2004, 'Hydrologic implications of dynamical and statistical approaches to downscaling climate model outputs', *Climate Change,* vol. 62, pp. 189–216.

Appendix A: Application of the LUCICAT model

A.1 LUCICAT model

The Land Use Change Incorporated CATchment (LUCICAT) model (Bari 2005; Bari et al. 2005; Bari & Smettem 2006a & b; Bari et al. 2007; Smith et al. 2007; Dixon & Bari, 2008) was used to simulate streamflow throughout the Serpentine Dam catchment. LUCICAT uses a daily water-balance model to represent the streamflow processes that occur within the catchment. The model consists of five main stores: dry, wet and subsurface stores, saturated groundwater store and transient stream zone store (Fig. A.1).

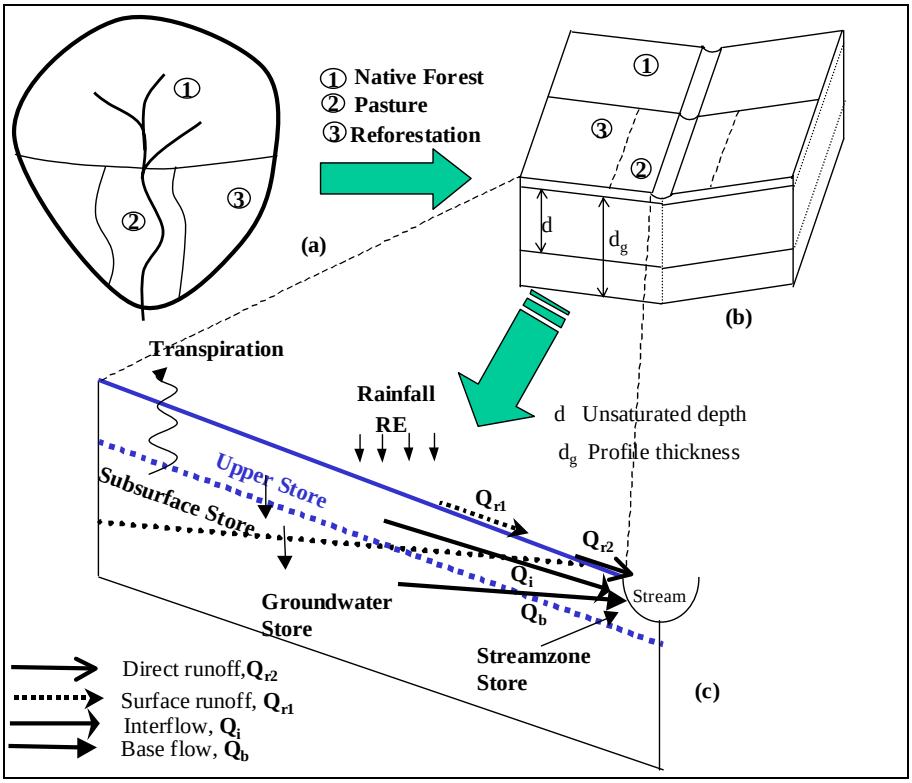

Figure A.1 LUCICAT model

The catchment being modelled is divided into smaller subcatchments, with each represented as an 'open book' catchment. The dry, wet and subsurface stores model vertical and lateral water flows and also describe the soil-moisture balance. The Groundwater Store controls baseflow to the stream and the contribution of groundwater to the streamzone. The transient streamzone represents parts of the catchment that have become saturated due to the influence of groundwater.

A.2 Data preparation and model set-up

The Serpentine Dam catchment was divided into 86 subcatchments, ranging in area from 2–16 km^2 (Fig. A.2). This scale of separation enables the application of spatially varied catchment characteristics, including attributes such as rainfall, pan evaporation, soil type and vegetation. To run LUCICAT, daily rainfall, daily pan evaporation, subcatchment attributes, groundwater data and land-use history for each subcatchment were required. Sub-catchments with gauging stations at the outlet also required daily flow data to be used for calibration.

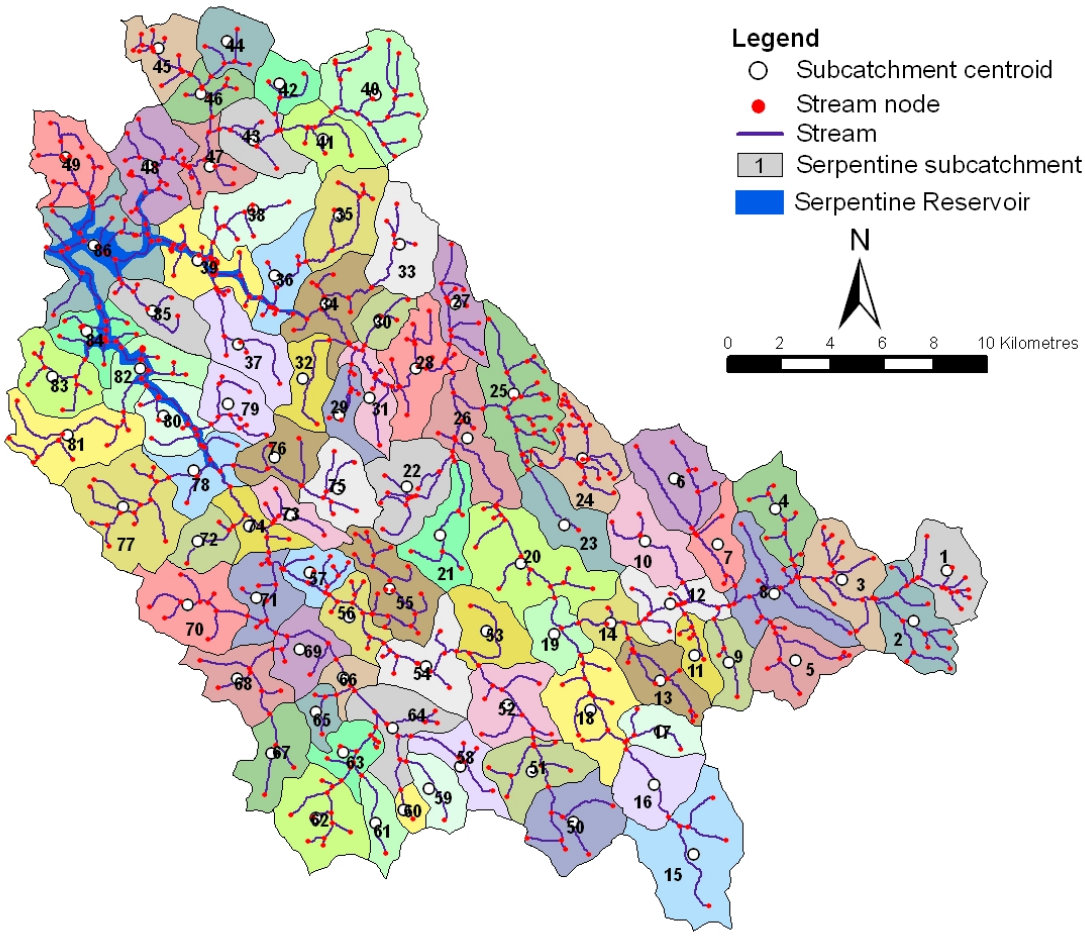

Figure A.2 Stream nodes and subcatchments of the Serpentine Dam catchment

Rainfall distribution

A total of 37 rainfall stations were used to create a spatial distribution of daily rainfall across the catchment (Fig. 2.2) using data collected between 1960 and 2004. The periods of record of the rainfall stations varied and only five stations had complete records from the 1970s to 2004. Based on the method described by Dean and Snyder (1977), for each day of the

simulation, a daily rainfall dataset was generated for each subcatchment using records from the three closest stations, or, to fill data gaps, using records from the closest rainfall station with data.

The average annual rainfall for the catchment over the period 1975–2004 ranged from 650 to 1150 mm, increasing from east to west (Fig. A.3).

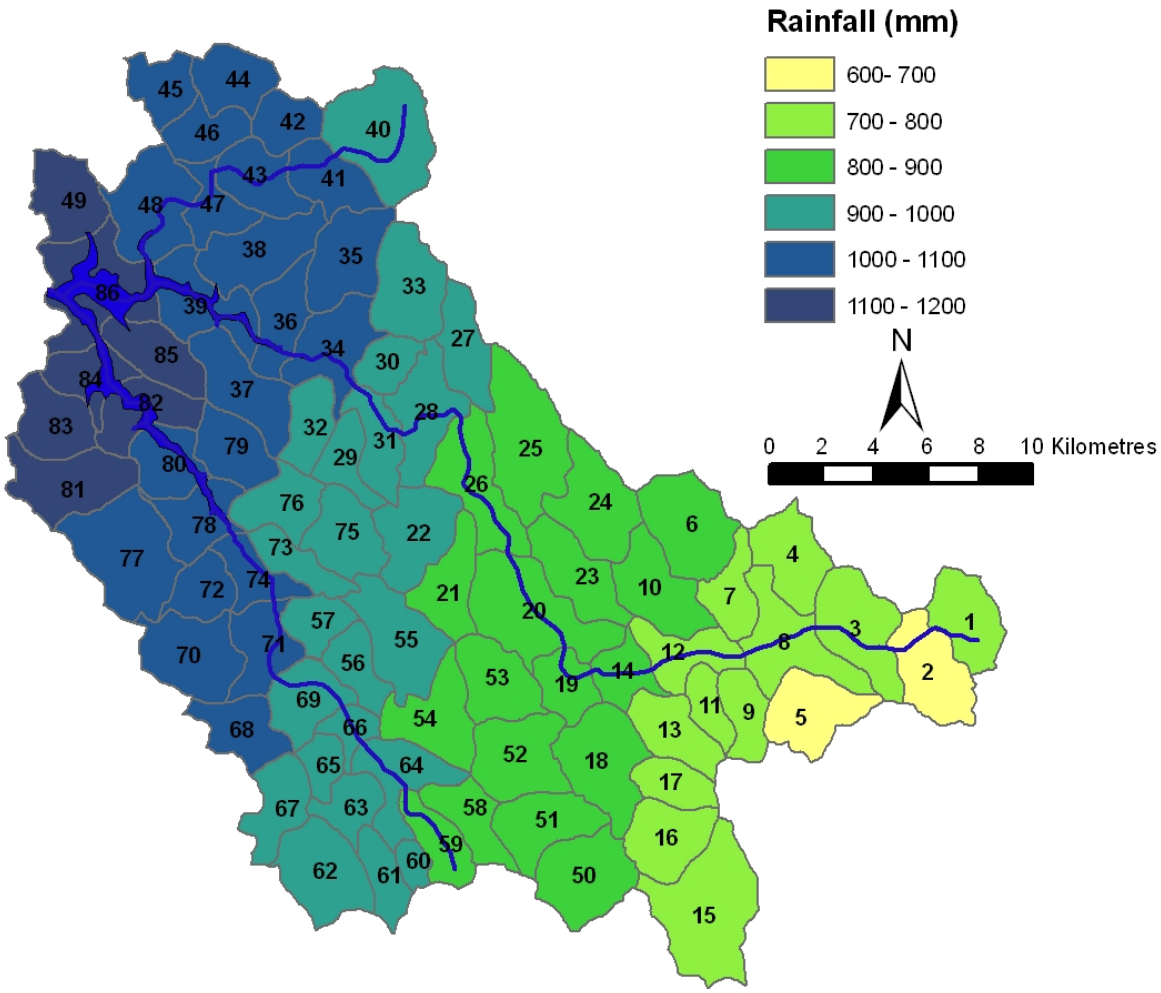

Figure A.3 Spatial distribution of average annual rainfall (1975–2004)

Mean monthly rainfall varied significantly across the catchment (Fig. A.4). The mean monthly rainfall for January at the dam outlet (Catchment 86) was 17 mm. The variation within the month was high — largely due to the high monthly rainfall totals of 32 and 120 mm respectively in 1990 and 2000. November to March also had low mean monthly rainfalls, with less variation than January. December had the smallest variation in mean monthly rainfalls of the three sites shown in Figure A.4.

At all sites mean monthly rainfall and the variation in monthly rainfall increased during the winter months (June–August). There was a significant increase in rainfall closer to the catchment outlet during the wetter months (May–September), with a less pronounced pattern during the drier months.

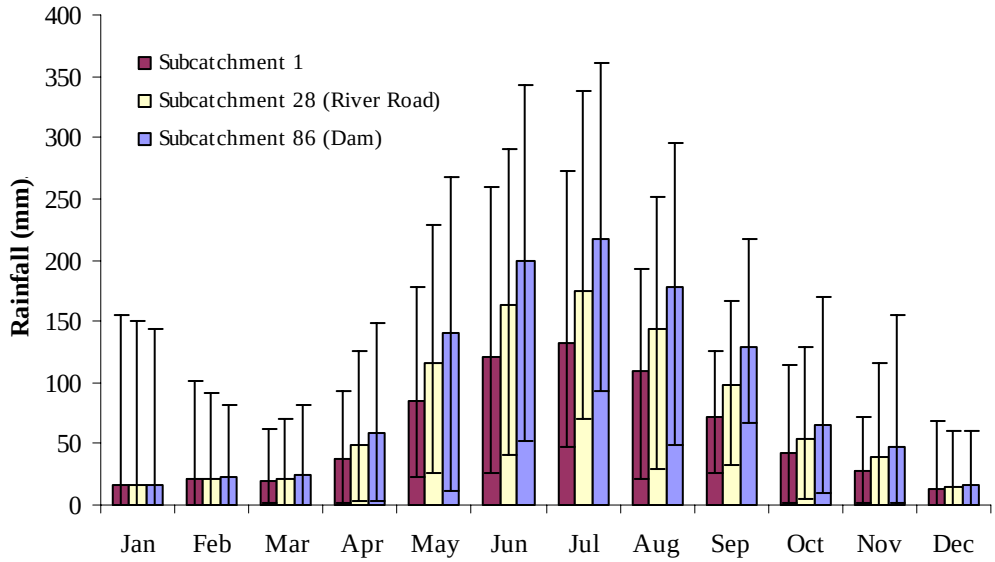

Figure A.4 Mean monthly rainfall 1975–2003

Pan evaporation

While pan evaporation is not recorded within the catchment, daily observed data are available at some rainfall stations west of the Serpentine Dam. Mean annual pan evaporation data at the centroid of all subcatchments were calculated from Luke et al. (1988) and then the figures converted into daily data using a harmonic function. The annual pan evaporation across the catchment ranged from 1600 to 1710 mm. The number of rainfall days was also a factor in determining daily rainfall, explaining some of the spikes in the data. The maximum daily evaporation throughout the catchment ranged from 8.3 to 8.9 mm, usually during the December–January period, and the minimum daily evaporation ranged from 0.5 to 2 mm, generally in the June–July period. Daily modelled pan-evaporation data from the Serpentine meteorological station (009039) compared well with the pan-evaporation data at Catchment 86 derived using the above methodology (Fig. A.5).

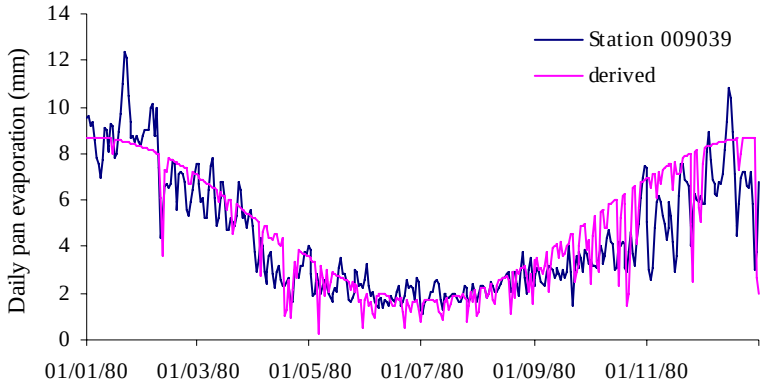

Figure A.5 Daily pan evaporation from daily modelled data (009039) and derived from annual data

Observed streamflow

Six gauging stations, with catchment areas between 2.1 and 243 km^2, were used to calibrate the modelled flows (Table 2.1). The Big Brook and River Road stations are located along the main tributaries, while the Cameron Central and Cameron West gauges are within smaller experimental catchments. The longest complete period of record (1983 to 2004) is from the Big Brook gauging station, followed by the Jack Rocks and River Road gauging stations, whose records cover 1981–99 and 1982–99 respectively. The Jayrup gauging station has a good record (1995–2003), as does the Cameron Central gauging station (1992–2003) — apart from a period of approximately one month when the quality of the data was recorded as poor. This period of poor records was dry and therefore does not bias any modelling results.

Land-use history

During the calibration of the LUCICAT model, full forest cover was assumed, with LANDSAT imagery used to calculate the leaf area index (LAI) of forest cover. The LAI values were used as a data input to the LUCICAT model as part of vegetation/water-balance calculations. The relatively small proportion of the catchment used for mining throughout the simulated period was not incorporated into the modelling.

LAI values were developed using the Microstation and Geographic Information Computation (MAGIC) model (Mauger 1996). This involved creating a grid about the catchment and dividing it into 25-m x 25-m cells. To separate forest cover from bare ground and water, the hues of each cell were used to characterise these land types. LAI values were determined for the years 1988, 1990, 1992, 1994, 1996, 1997, 1999, 2000, 2002 and 2003. The average LAI value within each subcatchment was determined and incorporated into the input file. For the years before 1988, the 1988 LAI values were used. For the years for which an LAI value was not available, the model interpolated a value. An annual plot of LAI values within selected subcatchments for the 1988–2003 period is shown in Figure A.6.

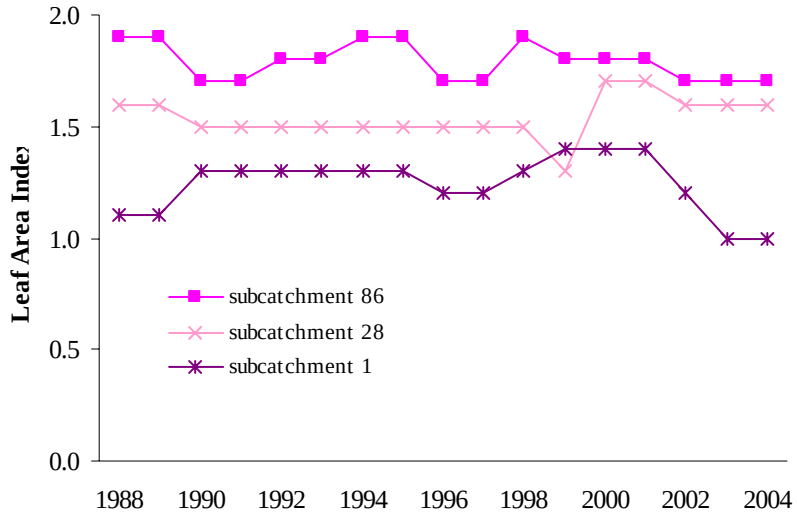

Figure A.6 LAI at three selected subcatchments

Groundwater

In the high-rainfall zone of south-west Western Australia, groundwater is commonly well connected to the stream channel. In the low-rainfall zone, however, groundwater can be 15–20 m below the stream channel. Not much groundwater data is available for the Serpentine Dam catchment, though some is available for the Cameron subcatchments. The limited recordings of groundwater levels at one site (61440352, subcatchment 69) show that the water level was close to the surface during October 1990 and June1991.

Subcatchment attributes

LUCICAT requires a variety of subcatchment attributes such as subcatchment elevations and areas; stream depth, width and length; surface slope; and soil thickness. This information has been extracted from the Department of Water's Geographic Information System.

A.3 Calibration

LUCICAT was manually calibrated for the annual, monthly and daily time scales, and simulations matched the observed data very well for all of them. The variations of some calibration parameters are shown in Table A.1. The value ranges are the results of calibrating LUCICAT to a wide range of catchments.

Table A.1 Parameters and their range

Parameter	Description	Unit	Value
d	Topsoil thickness	mm	1900–2900
w_i	Infiltration threshold		0.0001–0.0091
K_{ll}	Saturated hydraulic conductivity	mm/day	350
K_{uv}	Vertical conductivity	mm/day	27

Annual streamflow calibration

Annual runoff was calibrated at stream gauges throughout the catchment (Figs A.7 & 4.2). The correlations of the modelled and the observed streamflows for the six gauging stations are shown in Figure A.8. The annual averages are compared in Figure 4.3. For the Jack Rocks gauging station the observed and modelled data followed similar trends (Fig. A.7a). Both datasets record a high-runoff year in 1981 (Obs: 147 mm, LUCICAT: 178 mm) followed by a lower runoff year in 1982 (44 mm and 58 mm) and another high-runoff year in 1983 (163 mm and 214 mm). In all cases, LUCICAT runoff tends to be higher than observed runoff. A period of low runoff (60–100 mm) is recorded by both datasets from 1984 to 1987, after which records of annual runoff vary between 47 and 170 mm. LUCICAT simulated lower runoffs during the 1992–94 period and higher runoffs for 1996–98. The relationship between observed and modelled runoff (Fig. A.8a) records an R^2 value of 0.84. The statistics in Table 4.1 suggest that, during high runoff years, LUCICAT simulates higher than the observed, as the 90th percentiles of the observed and modelled datasets are 162.1 and 176.2 mm respectively. The statistics also indicate that LUCICAT simulates the low-runoff years well, as the 10th percentiles are the same (55.5 mm).

The observed and modelled runoffs at Big Brook gauging station (Fig. A.7b) follow a similar trend to that of the Jack Rocks station from 1983 to 1997. In 1983 LUCICAT models 46.5 mm compared to the observed 67.9 mm, following which both datasets show a decline in annual runoff until 1987. A range of high and low runoff years is seen until 1998, with both datasets matching well. From 1997 to 2003, annual runoff is low (1–35 mm), with LUCICAT generally simulating higher than the observed data. This is supported by the statistics in Table 4.1, as the modelled 10th and 90th percentiles (13.8 mm and 67.1 mm) are both higher than the observed (10.0 mm and 63.2 mm). The scatter graph (Fig. A.8b) also supports this, as the trendline sits above the 1:1 line and gives an R^2 value of 0.87.

The runoff for the Cameron Central gauging station is generally very low (0–12 mm), apart from 1996, for which observed and modelled annual runoffs are 26 mm and 37 mm respectively (Fig. A.7c). LUCICAT models lower runoff in the 1992–95 period and higher runoff from 1996 to 1999. Cameron Central has the smallest area of the gauged catchments, and also the lowest annual runoff values. As a result, the simulation discrepancies are more noticeable. Due to LUCICAT's high 1996 simulation, the modelled dataset has a higher mean

(8.0 mm) than the observed data (7.5 mm), while the observed dataset has higher 10th and 90th percentile values (Table 4.1). The high-runoff simulation for 1996 influences the scatter graph (Fig. A.8c), as the trendline is biased above the 1:1 line.

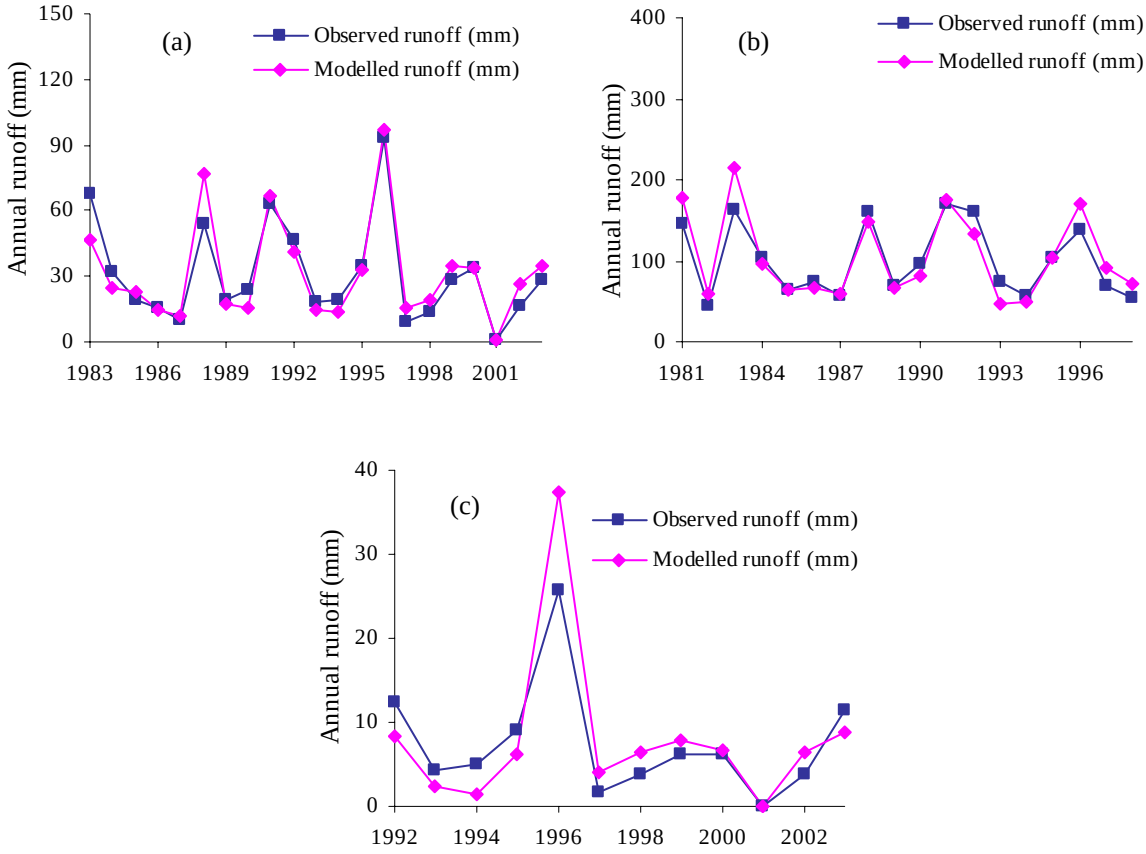

Figure A.7 Observed and modelled annual runoffs at (a) Jack Rocks, (b) Big Brook, and (c) Cameron Central

Modelled streamflows at Serpentine Dam during the 1975–2004 period are varied with a general decrease from the 1990s, mirroring the pattern of declining rainfall in that area. Five-year averages of summer streamflow (December–February) increased slightly from 1985–89 (0.19 GL) to the 2000–04 period (0.27 GL). Those of winter (June–August) and spring (September–November) have both increased from 1985–89 to 1995–99 and decreased from 1995–99 to 2000–04 (Table A.2).

Table A.2 Five-year averages of seasonal streamflow at the Serpentine Reservoir

	Five-year average of streamflow at Serpentine Reservoir (GL)					
Season	1975–1979	1980–1984	1985–1989	1990–1994	1995–1999	2000–2004
Summer	0.15	0.51	0.19	0.21	0.23	0.27
Autumn	0.47	0.80	0.55	0.72	0.40	0.42
Winter	18.26	31.66	22.93	29.19	29.48	21.98
Spring	6.57	16.24	9.35	9.56	16.99	9.31

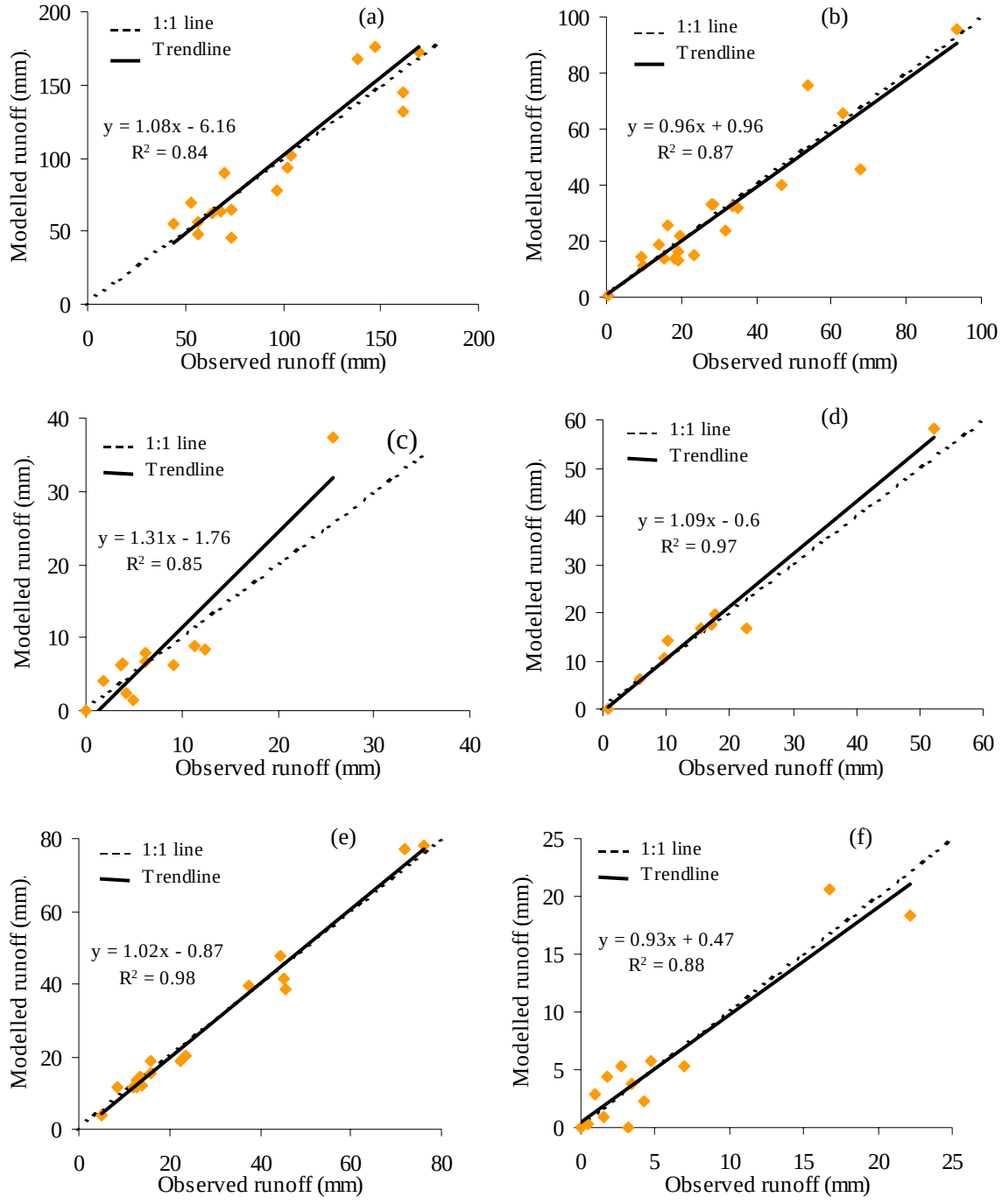

Figure A.8 Relationships between observed and modelled annual runoffs at (a) Jack Rocks 614031 (b) Big Brook 614037 (c) Cameron Central 614066 (d) Jayrup 614093 (e) River Road 614035 and (f) Cameron West 614064

The observed and modelled annual streamflows at the Jayrup gauging station were very similar (Fig. 4.2a). The low-flow period of 1997–2001 was predicted well, with 1996, 2002 and 2003 modelled slightly higher by LUCICAT. The scatter graph (Fig. A.8d) picks up this bias, as the trendline sits above the 1:1 line. The closeness of the two datasets is reflected in the R^2 value of 0.97. The percentiles are also very close. The modelled data has slightly lower 90th (27.4 mm/28.6 mm) and slightly higher 10th percentiles (4.9 mm/4.8 mm) than the observed dataset (Table 4.1).

The River Road gauge has a long period of record. The runoff varies throughout the 1982–98 period from 4.6 mm to 78.1 mm, and the modelled dataset follows the trend well, simulating both low- and high-runoff years well. The peaks are simulated well, with observed and modelled data recording 72 mm and 78.1 mm in 1983 and 76.2 mm and 79.5 mm in 1996. LUCICAT models a lower annual runoff in 1992 and higher runoff in 1997 and 1998. The mean annual runoff throughout the calibration period for the observed and modelled datasets is 28 mm and 29 mm respectively. The scatter graph (Fig. A.8e) supports the accurate calibration, with the trendline sitting on the 1:1 line and an R^2 value of 0.98. Further statistics reveal that LUCICAT tends to overestimate observed data for this gauging station. The 90th percentiles are 56.0 mm and 60.9 mm for the observed and modelled dataset respectively. The modelled median annual runoff is also higher (19.5 mm) than the observed (15.9 mm).

The Cameron West calibration is similar to that of Cameron Central, with mean annual runoff varying from 0 to 22.2 mm. During 1992–96 LUCICAT simulated lower than observed values, then simulated higher values during the low-flow periods of 1998–2000, 2002 and 2003. The balance of higher and lower than observed runoffs has produced a scatter graph with a trendline that sits very close to the 1:1 line (Fig. A.8f) and an R^2 value of 0.88. Further analysis reveals that the two datasets vary in certain statistical characteristics. The 90th percentiles are higher for the modelled data (16.2 mm) than the observed (14.8 mm), while the modelled 10th percentiles are lower than observed (Table 4.1).

Monthly streamflow

Plots of modelled and observed runoff at the remaining gauging stations are shown in Figure A.9. The flow period error index (EI), Nash-Sutcliffe criteria, correlation coefficient, explained variance (EV) and water-balance error were also determined for each gauging station (Table A.3).

Recorded monthly runoff maxima at the Jack Rocks gauging station ranged from 12 to 65 mm (Fig. 4.4). The flow period index error is very close to 1, indicating that the modelled and observed datasets are flowing for the same duration. The Nash-Sutcliffe criterion is also close to 1 (0.83), indicating that the modelled data fit well with the observed data.

Monthly maximum runoff at River Road ranged from 4 to 41 mm (Fig. A.9a). LUCICAT tended to cease-to-flow earlier than the observed cessation, which is indicated by the flow period error index value of 0.85, indicating that the modelled dataset is flowing for a smaller duration than the observed dataset. The Nash-Sutcliffe criterion was evaluated at 0.93, a

better result than for Jack Rocks. Similarly to Jack Rocks, LUCICAT tended to simulate higher figures than the observed data during the high runoff months.

The two Cameron sites received the smallest monthly runoffs. Statistically, the model outputs for these two sites don't perform as well as for the other gauging stations. Maximum monthly runoffs at Cameron West (Fig. A.9b) and Central (Fig. A.9c) were recorded at 10.6 mm and 12.5 mm respectively, both in August 1996. LUCICAT generally predicts the number of runoff days well, with a flow period error index of 0.79 at Cameron Central. The index at Cameron West is lower (0.54), which can be attributed to the July–October period of 1994 when LUCICAT modelled dry conditions.

The Jayrup gauging station has monthly records of runoff from May 1995 until April 2004 (Fig. A.9d). Maximum monthly runoff reached 21 mm in August 1995. LUCICAT mistimed and overjudged this peak, recording 17 mm in August and 25 mm in September. The Nash-Sutcliffe efficiency is close to 1 (0.86), indicating that the two datasets fit well. LUCICAT models the majority of runoff events satisfactorily, with a flow period error index of 0.76.

The Big Brook gauging station (Fig. A.9e) has the longest period of record, 1983–2004. The modelled dataset follows the observed data very well at all magnitudes of flow. The maximum monthly runoff was recorded in August 1996 (38.2 mm), which LUCICAT simulated very well at 38.5 mm. The flow period error index is close to 1 (0.81), indicating that LUCICAT is modelling the majority of runoff events. The Nash-Sutcliffe efficiency is also close to 1 (0.89), indicating a good fit.

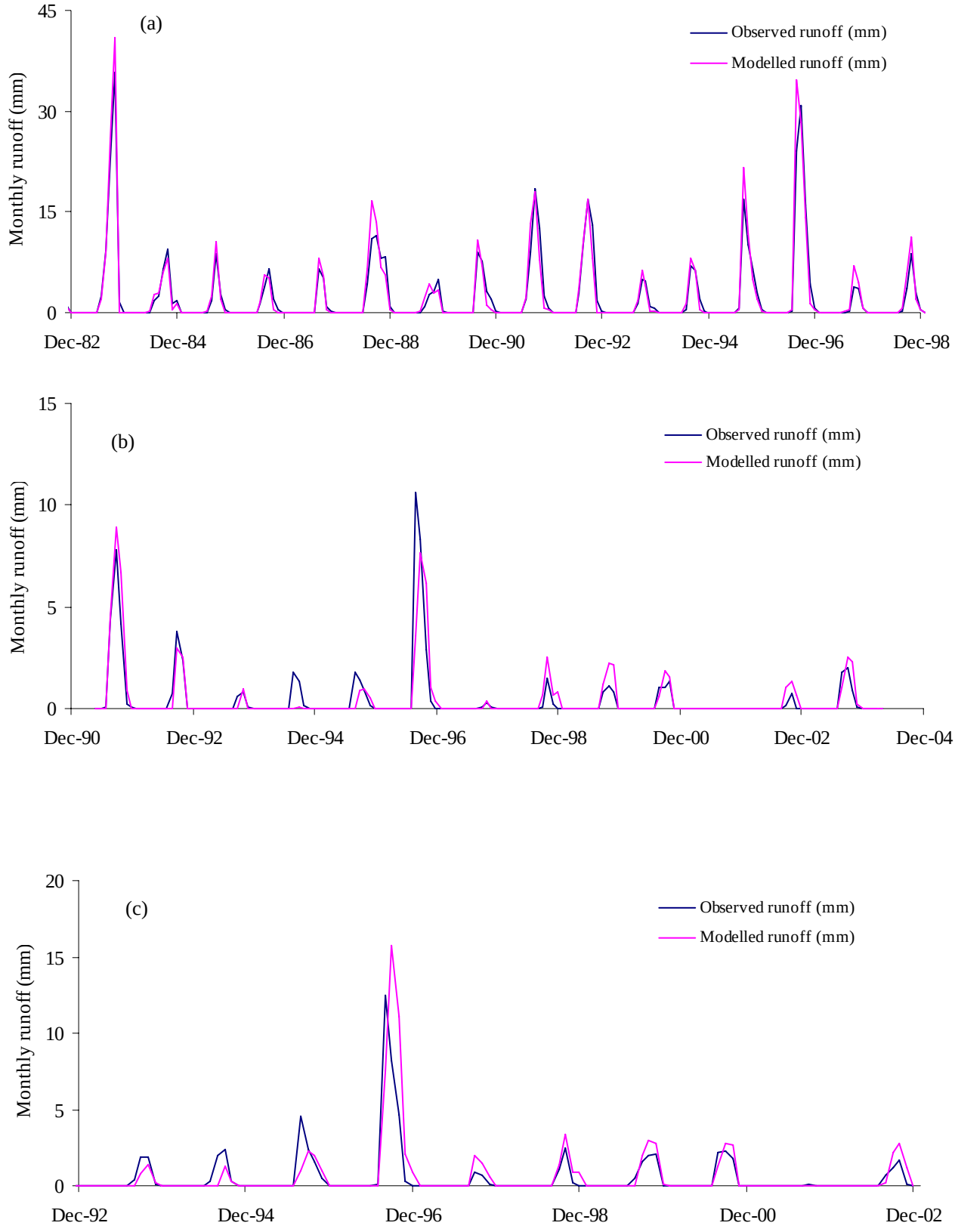
(a)
Observed runoff (mm)
Modelled runoff (mm)
Monthly runoff (mm)
45
30
15
0
Dec-82
Dec-84
Dec-86
Dec-88
Dec-90
Dec-92
Dec-94
Dec-96
Dec-98
(b)
Observed runoff (mm)
Modelled runoff (mm)
Monthly runoff (mm)
15
10
5
0
Dec-90
Dec-92
Dec-94
Dec-96
Dec-98
Dec-00
Dec-02
Dec-04
(c)
Observed runoff (mm)
Modelled runoff (mm)
Monthly runoff (mm)
20
15
10
5
0
Dec-92
Dec-94
Dec-96
Dec-98
Dec-00
Dec-02

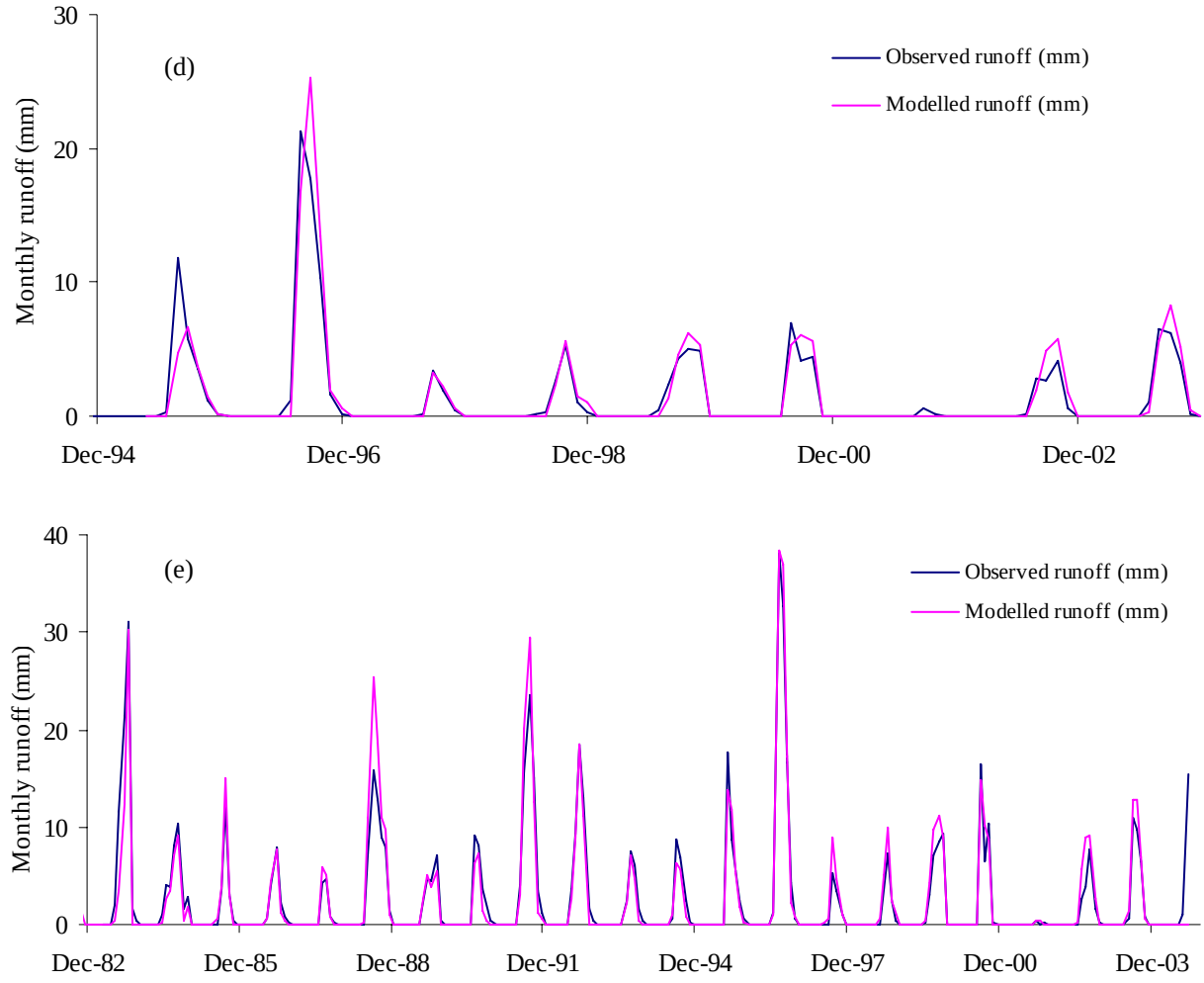

Figure A.9 Observed and predicted monthly streamflows at (a) River Road, (b) Cameron West, (c) Cameron Central, (d) Jayrup and (e) Big Brook gauging stations

Table A.3 Monthly statistics

Measure of fit	Value for best fit	Jack Rocks	River Road	Big Brook	Jayrup	Cameron Central	Cameron West
Flow period error index (EI)*	1	0.99	0.85	0.81	0.76	0.79	0.54
Nash-Sutcliffe criterion*	1	0.83	0.93	0.89	0.86	0.51	0.71
Correlation coefficient	1	0.96	0.97	0.95	0.94	0.80	0.85
Explained variance (EV)	1	0.83	0.93	0.89	0.86	0.51	0.71
Water-balance error (%)	0	+ 4.2	+ 3.3	+ 2.2	+ 5.4	+ 7.2	+ 4.9

* explained in Bari (2005)

Daily streamflow

Modelled and observed daily flows for Jack Rocks, Cameron Central, Big Brook and River Road are compared in Section 4.3 with graphs in Figure 4.6.

Daily runoff at Cameron West is very small, the maximum reaching only 2.3 mm in July 1996. Because runoff at this site is so small, discrepancies as small as 0.3 mm are significant deviations from the observed dataset. As a result, the modelled and observed daily runoffs at Cameron West are not as well matched as at other gauging stations. In the latter half of the dataset (1998–2003), LUCICAT simulates the correct flow duration and produces 'flashy' hydrographs (higher peak flows and early drying out). In the earlier half of the dataset (1991–97), LUCICAT records a shorter flow duration period and also tends to simulate higher peak flows. Daily runoff for 1991 is shown in Figure A.10a.

The modelled and observed daily runoff datasets at Jayrup are well matched. The average annual runoff rate at this catchment is 1.8% and so the maximum daily runoff recorded is quite low, 3.2 mm. There are a few instances where the LUCICAT simulation differs from the observed data, its flow duration being shorter in some cases than observed. During 1995, 1998 and 2002, due to the low magnitude, LUCICAT misses an early isolated runoff event and therefore modelled runoff begins later than observed. This is also the case for 1996 and 1999 (Fig. A.10b), where the modelled runoff begins 1–2 weeks later than observed. The modelled dataset simulates all magnitudes well, but at times doesn't model the full magnitude of the peak runoff events. This is particularly the case in 1995, when two peak runoff events were recorded at 1.7 mm and 1.2 mm, whereas LUCICAT simulated both as 0.7 mm. It also simulated a lower runoff during 2001; however, the runoff during that year was very low, with a maximum of 0.17 mm. During 1997, 1998 and 2000, runoff events in the 0.1–0.3 mm range tended to be modelled higher.

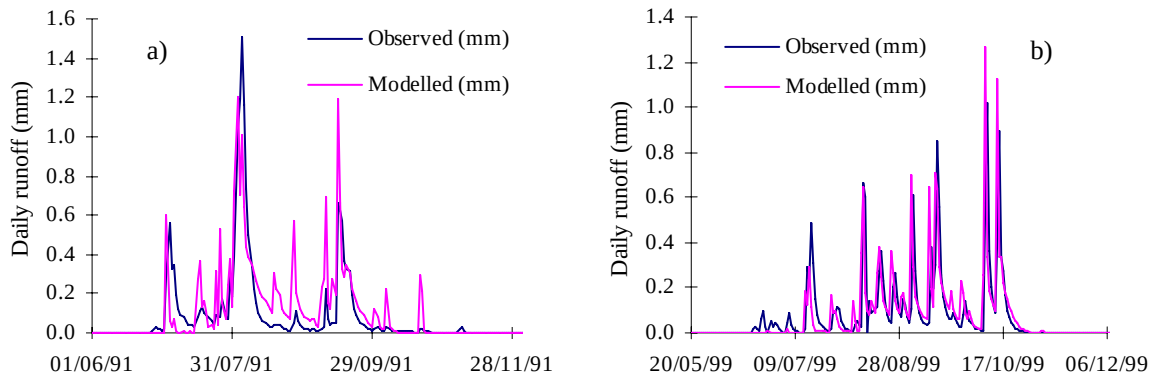

Figure A.10 Daily streamflows at (a) Cameron West (1991) & (b) Jayrup (1999) gauging stations

Daily flow duration

Daily flow-duration curves were created for each gauging station. The Cameron Central gauging station recorded flow data for the period 1992–2003 and the modelled and observed flow durations are similar (Fig. A.11a). This is also the case with the River Road and Big Brook gauging stations (Figs A.11b & c), for which the periods of record are 1982–99 and 1983–2004 respectively. Flow at Jayrup gauging station was recorded from 1995 until 2003. The flow-duration curve compared well for all magnitudes of flow (Fig. A.11d). The curves for Jack Rocks and Cameron West show good matches for the median to high flows and a deviation from observed flow in low-flow periods (Fig. 4.7).

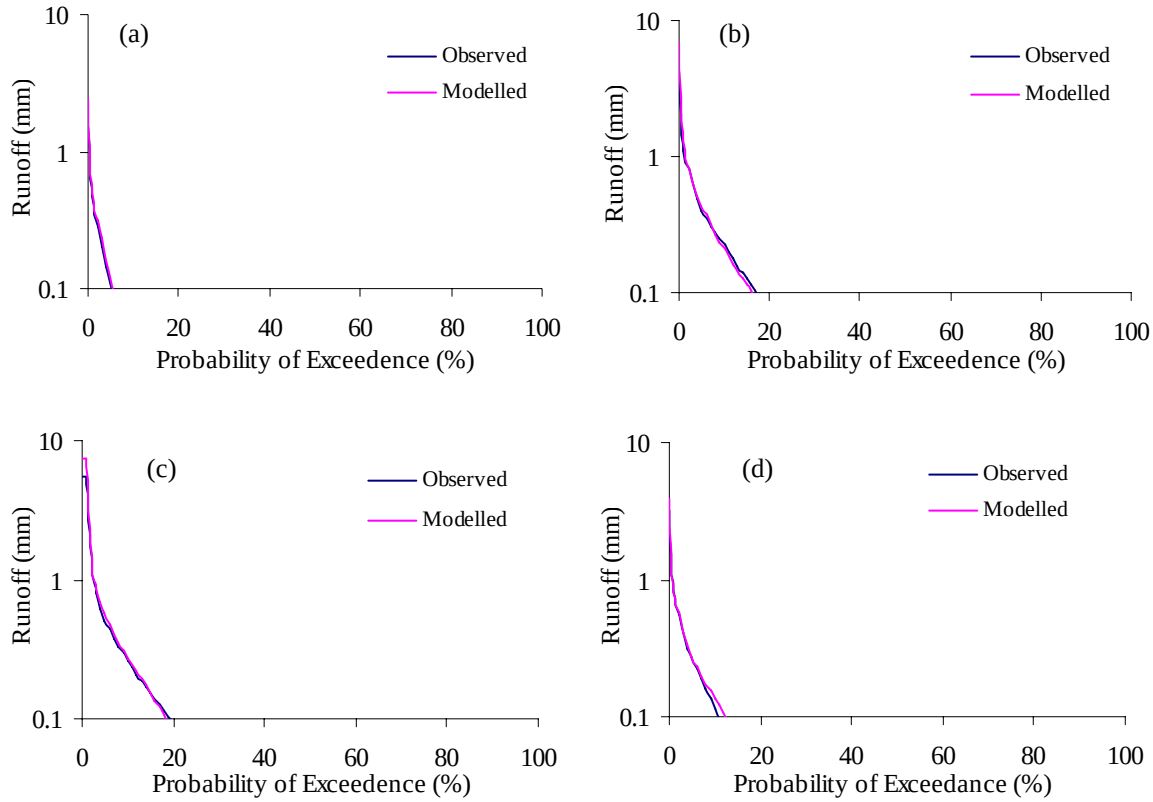

Figure A.11 Daily flow duration at (a) Cameron Central, (b) River Road, (c) Big Brook and (d) Jayrup gauging stations

Appendix B Calculation of spatial distribution of rainfall

Four rainfall stations surrounding the Serpentine Dam catchment were part of the group of 31 rainfall stations for which downscaled rainfall data were produced. The observed dataset, with which the modelled dataset is compared, used 37 rainfall stations throughout and surrounding the catchment (Fig. 2.2). As a result, the spatial distribution of rainfall calculated using the current-scenario CCAM-downscaled rainfall data was not the same as the spatial distribution calculated using observed data. These discrepancies are shown in Figure B.1, which illustrates that rainfall with the CCAM data is higher for the majority of the catchment, particularly the Big Brook and River Road subcatchment areas, and lower in the subcatchments close to the dam outlet.

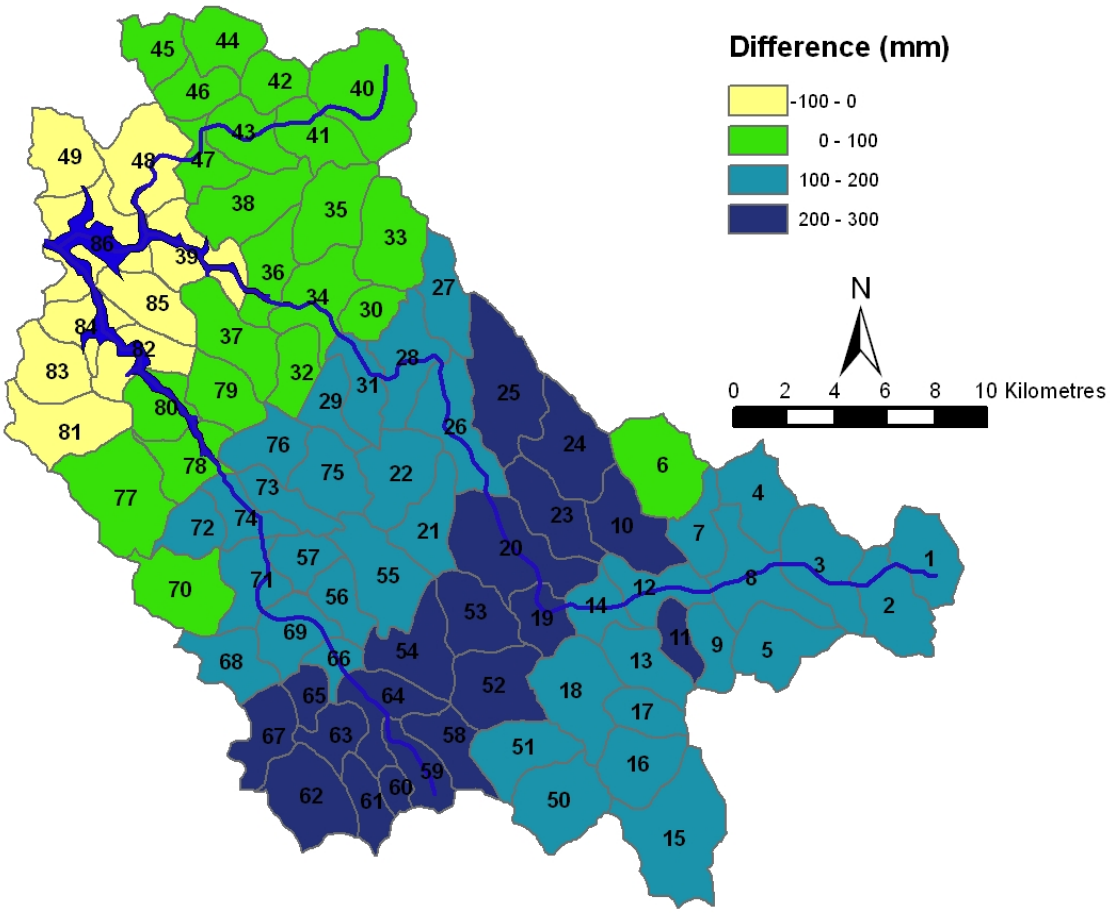

Figure B.1 Differences between the observed and the CCAM-downscaled annual rainfalls

As these results would bias the catchment yield results at the dam outlet, further analysis was carried out to form a relationship between annual rainfalls at each of the 86 subcatchments of the Serpentine Dam catchment and annual rainfalls at each of the four previously mentioned rainfall stations and then use this relationship to run the rainfall distribution for all of the GCMs. For each subcatchment, for the period 1975–2004, the following equation was solved:

$$y_{ij} = a_{ij}x_{1j} + b_{ij}x_{2j} + c_{ij}x_{3j} + d_{ij}x_{4j}$$

where

I = subcatchment number (1:86)

j = year (1975:2004)

y_{ij} = observed annual rainfall at subcatchment *I* during year *j*

x_{1j} = observed annual rainfall at Serpentine during year *j*

x_{2j} = observed annual rainfall at Jarrahdale during year *j*

x_{3j} = observed annual rainfall at Wandering during year *j*

x_{4j} = observed annual rainfall at Dwellingup Forestry during year *j*

a_{ij} b_{ij} c_{ij} and d_{ij} are unknowns for each subcatchment *I* and each year *j*

For example, annual rainfall at subcatchment 1 in 1975 is calculated by scaling the rainfall at each of the four rainfall stations and summing them.

Figure B.2 shows the average annual rainfall at subcatchment 86, which represents the catchment average. The observed dataset was created using the 37 available rainfall stations, and the calculated dataset was created using the scaled data from the four rainfall stations. The two datasets show similar trends. A plot of the residuals (Fig. B.3) shows that, at most, the observed and calculated data differ by 8 mm.

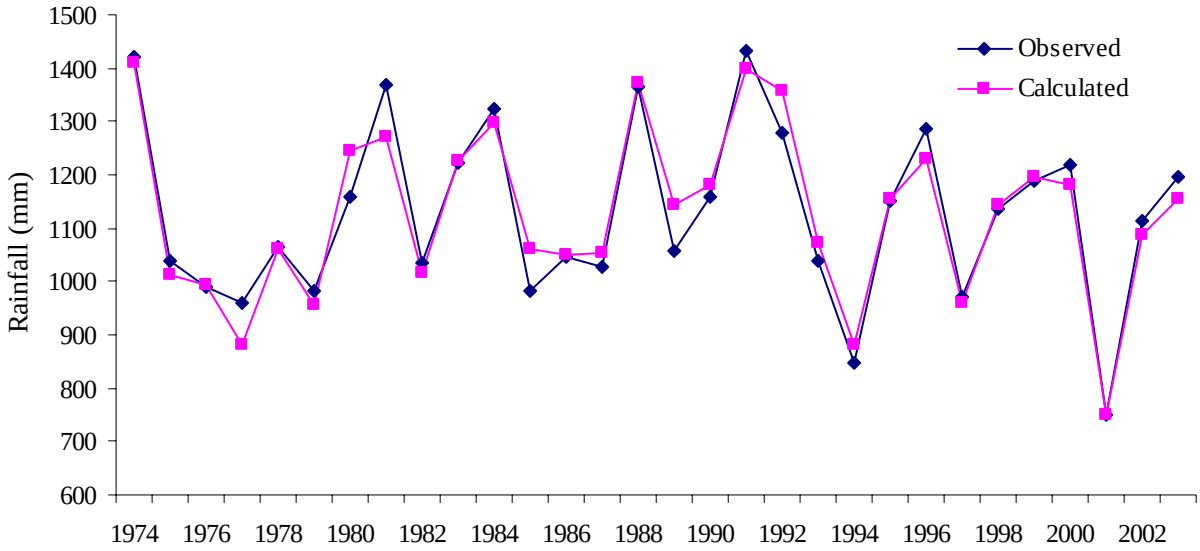

Figure B.2 Catchment average rainfall: comparison of observed data from 37 rainfall stations (observed) and scaled data from 4 rainfall stations (calculated)

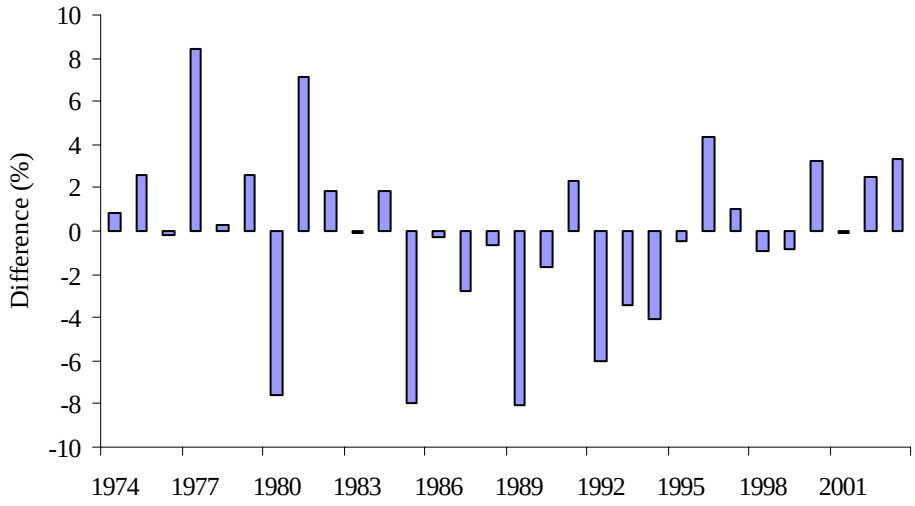

Figure B.3 Difference between observed and calculated data

Figure B.4 shows the differences in rainfall (in millimetres) between the observed data (distributed by LUCICAT) and the CCAM current-climate downscaled rainfall data — an average value for all 40 simulations and 30 years of data. Comparison of the two datasets reveals a large improvement: whereas in Figure B.1 the largest difference was 300 mm, the largest difference is now only 30 mm.

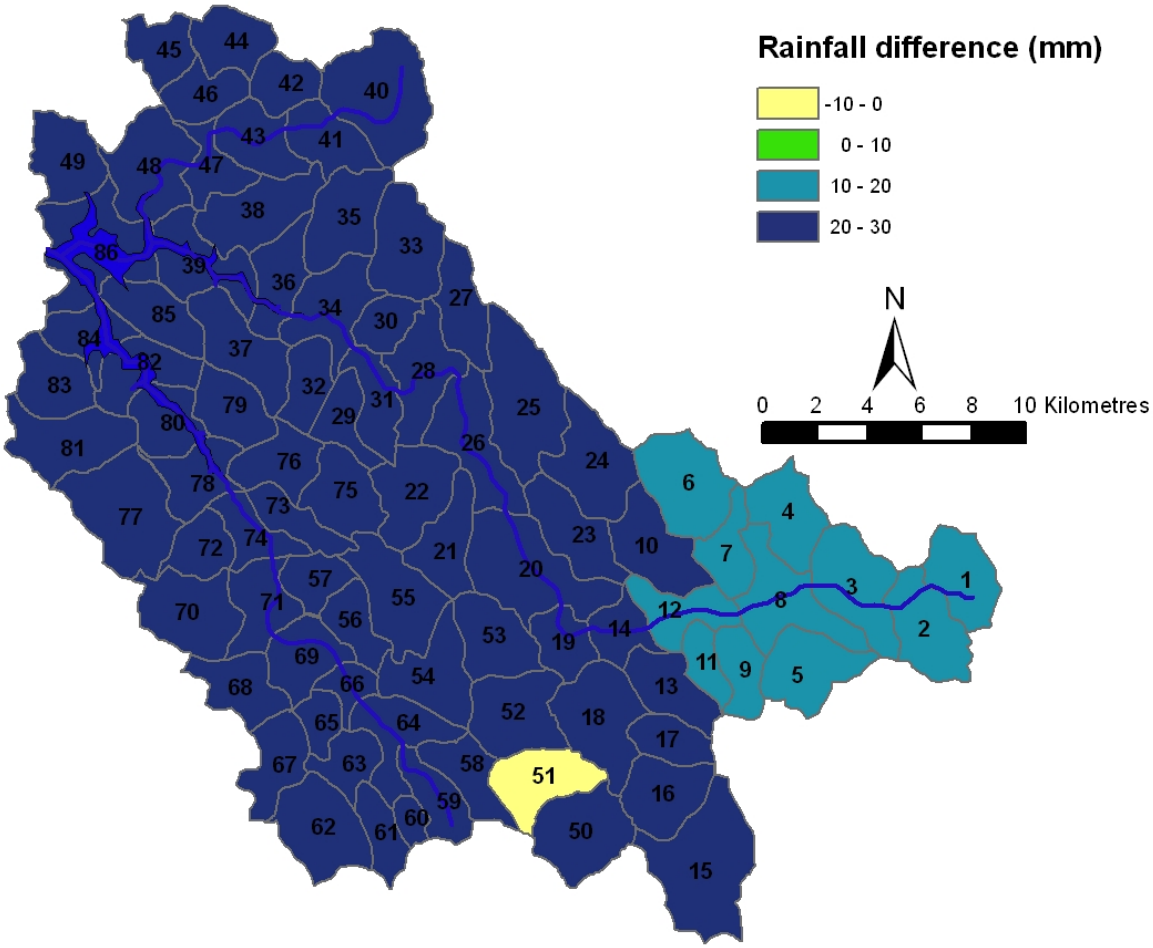

Figure B.4 Difference between observed and current CCAM downscaled rainfall data — using the statistical method

Table B.1 shows the monthly differences between the downscaled rainfall and observed data. The monthly rainfall for the GCMs refers to the average monthly rainfall for 30 years averaged for all 40 simulations. All data have been evaluated at subcatchment 86, which represents the entire catchment. The greatest variation when comparing current-climate monthly rainfalls occurs during the high rainfall months, as the projections for the dry months (November–March) are similar for all datasets (Fig. B.5).

The seasonality of the ECHAM4 model follows that of the observed well, despite simulating high rainfalls during June, July and August. The Mk3 displays a seasonal bias, causing the projection to be lower than observed in the early months of the annual hydrograph and higher than observed in the later stage. The CCAM and HadAM3P models both have a similar seasonality and a similar magnitude to those of the observed data.

Table B.1 Downscaled current-climate monthly rainfalls compared to observed data

	Jan	Feb	Mar	Apr	May	Jun	Jul	Aug	Sep	Oct	Nov	Dec
Observed data (1975–2004) Rainfall	17	22	21	49	117	165	176	145	100	54	40	15
ECHAM4 (1975–2004)												
Rainfall (mm)	20	21	34	59.9	117	199	220.6	166	105	44	35	25.2
Difference (%)	16	-4	38	18	0	17	20	12	5	-22	-14	41
Difference (mm)	3	-1	13	11	0	34	45	21	5	-10	-5	10
CCAM (1975–2004)												
Rainfall (mm)	25	24	31	47	93	163	173	152	121	72	39	27
Difference (%)	31	-28	37	-36	-36	-1	3	6	20	21	-6	25
Difference (mm)	8	2	10	-2	-24	-2	-3	7	21	18	-1	12
Mk3 (1975–2004)												
Rainfall (mm)	19	15	28.2	34	92	153	185	185	138	71	26	22
Difference (%)	11	-48	26	-42	-28	-8	5	21	28	24	-51	32
Difference (mm)	2	-7	7	-15	-25	-12	9	40	38	17	-14	7
HadAM3P (1960–1990)												
Rainfall (mm)	27	29	24.3	27	106	153	170.7	162	100	42	27	29
Difference (%)	36	24	14	-81	-10	-8	–3	10	0	-28	-48	48
Difference (mm)	10	7	3	-22	-11	-12	-5	17	0	-12	-13	14

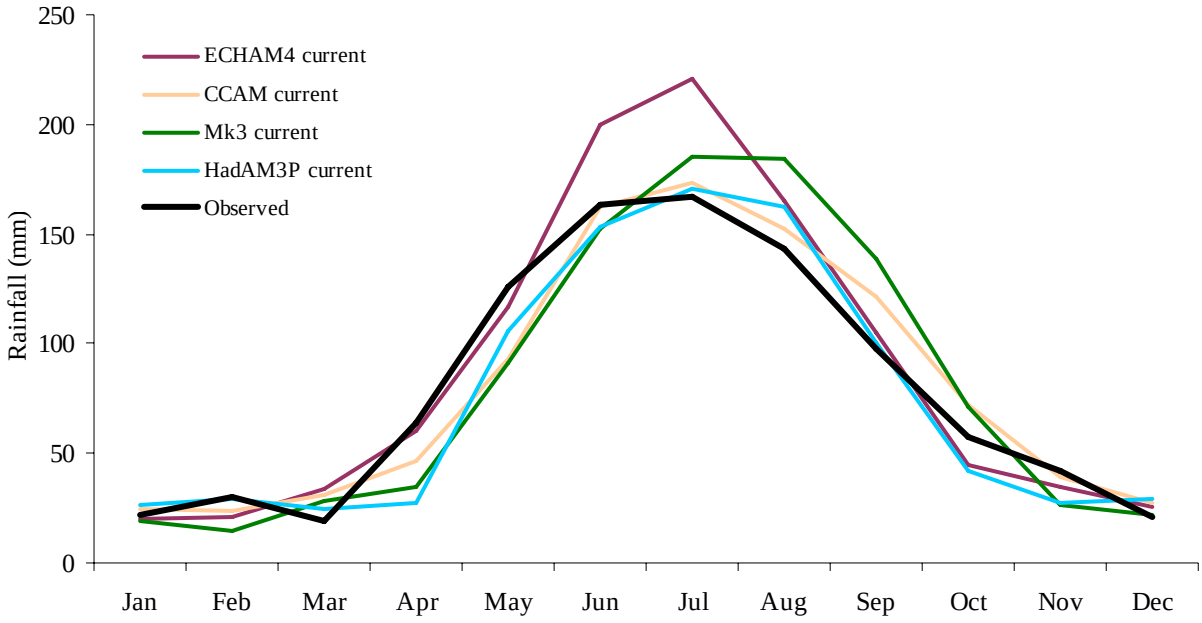

Figure B.5 Mean monthly rainfall, observed and current-scenario simulations

Appendix C: Statistical significance of sample size

The statistically significant sample size was determined in a similar way to Stage 1, using ten simulations. The standard deviations of the mean annual rainfall for each GCM dataset were used as the study variable. The following equation was used to determine the statistically significant sample size (Johnson & Bhattacharyya 1996):

$$n = \left[\frac{t_{0.05/2} S}{d} \right]^2$$

n = sample size

$t_{0.05/2}$ = t-value at the 95% confidence limit (2-tailed test, df = n (10) – 1)

S = standard deviation of the study variable

d = desired error margin

Using a desired error margin (d) of 5%, this methodology was performed using the first ten simulations of all of the GCM datasets. The current-climate CCAM dataset produced the highest sample size (n), at 40. The corresponding S value was 21.05 and the t value 2.262. This indicates that the testing of 40 simulations is required to ensure that the error estimation of the standard deviation does not exceed 5% at the 95% confidence level.

Appendix D: Simulated runoff statistics from downscaled rainfall

The following statistics relate to the 30-year average for monthly runoff, and its variation from the 40 simulations. The mean, maximum, minimum, 10th percentile, 90th percentile, standard deviation and coefficient of variation were all determined for the current and future scenarios of the CCAM, Mk3 and HadAM3P GCMs.

From the current to the future scenario in the CCAM simulations, the mean of the 30-year mean monthly runoff decreases every month. The maxima decrease in all months apart from March, and the minima decrease every month. The 10th percentile values remain similar; however, from June to November the 90th percentile values reduce significantly, by up to 50%.

The Mk3 simulations showed similar results to the CCAM simulations, with the mean, maximum, minimum, 10th percentiles and 90th percentiles decreasing from the current to the future scenario. Greater change was seen during the wetter months of July–September.

The statistics relating to the HadAM3P simulations showed different trends. The statistics for January indicated that runoff would increase for the future scenario. For the Mk3 and CCAM simulations, the standard deviation would either remain the same or decrease when compared with the future scenario. The HadAM3P simulations are a little different, as during January, February and November the standard deviation increases slightly.

Table D.1 CCAM monthly runoff statistics

CCAM	January		February		March		April		May		June	
	Current	Future	Current	Future	Current	Future	Current	Future	Current	Future	Current	Future
Mean of averages	0.16	0.11	0.09	0.08	0.09	0.09	0.18	0.11	0.54	0.34	3.26	1.61
Max of averages	0.29	0.16	0.13	0.10	0.18	0.12	0.23	0.18	0.71	0.41	4.29	2.18
Min of averages	0.10	0.07	0.06	0.04	0.07	0.06	0.12	0.08	0.42	0.26	2.51	1.27
10th percentile	0.12	0.09	0.07	0.05	0.08	0.06	0.14	0.08	0.45	0.28	2.82	1.39
90th percentile	0.20	0.14	0.12	0.10	0.11	0.11	0.21	0.14	0.63	0.39	3.80	1.87
St. Dev.	0.04	0.02	0.02	0.02	0.02	0.02	0.03	0.02	0.07	0.04	0.42	0.20
CV	0.23	0.18	0.20	0.22	0.21	0.19	0.15	0.21	0.14	0.11	0.13	0.12

CCAM	July		August		September		October		November		December	
	Current	Future	Current	Future	Current	Future	Current	Future	Current	Future	Current	Future
Mean of averages	12.77	8.29	20.41	12.71	16.07	10.43	6.93	4.39	1.62	1.02	0.38	0.31
Max of averages	16.48	9.54	27.65	14.58	19.57	12.54	8.28	5.40	2.22	1.50	0.56	0.47
Min of averages	9.16	6.93	15.99	10.71	12.65	8.70	5.74	3.36	1.15	0.70	0.25	0.17
10th percentile	11.05	7.29	17.18	11.56	14.04	9.08	6.16	3.79	1.34	0.85	0.27	0.23
90th percentile	14.30	9.03	22.89	13.97	18.62	11.60	7.86	5.09	1.89	1.19	0.47	0.37
St. Dev.	1.39	0.63	2.38	0.97	1.69	0.94	0.64	0.52	0.23	0.16	0.08	0.07
CV	0.11	0.08	0.12	0.08	0.10	0.09	0.09	0.12	0.14	0.16	0.20	0.22

Table D.2 Mk3 monthly runoff statistics

Mk3	January		February		March		April		May		June	
	Current	Future	Current	Future	Current	Future	Current	Future	Current	Future	Current	Future
Mean of averages	0.09	0.07	0.05	0.05	0.08	0.05	0.11	0.08	0.44	0.30	2.34	1.41
Max of averages	0.14	0.14	0.10	0.07	0.13	0.08	0.15	0.11	0.64	0.37	3.14	1.73
Min of averages	0.06	0.05	0.03	0.03	0.05	0.04	0.09	0.05	0.33	0.26	1.69	1.08
10th percentile	0.07	0.05	0.04	0.04	0.06	0.04	0.09	0.07	0.38	0.28	1.86	1.25
90th percentile	0.12	0.09	0.07	0.06	0.09	0.07	0.14	0.09	0.49	0.33	2.85	1.59
St Dev	0.02	0.02	0.02	0.01	0.02	0.01	0.01	0.01	0.06	0.02	0.36	0.14
CV	0.21	0.26	0.32	0.21	0.21	0.19	0.13	0.12	0.13	0.07	0.15	0.10

Mk3	July		August		September		October		November		December	
	Current	Future	Current	Future	Current	Future	Current	Future	Current	Future	Current	Future
Mean of averages	12.47	8.79	26.58	16.90	21.24	15.99	6.01	5.54	1.25	0.98	0.26	0.22
Max of averages	16.11	10.94	31.38	20.11	28.31	18.61	7.74	6.79	1.97	1.22	0.45	0.34
Min of averages	9.94	7.38	22.25	15.01	16.66	14.12	4.79	4.71	0.96	0.78	0.18	0.14
10th percentile	10.64	7.79	23.80	15.61	19.21	14.52	5.28	5.08	1.03	0.81	0.19	0.16
90th percentile	14.13	9.88	29.94	18.47	23.62	17.37	6.81	6.04	1.49	1.12	0.35	0.27
St Dev	1.43	0.76	2.34	1.29	2.12	1.12	0.67	0.45	0.20	0.12	0.07	0.05
CV	0.11	0.09	0.09	0.08	0.10	0.07	0.11	0.08	0.16	0.12	0.25	0.23

Table D.3 HadAM3P monthly runoff statistics

HadAM3P	January		February		March		April		May		June	
	Current	Future	Current	Future	Current	Future	Current	Future	Current	Future	Current	Future
Mean of averages	0.07	0.10	0.08	0.07	0.08	0.05	0.09	0.05	0.42	0.28	2.76	1.37
Max of averages	0.11	0.21	0.17	0.23	0.14	0.10	0.12	0.09	0.54	0.35	3.81	2.08
Min of averages	0.04	0.06	0.05	0.03	0.06	0.03	0.06	0.04	0.31	0.21	1.75	1.03
10th percentile	0.06	0.07	0.06	0.04	0.06	0.04	0.07	0.04	0.36	0.24	2.07	1.13
90th percentile	0.10	0.14	0.10	0.10	0.09	0.07	0.11	0.06	0.48	0.31	3.61	1.60
St Dev	0.02	0.03	0.02	0.03	0.02	0.02	0.01	0.01	0.06	0.03	0.60	0.23
CV	0.22	0.31	0.27	0.50	0.21	0.29	0.16	0.17	0.13	0.11	0.22	0.17

HadAM3P	July		August		September		October		November		December	
	Current	Future	Current	Future	Current	Future	Current	Future	Current	Future	Current	Future
Mean of averages	11.97	5.56	19.66	8.19	10.95	4.04	2.78	1.07	0.47	0.44	0.22	0.15
Max of averages	15.94	6.35	25.27	10.24	13.31	5.26	3.48	1.39	0.98	0.87	0.44	0.27
Min of averages	8.20	4.30	15.13	6.62	8.21	3.01	2.23	0.81	0.31	0.21	0.12	0.06
10th percentile	9.58	5.17	16.89	7.34	9.49	3.58	2.36	0.88	0.36	0.30	0.14	0.10
90th percentile	14.41	6.04	22.23	8.76	13.22	4.72	3.20	1.24	0.60	0.72	0.29	0.19
St Dev	1.95	0.38	2.28	0.73	1.30	0.47	0.32	0.14	0.12	0.16	0.06	0.04
CV	0.16	0.07	0.12	0.09	0.12	0.12	0.12	0.13	0.26	0.36	0.29	0.28

Government of **Western Australia**
Department of **Water**

www.water.wa.gov.au